Induction Machine Stray Loss from Inter-bar Currents

by

Steven C. Englebretson

Submitted to the Department of Electrical Engineering and Computer Science
in partial fulfillment of the requirements for the degree of

Doctor of Philosophy

at the

MASSACHUSETTS INSTITUTE OF TECHNOLOGY

September 2008

Author .....
Department of Electrical Engineering and Computer Science
September 4, 2009

Certified by ..
James L. Kirtley, Jr.
Professor of Electrical Engineering and Computer Science
Thesis Supervisor

Accepted by .....
Terry P. Orlando
Chairman, Department Committee on Graduate Students

Induction Machine Stray Loss from Inter-bar Currents

by

Steven C. Englebretson

Submitted to the Department of Electrical Engineering and Computer Science
on September 4, 2009, in partial fulfillment of the
requirements for the degree of
Doctor of Philosophy

Abstract

Stray load loss refers generally to the sources of induction machine loss not accounted for by typical calculations of primary or secondary copper loss, no load core loss, or friction and windage loss. Harmonic rotor bar currents from the non-sinusoidal distribution of the slotted stator winding contribute significant stray load loss. Rotor bars, especially on cast rotors for machines under fifty horsepower (37.3 kW), can be skewed, helically twisted from one end to the other, to reduce loss, torque, and noise from alignment of rotor and stator slots and from harmonic rotor currents. Inter-bar currents flowing circumferentially through the laminations between skewed and non-insulated rotor bars can significantly increase stray load loss.

Presented equations adjust the effective rotor resistance and skew factor of the extended per-phase induction machine equivalent circuit model in order to account for the impact of inter-bar currents. The average value of resistance between neighboring rotor bars significantly impacts calculations of rotor bar and inter-bar current and loss and has been determined for a number of measured rotors. Rotors fit into one of two distinct categories where either the bar-to-lamination contact resistance dominates the inter-bar resistance or the total resistance divides more equally between values of bar, lamination, and contact resistance.

Performance calculations using the adjusted equivalent circuit model are verified theoretically against previous calculation methods and experimentally by comparison to measured test results including variations in rotor skew, conductor conductivity, and inter-bar resistance. A number of different cast copper and aluminum five and ten horsepower test induction motors performed differently than originally predicted and variably between nominally identical machines. Inter-bar currents are part of the cause of both the variation and additional losses measured on these machines. The adjusted equivalent circuit equations improve estimations of motor performance and allow identification of means to increase machine efficiency by minimizing the stray load loss due to inter-bar currents.

Thesis Supervisor: James L. Kirtley, Jr.
Title: Professor of Electrical Engineering and Computer Science

Acknowledgments

Funding for this research was provided by the Copper Development Association and by the Army Research Laboratory. This work was completed with support by the Office of Naval Research, N00014-08-1-0080, ESRDC Consortium, and MIT Sea Grant College Program, NA06OAR4170019.

I would also like to thank the many people who contributed to this work through the use of facilities and equipment; help with machining, measurements, and testing; or guidance, advice, and encouragement along the way. First and foremost, it has been a privilege to learn from and work with Professor Jim Kirtley these past years. I was also fortunate to have Professor Jeff Lang and Dr. Tom Keim on my thesis committee. Still locally, I would like to thank Professor Chrys Chryssostomidis of the department of mechanical engineering and Director of the MIT Seagrant program for the opportunity to work on larger scale machines while wrapping up this thesis. Within the LEES laboratory, Professors Steve Leeb and Markus Zahn graciously lent the use of tools, software, and measurement equipment, Wayne Ryan helped with machining issues and rotor testing, and Vivian Mizuno tried to keep us all on track.

Many thanks to all of the cast copper rotor team, including John Cowie and Dale Peters from the Copper Development Association, Chuck Stark from ATI, Dan Seger and Dave Dunaway of Ramco Rotors, and Ken Young and Chris Rice of Vforge. Raj Rajmohan, Rich Schiferl, and Richard Budzynski from Rockwell Automation/Reliance Electric, now Baldor also provided invaluable advice, test rotors, and motor performance test results.

Additional thanks are due to Steve Nichols and Ray Roderick of Satcon Technology for the use of their dynamometer and measurement equipment.

Finally, I would like to thank my friends and family for there understanding, patience, and support along the way, especially my wife Bridget and mom Rosann for infinite editing help and who both suffered through some of the rotor testing.

Contents

List of Figures

List of Tables

Chapter 1

Introduction

This investigation began within a program developing copper rotor casting in an effort to explain why a number of different cast copper and aluminum five and ten horsepower induction motors performed differently than predicted, with lower than expected efficiency from increased stray load loss and variation between nominally identical machines. Calculations under-predicted stray load losses on both cast copper and cast aluminum rotors with skew. Inter-bar currents are a likely contributor to both the variation and additional losses measured on these machines. Traditional induction motor analysis assumes insulated rotor conductors. Inter-bar currents flowing between, instead of along, the rotor bars can alter the coupling between rotor and stator as well as the distribution of rotor current and loss. These cross currents between bars depend on the induced rotor voltage, bar impedance, rotor skew, and total impedance between bars which is often dominated by the bar-to-lamination contact resistance. The value of contact resistance can depend on the rotor geometry, material properties, and the casting process, varying both from one bar to the next on a given machine as well as between average values from motor to motor. Measurements will show significantly lower bar-to-core contact resistance for the cast copper compared to the cast aluminum machines. The design of the bar, or associated casting parameters, also appear to impact the contact resistance value. This thesis examines the ability of inter-bar currents to account for the differences between motor predictions and measured performance results as well as the variation in test results between

individual rotors.

Decreased efficiency due largely to increased full load stray loss was one significant rotor variation. Stray loss refers generally to any induction machine loss not accounted for by the standard calculations of primary copper loss, secondary copper (or slip) loss, core loss measured at no load, or friction and windage. Typically, stray load loss accounts for around two percent of the total input power of induction motors rated under fifty horsepower (37.3 kW), and several times this amount can be measured in extreme cases. Even these losses of a relatively small magnitude can be important both for the performance of individual machines as well as the aggregate power loss of the millions of electric motors in operation. Minimizing stray loss from inter-bar currents flowing circumferentially through the laminations between rotor conducting bars can slightly increase induction machine efficiency on skewed machines with imperfect bar insulation. Adjusting traditional induction machine equivalent circuit equations to account for total rotor bar and inter-bar losses can improve predicted values of stray loss. The adjusted calculations include the dependence of bar and inter-bar losses on bar-to-lamination contact resistance, rotor bar conductivity, and rotor bar skew. These approximate calculations allow improved, more general performance predictions as well as identification of means to increase machine efficiency by minimizing the stray loss due to inter-bar currents.

1.1 Motivation for Maximizing Efficiency

There are practical reasons beyond the interesting engineering challenge for attempting to wring out an additional percent or two from already efficient machines. An increase in efficiency of only a few percent can help to reach minimum required efficiency levels, to provide economic benefits to both motor manufacturers and owners, and to achieve significant net environmental benefits from avoided fossil fuel consumption.

With millions of motors in use, even small individual improvements can add up. Driving devices like pumps, belts, fans, and compressors, induction motors transform

significant amounts of energy in industrial and manufacturing applications as well as behind the scenes in refrigeration and building heating, ventilation, and air conditioning. Surveys of industrial, commercial, and residential electric motors in 1998 and 1999 estimated that around fifty percent of all of the electricity in the United States is consumed in electric motors.[1, 2] Similar figures have also been published for other industrialized nations.[3] The United States consumed almost 4.2 trillion megawatt hours of electric power in 2007 according to Department of Energy statistics, and the world wide estimate for 2007 is around 18 trillion kilowatt hours per year. More than two-thirds of this energy is produced by burning fossil fuels, primarily coal and natural gas.[4]

Governments and manufacturing organizations have recognized the potential benefits from small improvements in electric motor efficiency. The Energy Policy Act passed by the US Congress in 1992 set minimum required nominal full load efficiency levels for general purpose motors manufactured after October 24, 1997. The European Union likewise developed an electric motor classification scheme in 1999 to promote energy efficiency by specifying efficiency levels from the least efficient EFF3 to the most efficient EFF1. The National Electrical Manufacturers Association, NEMA, also publishes motor efficiency standards. Prior to the EPACT requirements, NEMA had classified "energy efficient" motors using similar minimum efficiency levels, ranging from 70% to 95.8% depending on motor size and type. NEMA has since established a "Premium Efficiency" designation for even higher efficiency motors ranging from 77% to 96.2% for 1 to 500 hp machines. The "Premium" labeling program is intended to help purchasers more easily identify high efficiency machines that can reduce power consumption, operating costs, and pollution from the avoided power generation.[5] With minimum motor efficiency standards required by governments or supported by manufacturing organizations, reducing stray loss can provide an alternative to completely redesigning an existing machine to achieve a small efficiency improvement.

Higher efficiency motors also provide a competitive edge among manufacturers and can be sold at higher prices for potentially greater profit. List prices for 10 hp motors available on line in 2007 varied with the frame size and the number of

poles (or motor speed) but generally ranged from around $700 to $1700. For these machines, an increase in motor efficiency of less than 3% corresponded to roughly a $300 increase in list price. With rising energy prices, the additional expense of higher efficiency machines can be more than offset by reduced operating costs. Increased efficiency can also potentially prolong a motor lifespan if the reduced loss results in a lower average operating temperature.

As environmental, political, and economic considerations fuel demand for ever higher efficiency machines, efficiency gains of only a few percent can be a significant improvement on an already good design, with the potential for substantial aggregate savings.

1.2 Stray Loss

For typical machine designs, about a percent or two of the total input power is attributed to "stray" losses, generally understood as the difference between input and output power not included in the fundamental frequency stator and rotor conductor losses, the no load iron loss, or the friction and windage loss. These losses range from 1.7% to 6.3% of the total input power (about 10% up to 27% of the total losses) on the 29 different cast 5 hp rotors measured as part of this project. Similarly, induction machine guru P.L. Alger found that typically, "[in practice] the stray-load loss may be between $\frac{1}{2}$ and 3 percent of the full-load input, or higher in poorly designed motors."[6] The 2004 IEEE 112 Standard Test Procedure for Polyphase Induction Motors and Generators lists values of stray-load loss to be assumed in common situations ranging from 1.8% percent of the rated load for machines less than 90 hp to 0.9% for 1851 hp and larger.[7]

Investigation into the source of stray losses have been ongoing ever since the earliest machines did not perform as well as expected. During the discussion of a 1932 Transactions of the American Institute of Electrical Engineering paper written by C.G. Veinott titled "Performance Calculations on Induction Motors," R.E. Hellmund, the then chief electrical engineer at the Westinghouse Electric and Manufacturing

Company, contributed the following statement:

> Those who designed induction motors many years ago and obtained at that time a rather close agreement between calculations and load tests undoubtedly wonder why new and improved calculation methods such as that presented by Mr. Veinott and others (see bibliography given in paper) should still be an active subject of discussion at Institute meetings. At the same time, it may be a surprise to many to learn that the discrepancy between the results obtained from load tests and those obtained by calculating methods from no-load values and other motor constants has been greater during recent years than it was, say, 20 to 25 years ago.

Hellmund then went on to discuss how the increased flux densities and ampere-turns required in motors of decreasing physical size for a given output can increase leakage flux and iron saturation, complicating performance calculations. Since then, material advancements in the laminations and insulations have contributed to the continued reduction in physical size of induction machines for any given power rating. Meanwhile, papers on both the measurement and calculation of "stray," neglected or misrepresented motor losses have continued to be published. More recently, a letter in the February 1997 issue of the IEE Power Engineering Journal, "Stray losses - a residue of ignorance" by Steve Williamson and another paper by C.N. Glew, "Stray load losses in induction motors; a challenge to academia," from the 1997 8th IEEE International Conference on Electrical Machines and Drives have addressed the continuing issue.

1.2.1 Stray Loss "Measurement"

Traditionally, fixed, assumed (and potentially too low) magnitudes have been assigned to stray loss regardless of the actual value because of the relatively small, second order impact and the difficulty in accurately calculating or measuring the loss. Typically, the reference values of stray loss from measured tests at any load point are not directly measured but rather determined by subtracting out all of the other calculable losses.

A testing facility with measurement equipment of sufficient precision to observe small changes in potentially large values of power, torque, and speed, as well as a consistent procedure are required to obtain repeatable results. Test equipment and available power must match the machine under test and may only be appropriate for a limited range of motor ratings. Any errors in alignment, measured temperature, input power, or output power can significantly impact determined values of stray load loss.

The 2004 IEEE 112 Standard Test Procedure for Polyphase Induction Motors and Generators "Efficiency Test Method B" is an input minus output power measurement including segregation of losses commonly used for determination of stray load loss. The stator copper losses can be calculated using the measured input current and the dc, room temperature, winding resistance adjusted to the winding temperature measured for the given operating point. The "friction and windage loss" can be determined by extrapolating the measured no load power loss with the stator copper loss removed, roughly a function of the square of the voltage, down to the zero applied voltage intercept. The "no load core loss" can be determined for full load voltage by subtracting out the stator copper and friction and windage losses from the measured total power loss. The rotor copper loss can be calculated as the slip times the input power minus the stator copper and no load core loss. Despite the well defined procedure, errors in measurement or calculation of the various loss components can impact the determined values of stray loss. A dynamometer correction factor accounts for any additional loss contributed by the dynamometer, showing up as a vertical offset on the otherwise measured stray loss. Curve fitting is also used to help eliminate error from the stray loss, assumed a function of the square of the load torque.

Temperature rise can also have a significant impact on conductivity and measured currents and losses. Values must be recorded quickly and temperatures accurately measured. Motors are often tested at reduced voltage to reduce the temperature rise, and the motor behavior must scale as expected with voltage in order for these measurements to accurately predict the full voltage operation. Thermocouples measure motor temperature on each phase of the stator both along the winding length

and at the end turns. There is the possibility of some difference in temperature between the rotor and stator, especially on non-steady-state measurements where the motor temperature is increasing. An increased rotor temperature decreases the rotor conductivity, increasing the rotor resistance.

The performance test results later used for comparison to calculations in this investigation were completed at a Rockwell/Reliance Electric, now Baldor, industrial motor testing facility. This dedicated testing facility has the personnel and measurement and test equipment for fast and reliable results. Five different cast aluminum rotors with no skew, and no expected loss or variation from inter-bar currents, measured extremely consistent stray losses, all within the range from 77 to 82 watts. Five skewed cast aluminum rotors, expected to show some variation in stray loss due to variation in contact resistance and inter-bar currents, still measured a reasonable spread in stray load loss from 151 to 180 W. The stray loss measurement procedure is consistent, repeatable, and capable of observing variations in stray loss and motor performance on five and ten horsepower motors.

1.2.2 Previous Stray Loss Investigations

Many different sources of stray loss have been identified and investigated over the past century. Some losses, like those from space harmonic rotor bar currents, can be relatively easily calculated and included in an extended equivalent circuit machine model. Certain losses, from sources like induced currents in motor housings and stator conductor eddy currents, have been identified, can be minimized through design considerations or using stranded conductors, and are minimally impacted by rotor variations. Many losses lack simple and generally applicable mathematical descriptions. Approximate formulas exist to estimate stator iron losses, but empirical correction factors are typically included. Losses from skew leakage flux or high frequency variations around the rotor surface and stator tooth tips are difficult to evaluate. The challenge with "stray loss" is to identify which of the many potential sources of stray loss apply for the given machine, with the goal of determining a generally applicable equation to calculate the loss and ultimately minimize the loss once the source and in-

fluencing factors are known. Stray loss dependent on the rotor are observed by testing and comparing different rotors inside the same stator and housing. This investigation focuses on stray loss from inter-bar currents, including both the conduction losses in the iron paths between bars as well as the accompanying harmonic currents in the rotor bars and end rings completing the current loops.

Loss from currents flowing through the iron laminations between skewed rotor bars, varying with the contact resistance between bars and laminations, is one generally accepted source of stray loss and discrepancy in test results between otherwise identical machines. New York University's S.S.L. Chang in 1954 classified stray losses according to their origin as either "theoretical imperfections" or "industrial imperfections," arising from either inadequate calculation methods or manufacturing issues. He asserted "the predominant cause of stray load loss due to manufacturing processes is the short circuiting of the rotor cage bars by the laminations. As these short-circuit paths effectively circumvent the rotor skew, a substantial amount of rotor harmonic current would be induced by the tooth harmonics."[8] As another investigation into this subject, this thesis focuses on stray loss resulting from inter-bar currents in an attempt to explain the differences in measured performance between nominally identical rotors and to improve motor performance predictions on a variety of five and ten horsepower cast copper and aluminum motors.

1.3 Inter-bar Current Losses

This present study would not exist without the solid foundation of previous investigations to build upon. A number of papers specifically examining inter-bar currents have been published since the 1930's.

Rossmaier wrote one of the earliest referenced papers on machine losses due to uninsulated rotor bars in a 1939 article published in Elektrotechnik und Maschinenbau.[9] This foundational paper derived the differential equation for rotor bar current as a function of position along the rotor length. The approach assumes sinusoidal variation around the rotor periphery and includes the continuous cross-path between

neighboring bars. Based on this initial work, Odok in 1958 added experimental measurements of inter-bar resistance and equations for harmonic rotor loss in the case of negligible end ring impedance. The losses from currents between neighboring bars were found to peak at a certain intermediate value of inter-bar resistance, decreasing as the resistance approached zero or as the bars became more perfectly isolated with zero cross currents.[10] In 1966 Weppler incorporated the inter-bar calculations into the equivalent circuit framework using a complex, real and reactive, skew factor to adjust the referred rotor resistance and reactance values to account for the inter-bar current paths.[11]

A series of more recent papers aimed at determining both numerical values of the inter-bar resistance for a particular rotor as well as the general impact of bar-to-bar currents on motor performance. Williamson and Smith in 2002 measured a reduced starting torque, found an increase in harmonic rotor losses, and derived a complex "inter-bar factor" to adjust each harmonic of the equivalent circuit, similar to the complex skew factor used by Weppler.[12]

Studies commonly used dc resistance measurements between neighboring bars to determine a value of bar-to-bar resistance on cast aluminum rotors. Willimason, Poh, and Smith in 2004 measured average bar-to-bar resistance values between neighboring bars on a set of 40 different rotors from 11 different machines, illustrating the increase in bar-to-iron contact resistance from quenching cast aluminum rotors.[13] Using a slightly different approach for determining bar-to-lamination contact resistance, Watterson, Prescott, Bradford, Lockwood, and Bagk considered currents traveling around the lamination iron, using measurement points on the same or opposite ends of bars with one and two intervening bars, instead of only between neighboring bars.[14] The general conclusions on stray losses from inter-bar currents have been consistent with Odok's predictions. Both increased or decreased contact resistance between the rotor bars and laminations can either raise or lower the stray losses depending on the machine design and value of average resistance between bars.

1.4 Thesis Contributions

The main contribution of this thesis is a transparent loss calculation to directly adjust equivalent circuit parameters to account for inter-bar currents. The new method checks against previous calculations after slight modifications to the earlier work and can be used with any equivalent circuit. The new approach still uses long and complicated equations, but the direct adjustments to equivalent circuit resistance and skew factor are simpler and more intuitive than using a complex skew factor. The new method also directly applies to a wider range of skewed equivalent circuits, and can be used on circuit models that divide the rotor skew equally between the rotor and stator. It is hoped that the new adjustments may find more widespread use in computer programs for motor performance calculations.

Average values of inter-bar resistance are necessary for calculations of rotor bar current and total rotor loss. Average values of contact and total inter-bar resistance from measurements on a number of both cast copper and cast aluminum rotors using several different slot shapes are also presented. The procedures and values are consistent with earlier efforts going back at least to the 1950's, but some adaptation is required for determining the lower contact resistance values of the cast copper rotors. Additional published data, especially for cast copper rotors, will be useful for estimating values of rotor loss.

The final comparison between calculations and measured test data is also useful for validating the new approach and examining the extent of the impact of inter-bar currents on stray load loss. This process has helped to identify equivalent circuit parameters impacting stray loss and inter-bar currents as well as additional potential sources of stray load loss that could be investigated in greater depth in future work.

1.5 Chapter Organization

This section presents a brief overview of the following chapters.

1.5.1 Chapter 2: Induction Machine Extended Equivalent Circuit

Realistic rotor bar and inter-bar loss calculations require a reasonably accurate model of the entire motor, including the interaction between the rotor and stator. The second chapter introduces the extended induction machine equivalent circuit, a common tool for approximate calculations of steady state behavior. This initial circuit model will later be used as the framework for the calculation of rotor bar and inter-bar currents and losses. Ultimately, the effective values of skew factor and rotor resistance will be adjusted in order to account for the impact of the rotor cross currents. The second chapter examines the traditional circuit model unmodified by inter-bar currents. The first sections define and present standard formulas of resistance and reactance terms before discussing the different methods often used to incorporate the impact of rotor skew into the circuit model. The variables with the greatest impact on the motor calculations in general and inter-bar loss calculations in particular are also highlighted.

This circuit model should be able to estimate motor behavior in the case of non-skewed machines without high end ring impedance or skewed machines with insulated rotor bars. Predictions of motor performance using this circuit model are compared to measured test results on a series of non-skewed, five horsepower cast aluminum induction motors. Modification of the equivalent circuit in order to account for skew in the ideal case of insulated rotor bars is also examined in detail since this factor will later change with the rotor current distribution in the presence of inter-bar currents.

1.5.2 Chapter 3: Inter-bar Loss Equations

The third chapter examines the calculations of bar and inter-bar rotor currents and losses. This chapter begins with a derivation updating, extending, and adapting to the circuit model the approach used by Odok with help from Kirtley to obtain the differential equation for rotor bar current including inter-bar paths. Alternate boundary conditions are also presented for arbitrary impedance end rings consistent with Subba Rao, Weppler, and Rossmaier.[15, 11, 9] The resulting solution for the

equation of rotor bar current and the calculated induced bar voltage are integrated along the rotor length to determine rotor loss along and between bars. Assuming linearity, the process can be repeated to include the impact of any number of higher order harmonics. The end ring losses are also added but are generally negligible except for the fundamental. Plots display the predicted change in stray loss from harmonic rotor bar and inter-bar currents with variation of bar-to-lamination contact resistance under the constraint of fixed stator current and rotor slip.

These equations for rotor current and loss are a function of the equivalent circuit parameters such as the mutual and leakage reactance values and the rotor impedance. The current and loss equations also require previously measured or otherwise calculated values of motor operating slip and input stator current. Incorporating the rotor loss equations into an equivalent circuit model will help to provide all of the required variables as well as more directly and accurately calculate losses when the inter-bar currents are significant enough to alter the motor operating current or slip. However, before an adjusted equivalent circuit can make predictions for any given machine, an average value of the impedance between bars must be determined.

1.5.3 Chapter 4: Determination of Resistance Between Bars

One of the critical parameters determining the value of inter-bar currents and loss is the impedance between neighboring bars per axial unit length. This study assumes the inter-bar impedance is primarily resistive and only dc current and voltage measurements were used. The total inter-bar resistance is a combination of contact resistance and the resistance of the lamination path between bars. Often, the bar-to-lamination contact resistance dominates the resistance between bars. All of the rotors examined can be grouped into one of two distinct categories of contact resistance, with different measurements and calculations effective for each type. Rotors with relatively high contact resistance can be measured directly, while lower contact resistance values require comparison between measured and simulated sets of voltage data. The fourth chapter presents the procedures used to determine the contact resistance values and the results for the five and ten horsepower rotors. The con-

tact resistance varies significantly from one bar to the next, but approximate average values are identified for use in rotor current and loss calculations.

1.5.4 Chapter 5: Equivalent Circuit Modification

This chapter presents the equations to modify the equivalent circuit effective skew factor and rotor resistance to account for inter-bar currents. The method is first verified theoretically by comparison to previous calculation methods by Weppler and by Williamson and Smith.[11, 12] Then experimental verification is provided by comparing the calculated motor loss and performance to measured test results. Variations between similar machines are examined. Comparison between calculations with and without inter-bar currents as well as the impact of variation in rotor skew, conductor conductivity, and bar-to-lamination contact resistance are presented.

1.5.5 Chapter 6: Conclusions and Suggestions for Future Work

The thesis ends with a discussion of the results, recommendations for reducing stray loss resulting from inter-bar currents, and suggestions for additional work that could help to improve future motor loss calculations.

Chapter 2

Induction Machine Extended Equivalent Circuit Model

Even though calculations of rotor bar and inter-bar loss focus on neighboring pairs of rotor bars, complete equations must be integrated into a larger machine model in order to account for the interaction between the rotor and stator. In addition to the rotor geometry and material properties, the bar-to-bar current and loss depend on the induced rotor voltage as a function of the stator current, rotor slip, and coupling between stator and rotor magnetic circuits. The extended induction machine per-phase equivalent circuit can provide the required reactance and input values for inter-bar loss calculations. Depending on the circuit parameters used, calculated harmonic rotor losses including inter-bar currents can range from unrealistically small to unrealistically high values. The entire system model must be reasonably accurate in order to correctly identify the impact of inter-bar currents.

Provided that the rotor end rings do not have unusually high impedance, inter-bar currents significantly impact only motors with skewed rotors and non-insulated conductors. Skew, a helical twisting of usually the cast rotor bars, is a common design attribute in smaller induction motors and one of the fundamental variables significantly impacting slot harmonic bar and inter-bar currents and loss. Intended to reduce noise, improve starting, and decrease pulsations and loss from the slot harmonics, the resultant harmonic loss from inter-bar currents can increase with

certain combinations of skew angle and inter-bar resistance. This chapter presents and discusses different possible modifications to the equivalent circuit to account for skew, all a function of the same traditional skew factor. In later chapters, adjustments to the equivalent circuit to account for inter-bar currents alter the traditional skew factor.

This chapter presents a common equivalent circuit machine model often used to predict motor performance. All circuit models are necessarily based on approximations and simplifications of the complicated machines they represent. One of the underlying assumptions behind the circuit model is perfect insulation of the rotor conductors restricting all currents to the rotor bars and end rings. After an overview of the induction machine equivalent circuit including an introduction to the most significant terms for calculating motor performance and inter-bar loss, calculations are compared to measured performance on rotors with no skew. Modifications are then made, particularly to the harmonic leakage reactance values, to improve the correlation between prediction and test.

2.1 Basic Induction Motor Equivalent Circuit

One of the most fundamental and widespread tools for examining induction machines is the equivalent circuit. The classic Steinmetz single phase equivalent circuit shown in Figure 2-1 is based on the transformer model and can be used for quick, rough analysis of induction machines.[16] The circuit includes winding resistance and leakage reactance terms for both the stationary stator, R_1 and X_1, and rotating rotor winding or conductor cage, R_2 and X_2, as well as a core resistance, R_c, to model losses in the iron laminations and a magnetizing reactance, X_m, representing the inductance and energy storage in the air gap of the machine. This circuit helps to define stray load loss as the component of loss not included in the circuit model or rotational losses. Rotational friction and windage loss is an exception, missing from the model originally applied to stationary transformers, but otherwise the stator and rotor I^2R losses and the iron loss, typically measured at no load, are all included. Values of the

equivalent circuit elements can be estimated through design calculations as a function of geometry and material properties or from measured locked rotor and no load motor tests. Equations for circuit terms often include empirical correction factors based on previous experience with similar machines already built and tested.

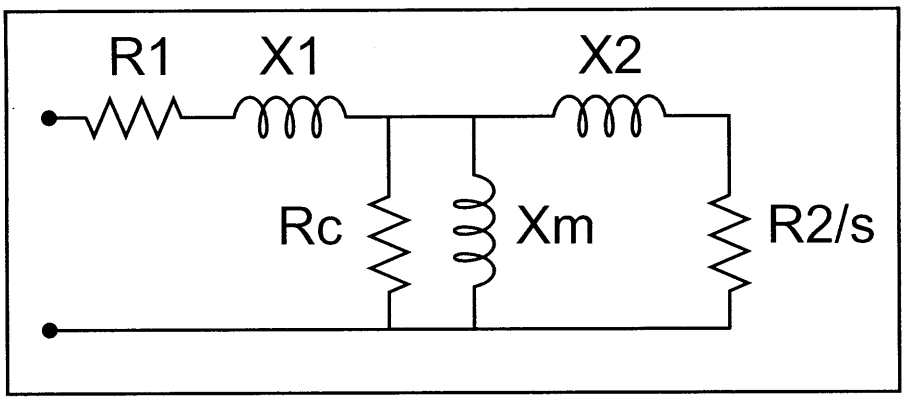

Figure 2-1: Induction motor equivalent circuit

The simple circuit represents most main aspects of motor behavior but cannot exactly model all of the attributes of induction machines over their full range of operation. The approximation omits elements required for more detailed analysis and the parameters that are included are not always fixed constants. The terms in the circuit vary with temperature, iron saturation, and frequency effects from no load to full load and locked rotor conditions. Partly due to these changing parameters dependent on the fields and currents in a machine, it can be difficult to accurately model and predict the performance of induction motors. Many different programs and formulas are used, generally based on an extended version of the equivalent circuit model. Additional elements can be added, and the values can be adjusted to include the effects of rotor skew, iron saturation, and changing impedance with frequency, especially at start up or locked rotor.

2.2 Extended Equivalent Circuit

The basic circuit can be extended as shown in Figure 2-2 to try to account for harmonic torques and losses by including any number of additional sets of series elements

representing the n^{th} order stator winding space harmonic.[6] All calculations in this study, with or without inter-bar currents, assume perfectly sinusoidal stator input voltage and current. Time harmonics from distorted input at low loads or inverter fed machines are not considered in this work, but could be similarly calculated if they are approximately independent of the fundamental, space harmonics, and other time harmonics. Any mention of harmonics hereafter refers to "space" harmonics. These higher order fields arise from the pulsed and stepped distortions of the spacial distribution of the stator winding coils in discrete slots, despite the assumed perfectly sinusoidal stator current. The harmonic fields can induce harmonic rotor bar currents, translated to higher frequencies by the motion of the rotor. The rotor frequencies depend on the harmonic values of slip, and resulting in variation of the harmonic rotor impedance values with frequency, analogous to the rotor fundamental with the varied fundamental slip frequency.

The new parameters of the extended equivalent circuit for the higher order harmonics are not directly measurable but determined from design calculations. As with the fundamental circuit elements, these harmonic additions will also vary with rotor skew, iron saturation, and frequency. Alger defines stray load loss, absent from the basic circuit model, as "additional core and eddy-current losses caused by the increase in air-gap leakage fluxes with load and by the high-frequency pulsations of these fluxes." He continues "a large part of the stray-load loss is due to induced harmonic currents in the secondary winding, which can be calculated by the extended equivalent circuit."[6]

Odok uses the same equivalent circuit to investigate stray losses in machines with insulated rotor bars.[17] Although less clear from the per rotor bar notation in his condensed AIEE paper, Odok's approach to calculating rotor loss is consistent with equivalent circuit analysis. His equations for rotor loss require values of stator current, rotor slip, and a number of unmeasurable reactance values, all calculable as part of an extended equivalent circuit.

The extended equivalent circuit, even corrected for rotor skew and including inter-bar current losses, still cannot account for all stray load losses. More complicated

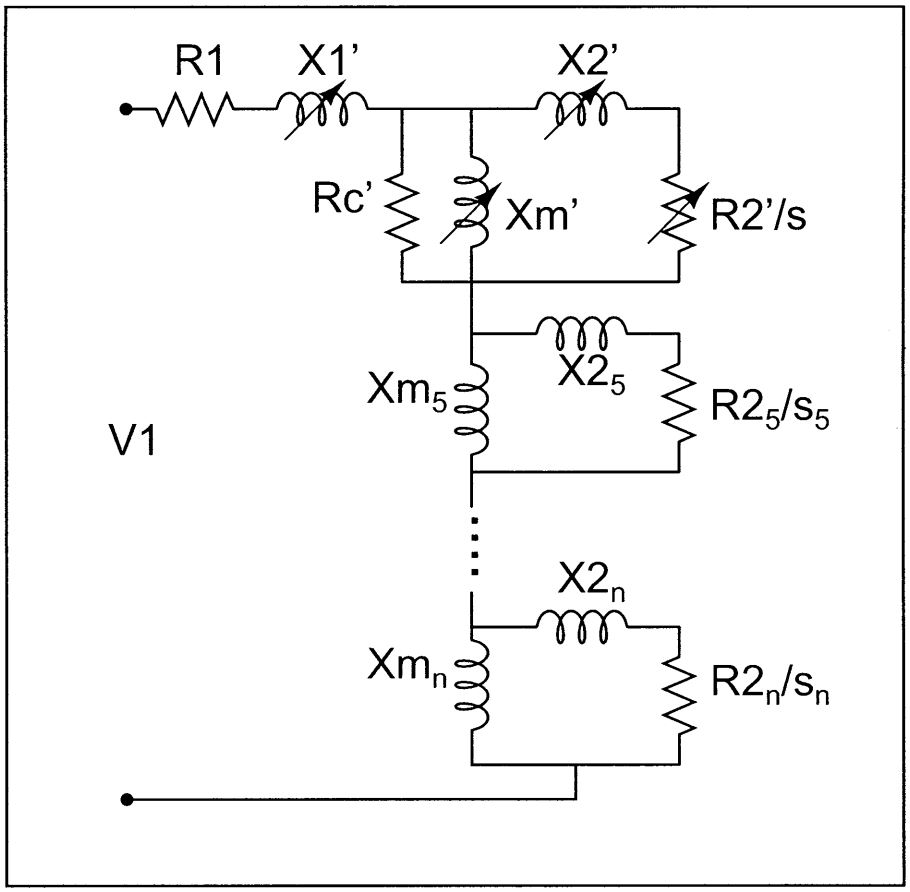

Figure 2-2: Extended induction motor equivalent circuit

circuits including terms to account for permeance harmonics and other losses are possible, but the additional effort may still fail to accurately represent a machine.[6]

Equivalent circuit calculations can incorporate adjustments to account for frequency effects in bar and end ring impedance and rotor bar skew. Fundamental and harmonic rotor bar currents and losses are included and adjustments for inter-bar currents and loss will be added. However, the stator teeth and tooth tips, rotor surface, and rotor teeth are additional sites of potential loss not usually included in the extended equivalent circuit or investigated here.

The equivalent circuit is a tool used to approximate motor behavior. The goal is to improve the approximation in later chapters to apply more generally to all rotors, including those with skewed, non-insulated bars, by adjusting terms to incorporate the impact of inter-bar currents. However, inter-bar currents are only one of many

possible sources of stray load loss. The total stray load loss from measured tests provides only an upper limit on the calculated losses due to harmonic bar and inter-bar currents. The extended equivalent circuit may still not account for other significant sources of stray loss and as a result fail to accurately estimate all aspects of motor performance. Nevertheless, especially on these smaller-sized, five and ten horsepower machines, where conduction losses are more significant than iron losses, the harmonic bar and inter-bar currents are expected to be the most significant source of stray loss. Improved calculations of these losses should help equivalent circuit motor performance prediction to better match measured test results.

2.2.1 Resistance Calculations

Terms of dc resistance are calculable using the total conductor length, area, and conductivity. The dc stator winding resistance can also be measured directly and the estimated length of the winding end turns adjusted to minimize any error. The equivalent rotor bar resistance is usually increased to account for the end ring losses, assuming a sinusoidal rotor current distribution.[6] Some uncertainty remains as to the exact value of rotor conductivity after casting, but there is a fixed upper limit. The impact of operating temperature on conductivity must also be considered, as well as frequency effects on the rotor bars with changes in the slip frequency. These two factors can significantly increase rotor resistance values.

The core resistance term can be approximated using power loss density curves from the lamination manufacturer along with calculated values of mass and peak magnetic flux density for the motor teeth and back iron. This calculated value is typically low by about a factor of two.[18] The large core resistance value usually has minimal impact on overall motor performance and the calculated loss can be checked against test values of no load core loss. The combined values of no load core loss and friction and windage loss can appreciably impact the value of stray load loss from test results. Overall, the resistance terms are generally simpler to determine and check than the reactance values.

2.2.2 Reactance calculations

The reactance terms are the most difficult equivalent circuit parameters to calculate. These mutual and leakage inductances represent portions of the machine net magnetic field linking all or part of one or both of the motor windings. The complicated machine geometries, rotation of the rotor and fields, and material properties that change with temperature and magnetic flux density make exact calculations unrealistic in many cases. However, the equivalent circuit's goal is to quickly provide approximations, and many people have worked on proposing, evaluating, and refining useful reactance equations over the past century. A number of equations exist for calculating machine reactance values. As these values govern the voltages induced in the rotor, they are essential for accurately calculating rotor bar and inter-bar currents and losses. Any reactance equations can be substituted into the general calculations for rotor current and total rotor loss. Typical reactance calculations used in later rotor calculations are presented here.

The air gap or magnetizing reactance can be approximated as the measured voltage divided by the input current from no load test points taken at varying input voltage or calculated for the n^{th} stator space harmonic on a non-skewed motor using the following equation.

$$X_{ag(n)} = \frac{2\,q\,\omega\,\mu_0\,N_a^2\,k_{wn}^2\,R\,L}{\pi\,(n\,P)^2\,G} \tag{2.1}$$

In this equation q is the number of phases, ω is the stator electrical frequency, μ_0 is the permeability of free space, N_a is the number of stator turns per phase, k_{wn} is the total winding factor for the n^{th} harmonic, R is the rotor radius, L is the stack length, nP is the number of harmonic pole pairs, and G is the equivalent air gap length. The fundamental magnetizing reactance is typically a relatively large value that can be reasonably well approximated. This equation seems to be universally accepted. The effective air gap, G, is larger than the physical gap by a proportion calculable using the Carter coefficient to account for slotted, non-smooth stator and rotor air gap surfaces.

The air gap reactance equation assumes infinite lamination permeability, but a

"saturation factor" less than one is often included in the denominator, in part to account for the actual lamination permeability.[19, 20] The reactive power stored and the mmf "absorbed" by the laminations in the motor reduce the effective magnetizing inductance, similar to a physically lengthened air gap. To adjust for this non-ideal lamination behavior, Kirtley includes an additional core reactance in parallel with the magnetizing reactance and core resistance. The core reactance can be calculated similarly to the core resistance, using lamination manufacturer rms volt-amp exciting power and real power loss density data along with calculated motor flux density and mass for the motor teeth and back iron.[21]

There are many possible ways to breakdown and calculate leakage reactance values resulting from the flux not completely linking both windings. All calculations provide only rough estimates. Veinott is one author who presents equations of leakage reactance components useful for motor performance predictions. He also describes how a detailed study showed his equation for end turn leakage reactance to calculate values lower than measured.[20] Still, when combined with the rest of his design calculations, the results closely match measured test results. Some complimentary error in another component of the total reactance value seemed to regularly account for the incorrect end turn reactance. There is not always a unique solution to match measured tests results, and it can sometimes be difficult to differentiate between a complete, theoretically sound solution and a combination of canceling errors.

The fundamental leakage reactance includes both stator and rotor terms. The calculated fundamental stator leakage reactance includes components of slot, end turn, and potentially a component of skew leakage reactance, depending on how the rotor skew is included in the circuit model. The fundamental and all higher order rotor leakage reactance values are calculated as the combination of slot, skew, and rotor zigzag leakage reactance. The next section examines the rotor skew and skew leakage reactance in detail. The fundamental and harmonic rotor slot leakage reactance are determined together with the rotor resistance as both change with slip frequency using a calculation routine developed by J. L. Kirtley, Jr. that breaks the bars into thin slices and builds up the total impedance for any given frequency, conductivity, and bar

shape.[22] This method is similar to a circuit approach used by Babb and Williams in their 1951 AIEE paper on the calculation of ac bar impedance.[23] The rotor impedance is the only parameter adjusted with slip in this version of the equivalent circuit model.

Alger gives the following "very rough" approximation for stator end turn leakage reactance.[6] The uncertainty in coil end leakage gives some leeway for small adjustments to the total stator leakage reactance.

$$X_e = \frac{7\, f\, q\, N_a^2\, D}{P^2\, 10^6}(p - 0.3) \tag{2.2}$$

In this end leakage equation f is the stator electrical frequency, q the number of phases, N_a the number of series turns per phase, D the air gap diameter in meters, P the number of pole pairs, and p the winding pitch expressed as the ratio of the coil span to the pole pitch.

The zigzag leakage deserves particular attention because of its importance in determining the harmonic bar and inter-bar rotor losses. The following equation from Kirtley calculates rotor zigzag leakage reactance.[21]

$$X_{2z(n)} = X_{ag(n)}\,(n\,P)^2 \left(\frac{1}{(N_R + n\,P)^2} + \frac{1}{(N_R - n\,P)^2} \right) \tag{2.3}$$

$X_{ag(n)}$ is the n^{th} harmonic air gap reactance, P the pole pairs, and N_R the number of rotor bars. This equation can account for some of the interaction between the number of stator slots (through the slot harmonic numbers for n) and the number of rotor bars.

An alternative approach uses the more broadly encompassing harmonic or differential leakage reactance instead of the zigzag leakage. Liwschitz-Garrick defines the differential leakage as the reactance accounting for the difference between the fundamental and the total machine flux.[19] The components of differential leakage reactance are built up using infinite series for each harmonic of interest to try to account for the large number of interacting fields. Odok also includes a value of differential leakage in place of the zigzag leakage terms used here. Both Liwschitz-

Garrick and Odok use the next equation to calculate values of differential leakage reactance, roughly equivalent to the zigzag leakage reactance calculated using (2.3), especially for the higher order harmonics.[17, 19]

$$X_{2d(n)} = X_{ag(n)} \left[\left(\frac{\left(\frac{\pi n P}{N_r}\right)^2}{\sin^2\left(\frac{\pi n P}{N_r}\right) K_{sk}^2} - 1 \right) \right] \tag{2.4}$$

The two equations for zigzag and differential leakage generally give similar results and are each used by different authors to combine with rotor slot leakage to calculate the total harmonic rotor leakage reactance.[6, 19] The harmonic rotor leakage reactance, however calculated, together with the harmonic magnetizing reactance are two of the key terms determining the magnitude of the harmonic rotor bar and inter-bar losses. Calculated values of rotor bar and inter-bar loss depend on the reactance, but the approach and general rotor equations can be used with any reactance equations. The difficulties in calculating the measured performance on the non-skewed aluminum rotor in Section 2.3, with insignificant inter-bar currents, suggest that neither of these similar reactance equations are ideal for all cases. Determining equations for equivalent circuit parameters applicable to a wide range of machines and operating points continues to be a significant challenge.

All later calculations use the zigzag reactance equation because calculations using the differential leakage reactance appear to underestimate measured stray loss. The zigzag reactance does not increase as fast as the differential leakage reactance, allowing increased second order slot harmonic loss. However, the corrections to rotor bar and inter-bar currents can be applied independent of the specific equations used to determine the equivalent circuit parameters in order to include the impact of inter-bar losses and more accurately predict motor performance.

2.2.3 Determination of Parameters from Tests

The basic equivalent circuit parameters for the fundamental motor circuit can be approximated from measured tests. The stator resistance is the only value directly

measurable. Determination of total impedance from the applied voltage and current under locked rotor conditions gives roughly the sum of the rotor and stator resistance and reactance. The rotor resistance can be solved by subtracting out the measured stator resistance, adjusted to the measured operating temperature, and the reactance can be split between stator and rotor. The values of rotor resistance and reactance are measured at the full stator input frequency during the locked rotor test, and the rotor resistance may be substantially higher and the rotor reactance lower than under full load at slip frequency. The distribution of magnetic fields in the motor can also vary substantially from no load to full load and locked rotor. At locked rotor, the magnetic flux density concentrates around the air gap. The higher flux densities can alter the permeability of sections of the laminations, potentially saturating leakage reactance paths, and further reducing the reactance measured at locked rotor compared to normal, full load operation. The magnetizing reactance and core resistance can be estimated from no load tests. Impedance values for the higher order harmonics are more difficult to measure so are typically calculated from the design equations previously discussed.

2.3 Equivalent Circuit Calculations with No Skew

A set of four cast aluminum, five horsepower rotors are the only available test samples with no skew. These rotors are more easily calculable since inter-bar currents are typically insignificant on non-skewed rotors. Low enough bar and end ring resistance values provide a low impedance path to effectively short circuit any voltage between bars. The non-skewed aluminum rotors measured roughly half of the full load stray loss of the skewed counterparts, at about 80 versus 160 W. The skew was the only parameter intentionally changed and all rotors were tested within the same stator.

Equivalent circuit parameters are determined by test results whenever possible. Both the rotor and stator conductivity are adjusted to the measured temperature at each point. Measured torque, speed, current, input power, and stator winding temperature are used for comparing measured motor performance to calculations. The

dc stator winding resistance as well as the measured locked rotor impedance are also checked against design calculations and used to set equivalent circuit parameters. No load current-voltage curves provide an upper limit on the calculated magnetizing reactance. No load voltage and power measurements are also used to determine friction and windage loss by extrapolating the power at the two lowest voltage measurements to zero voltage, using a quadratic approximation for the voltage curve.

The five horsepower pump motors examined here are designed to run submerged in water. When tested in air at full voltage, they heat up dangerously fast. The conductivities at each point of the torque speed curve use the temperature value recorded with each measurement point. Due to the potentially extreme temperature rise, most of the low speed torque measurements were taken using one half of the rated voltage. The measured torques for these points have been multiplied by a factor of four for comparison and plotting with the full voltage low slip points. In two instances, the scaled torques were indistinguishable between similar rotors tested at both full and half voltage. Still, it is possible that the reduced voltage measurements could miss certain effects or not always be exactly representative of the full voltage values.

Temperature corrections to conductivity are made at each point and have a significant impact, much greater than frequency, on the rotor (and stator) resistance values. The torque speed curves can be inconsistent between the high and low slip regions, since high slip points were taken at half the rated voltage to limit currents and reduce temperature rise.

Equivalent circuit calculations at varied load points are compared to measured torque speed curves first for the non-skewed, five horsepower, cast aluminum rotors. The measured speed and temperature are used in the circuits for each operating point. Figure 2-3 compares the measured torque speed curve to an initial calculation using the equivalent circuit.

The stars show the measured torque-speed points while the solid line gives the equivalent circuit prediction. Typical error in measured torque is less than a tenth of a newton-meter. The dashed line shows the equivalent circuit calculation for funda-

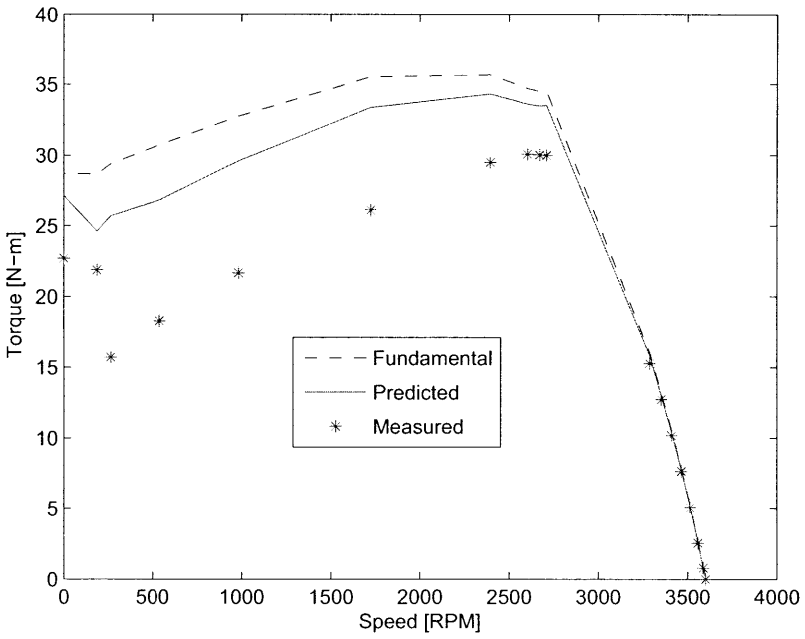

Figure 2-3: Non-skewed aluminum equivalent circuit approximation

mental torque. The initial calculation underestimates stray loss and fails to reproduce the dip in torque. The dip in the measured torque at the high slip points suggests that there are significant stator slot harmonics influencing the torque speed curve and stray load loss. These losses depend strongly on the values of harmonic magnetizing and leakage reactance. Reduced magnetizing reactance decreases the induced harmonic rotor voltage and current, moving towards the extreme case of eliminating the harmonic rotor currents by providing a parallel short circuit path. Increased harmonic leakage reactance reduces the harmonic rotor current for a given induced voltage, moving towards eliminating the harmonic currents and losses by effectively open circuiting the high impedance harmonic rotor branch.

Minor adjustments have slightly reduced rotor bar conductivity, calibrated core resistance and reactance, set the correct value of friction and windage, and increased the stator end turn leakage reactance to better align the measured and calculated curves.

Adding a correction factor to decrease the harmonic leakage reactance, or equivalently, to increase the harmonic magnetizing reactance, or a combination of both,

increases the calculated stray load loss. The adjustment increases stray load loss in the rotor bars from induced high frequency stator slot harmonic currents and exaggerates the torque dip at high slip, as shown in Figure 2-4. Again, the stars show the same measured torque-speed points, with an error of about 0.1 newton-meter, while the solid line gives the equivalent circuit prediction, now including a correction factor to reduce the harmonic leakage reactance. The dashed line shows the equivalent circuit calculation for fundamental torque.

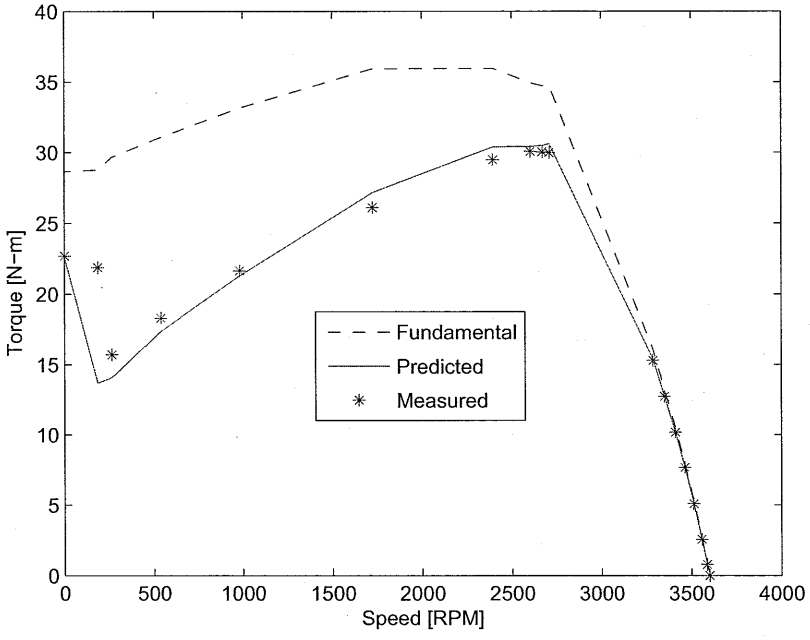

Figure 2-4: Equivalent circuit approximation with altered leakage reactance

The adjusted harmonic reactance value is not the only possible solution to improve the match between measured and calculated motor performance. A core loss varying with slip and significantly increasing towards locked rotor or an unsymmetrical ratio between the reactance values for two counter-rotating slot harmonics are two alternative adjustments to the equivalent circuit that could also improve the correlation between measured and predicted values of torque and loss. The slot harmonic leakage reactance is the value most likely to require correction, because significant increase in the magnetizing reactance can increase the total motor reactance and the altered core loss reduces the fundamental rotor losses more than seems consistent with measured

tests. However, in general, with skewed machines, some combination of decreased harmonic leakage reactance, slightly increased magnetizing reactance, and the addition of a load and skew dependent iron lamination loss seem to be necessary along with the inter-bar adjustments for matching calculated and measured test results.

Adjusting the rotor conductivity to 91% of the ideal, 100% IACS value and adding a 0.08 correction factor to largely eliminate the harmonic zigzag or differential leakage reactance terms generates a qualitatively good fit between calculated and measured performance for the non-skewed aluminum rotor. The fundamental magnetizing reactance used was 180 ohms and the fundamental leakage reactance terms were arbitrarily set to match the locked rotor conditions. The change in conductivity is not unreasonable considering the potential for conductor voids and impurities during the casting process.

The predicted torque for the low slip points around the machine operating region is easier to match and agrees fairly well with measured test results for most of the examined machines. However, it is possible to closely match the measured torque and still have a poor representation of the actual motor from difference between other measurements and calculated predictions of total input real or reactive power or current, for example. Total equivalent impedance, efficiency, power factor, and losses are also useful values for comparison between calculations and tests. The calculated stray loss from harmonic bar currents is only 21 watts without the reactance correction factor compared to 91 watts with the adjustment and about 82 watts measured. A comparison of the calculated and measured stray losses for a range of load points is given in Table 2.1. The approximate error in measured stray loss in this case is about ten percent of the measured value. This is roughly equal to the measured spread of about eight watts in the values of full-load stray loss for the non-skewed rotors. The un-adjusted calculations significantly underestimate both stray load loss in the operating region and the torque dip approaching locked rotor in Figure 2-3. Including the reduced harmonic leakage reactance results in a much closer approximation for both stray load loss and torque.

Inter-bar currents are not yet a factor in this non-skewed case with low conductiv-

ity end rings. However, the traditional reactance equations still seem to require some adjustment, especially for the stator slot order harmonics which have the greatest impact on both stray load loss and harmonic torques in this case, in order to bring equivalent circuit calculations closer to measured test results. The slot harmonic reactance values will similarly impact the calculated rotor losses in the skewed rotor cases discussed in Chapter 3, complicated there by the presence of inter-bar currents.

Table 2.1: Comparison of stray load loss cast aluminum no skew

Load	Calculated No Adjustment	Adjusted Harmonic Leakage	Measured
25%	3	12	5
50%	6	28	20
75%	12	54	45
100%	21	91	79
110%	32	142	123
125%	48	210	178

Besides the stray losses, the full load prediction remains nearly unaltered. There is a more significant difference in torque, current, input power, efficiency, and power factor at locked rotor and high slip, favoring the circuit with adjusted reactance values.

The three plots below, Figures 2-5, 2-6, and 2-7, illustrate the impact of varying the rotor conductivity, harmonic leakage reactance, and magnetizing reactance. Excellent agreement is possible on the steep slope, at high speed and low slip around the normal motor operating points. Matching the measured test results becomes more difficult at the peak torque and especially at locked rotor and in the region of low speed, high slip. The expected error in measured torque for these plots is again less than a tenth of a newton-meter.

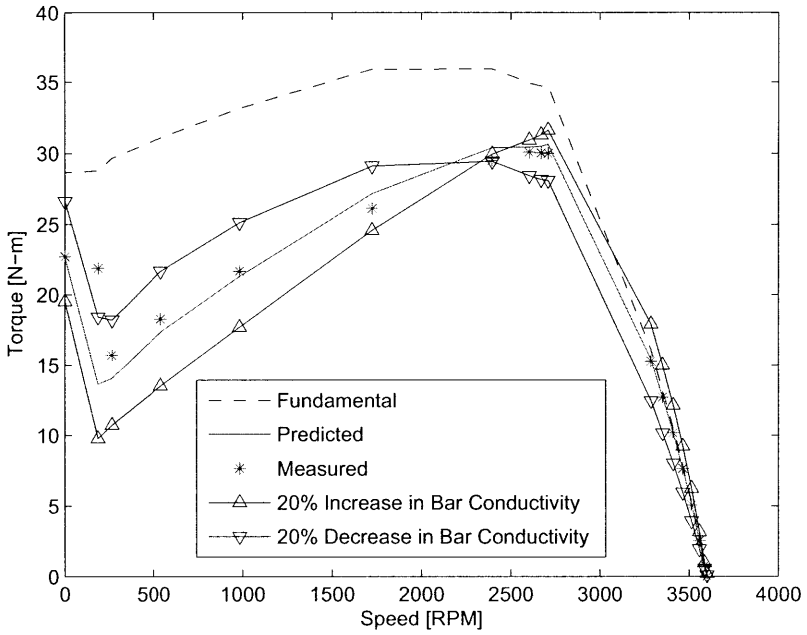

Figure 2-5: Equivalent circuit predicted and measured torque-speed curve - varied rotor resistance

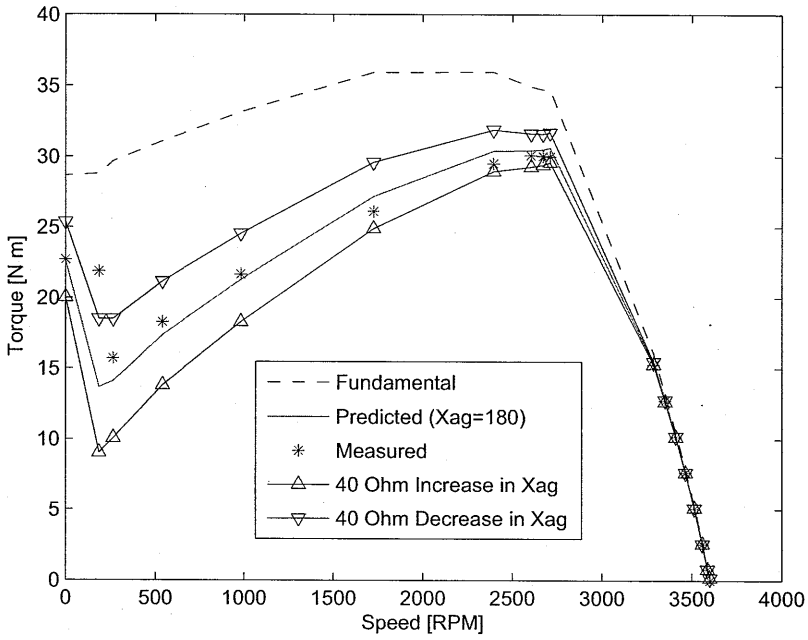

Figure 2-6: Equivalent circuit predicted and measured torque-speed curve - varied magnetizing reactance

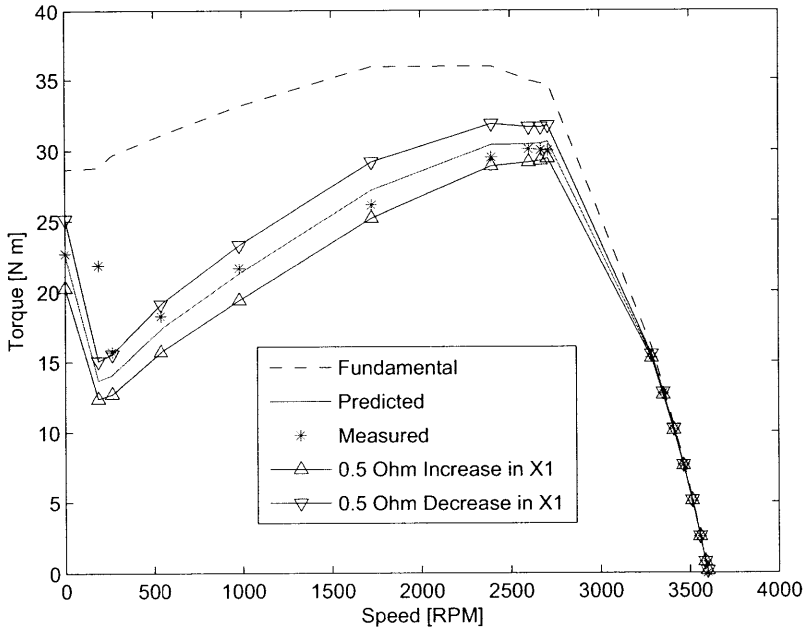

Figure 2-7: Equivalent circuit predicted and measured torque-speed curve - varied leakage reactance by about 25%

2.4 Rotor Bar Skew

At least as of 1970, "the majority of induction motors have skewed slots, most commonly on the rotor, but sometimes on the stator; and, with small machines, skewing is virtually the rule."[24] Conversely, another perspective from 1974 held a different view.

> It is well known that harmonics give rise to important losses, particularly when the rotor insulation is not perfect. In this case, it is not possible to reduce the harmonic currents by means of an appropriate skew. This explains why most manufacturers forgo the rotor skew.[25]

Experience with skew on the motors of this study has been equally confusing, and these two authors may both be correct in talking about different classes of machines. The second quote also mentions how skew fails to reduce harmonic losses when inter-

bar currents are present. New equations to calculate this long observed effect are presented in Chapter 5 to adjust the effective skew factor.

Rotor skew is an important variable in the calculation of inter-bar currents and losses. This section examines how variations in rotor skew impact insulated rotor equivalent circuit models without inter-bar currents.

2.4.1 Theoretical Impact of Skew

Skew is a common design and manufacturing variable interlinked with stray losses. Rotor bars are skewed, twisted from one end to the other, in order to reduce loss, torque, and noise from slot permeance and mmf effects.[26, 18] Interaction between the discrete stator teeth and rotor bars can result in cogging, current and torque pulsations, and losses in both the rotor bars and iron laminations from the high frequency variations in fields and currents. Skewing the rotor bars, typically through the angle between adjacent stator slots, creates a relative phase change along the length of the rotating bar, with each bar section opposite a slightly shifted air gap flux. This helps to smooth out the fluctuations in induced rotor harmonic currents caused by the bars alternately passing through regions of high flux density directly below stator teeth to regions of low flux density opposite stator slot openings.

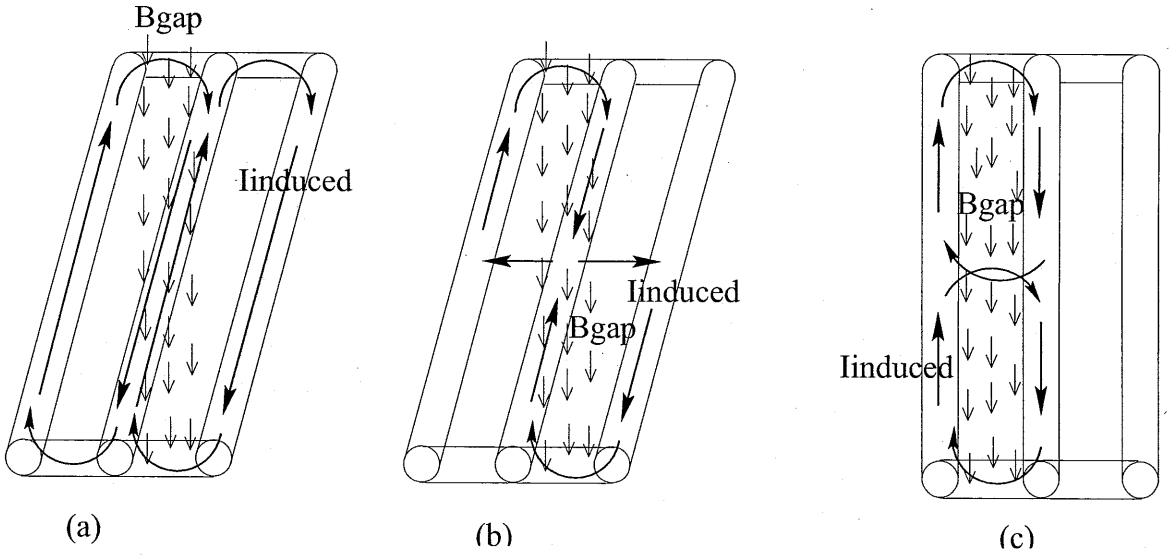

Figure 2-8: Cartoon explanation of skew and inter-bar currents

As shown in the cartoon of Figure 2-8(a) for the case of skewed, insulated bars, the currents induced by the locally increased flux density cancel out in the center bar. The currents of the outside bars would similarly cancel with the induced currents from neighboring tooth fields. Alternatively, if the neighboring poles of oppositely directed harmonic flux were also included, the net flux linked by the skewed loop of any two neighboring bars is roughly zero. Imperfect insulation between the rotor bars and laminations creates additional current paths through the iron between bars. With currents no longer restricted to the bars and end rings, any region of changing flux density between bars can induce currents in local loops formed, for example, by neighboring pairs of bar halves, as in Figure 2-8(b), with increased stray loss due to the currents now flowing along parts of the bars and through the iron laminations between bars.

With non-skewed rotor bars, the typically much lower impedance path through the sections of bar and end rings short circuit the inter-bar path. Plus, any cross currents through the iron would also tend to largely cancel each other out as in Figure 2-8(c). In a real machine, any inter-bar currents distribute along the full length of the bars, and the rotor bars carry a combination of fundamental and harmonic field currents. Furthermore, components of the air gap magnetic flux density tangential to the rotor surface from the combined stator and rotor leakage flux complicate the picture of slot flux radially directed and conveniently aligned with the stator teeth and slot openings.

Ignoring the discretization effect of slots and bars, skew introduces a relative phase shift, varying with position along the motor stack length, between the ideally sinusoidal stator and rotor current distributions. Since the resultant air gap magnetic field is a function of both rotor and stator currents, the phase shift with skew results in an air gap field varying along the rotor length, strengthened at one end and reduced at the other for the fundamental.[27] Neglecting the slight increase in skewed rotor or stator resistance from the slightly increased length and reduced area of the angled conductors, the air gap field, motor loss, and performance are theoretically identical when applying equal (and opposite) skew to either rotor or stator conductors or any equivalent combination to both.

Motor symmetry also requires ideally equal impact from either a positive or negative skew angle. Flipping the axial orientation of a uniform rotor, inside a uniform stator will have no impact on the motor's performance. Linked flux and induced voltage are identical whether the rotor or stator are skewed a positive or negative given skew angle.

In addition to smoothing out the slot harmonics, skewing the rotor also slightly reduces the coupling between stator and rotor and marginally increases the length and decreases the area of the rotor bars, adding an additional leakage reactance component and slightly increasing the rotor resistance.[24, 6] Apart from skew, different combinations and larger numbers of stator slots and rotor bars, magnetic slot wedges, and controlled starting can help to minimize the impact of slot effects; so typically in practice, smaller machines are often skewed while larger motors and generators, with more design flexibility and more difficulty in skewing fabricated rotor bars, are straight.[18]

However, even with smaller machines, there does not seem to be universal consensus on the benefits of skew, firm rules on optimal skew angles, or one generally accepted method to model the effects of skew. Butler and Birch in 1971 published a paper discussing the reasons for skewing rotors and examining five different ways that authors have modified induction motor equivalent circuits to account for the effects of skew.[28] With and even without inter-bar currents, the net result of skewing the rotor bars can vary between seemingly identical machines. The sometimes puzzling results from rotors tested in this study can be explained by both variations in the average resistance between bars as well as variations in the manufactured angle of skew. Confusion can easily arise over what angle defines the rotor skew, and even with agreement on the designed skew angle, skewing a stack of rotor lamination exactly a desired amount can still be a challenge. The resultant bar skew as manufactured may only be visible from any shifting in the lamination keyway of closed slot rotors, and accurate measurements of the skew angle as cast are difficult even with visibly skewed bars. Designed or unintended variations in skew between otherwise identical machines impact measured motor performance, peak torque, and stray load loss.

A number of different adjustments to the equivalent circuit are possible to try and predict the impact of skew on the motor performance.

2.4.2 Impact of Skew on Equivalent Circuit

The standard induction machine equivalent circuit can be modified to more accurately model a skewed rotor motor. The reduction in magnetic coupling and corresponding increase in leakage reactance due to rotor skew are universally calculated using an established skew factor. However there is no single accepted method on how to apply the skew factor to adjust the equivalent circuit. The two different circuit models most commonly used are shown in Figures 2-9 and 2-10. These two circuits are functionally equivalent, and can be used interchangeably to calculate identical total motor impedance, losses, and performance. The circuits can be derived from the original equivalent circuit by applying skew to either the rotor for Figure 2-9 or splitting the skew equally (and oppositely) between the rotor and stator for Figure 2-10. Butler and Birch include a derivation of the circuit in Figure 2-9 in their paper examining different equivalent circuits used to include the impact of skew.[28] Both Vienott in his 1959 book, *Theory and design of small induction motors* and the Appendix of the 1954 AIEE paper "Speed-Torque Calculations for Induction Motors with Part Windings" by Alger, Ku, and Pan include derivations of the circuit with equally divided skew shown in Figure 2-9.[20, 29]

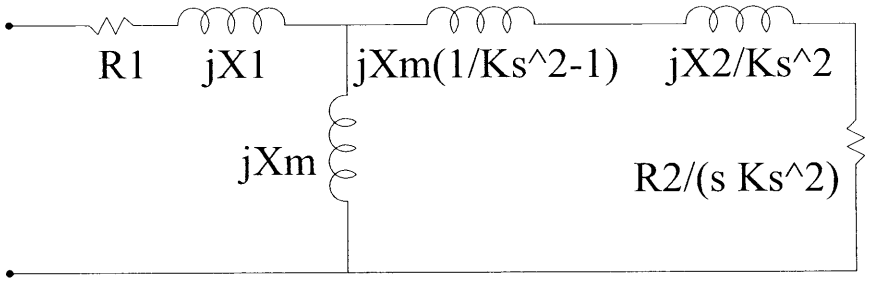

Figure 2-9: Equivalent circuit adjusted to include a skewed rotor

The circuit component values are different in the two cases because of the altered winding and referral factors. The skew factor is an additional winding factor that must be accounted for on either the rotor or stator winding or both when referring

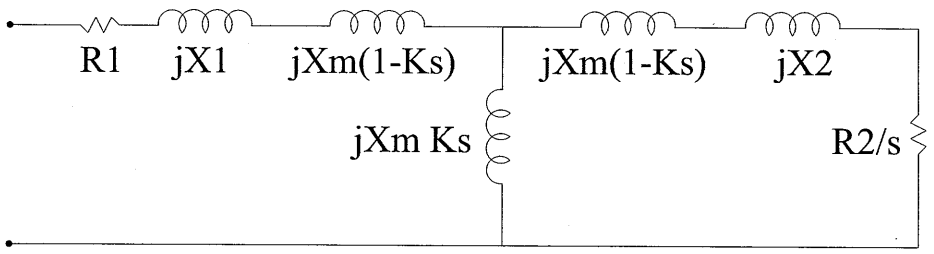

Figure 2-10: Equivalent circuit adjusted with equal and opposite skew split between rotor and stator

the per-bar rotor component values to the stator winding. With equally split skew, the two factors cancel out and the commonly used referral factor with the rotor cage winding factor equal to unity, $k_2 = 1$, can be used.

$$\left(\frac{q_1(N_1k_1)^2}{q_2(N_2k_2)^2}\right) = \left(\frac{3(N_ak_w)^2}{N_r 0.5^2 1^2}\right) = \frac{12N_a^2k_w^2}{N_r} \tag{2.5}$$

In (2.5), q gives the number of phase for either the stator or rotor, depending on the subscript; N is the number of turns per phase except N_r is the number of rotor bars; and k is the total winding factor. With a fully skewed rotor, the rotor winding factor equals the total skew factor, and the effective turns ratio and impedance referral factor must be increased accordingly.

Additional combinations could differently divide the skew between the rotor and stator conductors to create new alternative equivalent circuit models. Two of the most useful and popular circuit models have already been presented in Figures 2-9 and 2-10. The split skew model eliminates the skew factor from the referral ratio. The skewed rotor includes the additional leakage reactance from skew only in the rotor branch. At the opposite extreme, one alternative circuit skews only the stator conductors. This results in the circuit model given in Figure 2-10 with the skew leakage reactance confined only to the stator branch.

Final calculations generally use the equivalent circuit of Figure 2-9, because the skewed rotor circuit most accurately represents the physical motors with skewed rotors and the existing, complex skew factor equations by Weppler and by Williamson and Smith require the skewed rotor circuit. The circuit model of Figure 2-10 was also used regularly to check the calculated values. With consistently calculated circuit

elements, no errors, and the new rotor adjustments, the two circuits give identical results and can be used interchangeably.

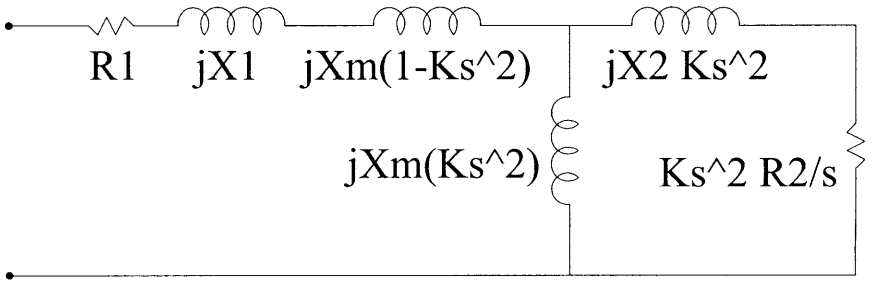

Figure 2-11: Equivalent circuit adjusted for a skewed stator

2.4.3 Skew Factor

Without exception, all of the different versions of skewed equivalent circuit models use the same universal skew factor in their varying calculations to adjust values of resistance and reactance. The skew factor gives the reduction in induced voltage of a skewed compared to a non-skewed rotor bar. The skew factor can be derived, among other methods, from examining the change in flux linked by a non-skewed, full-pitched square rotor bar loop with an angled, trapezoidal, skewed cross-section.

$$k_{sk,n} = \frac{\sin(\frac{n\alpha}{2})}{\frac{n\alpha}{2}} \tag{2.6}$$

In this equation n is the harmonic number and α is the electrical angle of skew measured as the electrical angle of rotation of the face of a rotor bar from one end to the other around the axis of the machine. For one stator slot pitch, and P pole pairs, this angle is $2\pi P$ radians divided by the number of stator slots. This angle is another opportunity for confusion, and the rotor skew can also be described by the more visible angle for open slot designs measured between a skewed bar and a line parallel to the straight axis of the rotor.

Figure 2-12 illustrates the two angles involved with skewed rotor bars. The circle represents the face of one end of the rotor and the lighter lines, axially straight down the rotor, would be the location of non-skewed rotor bars. The darker line is a rotor

bar skewed through one rotor bar pitch, the angle between rotor bars. The mechanical skew angle is measured as an angle of rotation around the rotor axis, equal to $\frac{2\pi}{N_R}$ in this case with N_R rotor bars. This translates to the electrical skew angle, α, by multiplying by the number of pole pairs, P. The more visible angle, β, is a function of the bar length and rotor radius. The skew is often specified as a fraction of rotor or stator slot pitch to try and avoid any confusion with the different angles.

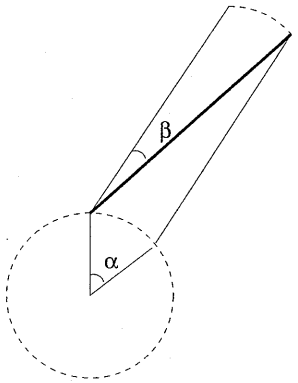

Figure 2-12: Angles of skewed rotor bars

Including the skew factor typically has only a slight (few percent or less) impact on the rotor fundamental values but can significantly reduce the rotor slot harmonic current, torque, and loss by a combination of increased slot harmonic leakage reactance and possibly a decrease in slot harmonic magnetizing reactance, depending on the choice of equivalent circuit. The rotor skew often aims to eliminate the stator slot harmonic currents unreduced by the winding factor and otherwise contributing potentially significant harmonic loss and torque. However, with inter-bar currents flowing between imperfectly isolated rotor bars, the skew is less effective at canceling out the slot harmonic currents. In fact, measured stray loss and torque dip increased for the skewed cast aluminum rotors compared to the only available non-skewed case.

The *non-skewed* equivalent circuit calculations better matched measured results with an adjustment to the slot harmonic reactance values. Equivalent circuit calculations of the *skewed* five horsepower aluminum rotors require an even further decrease in slot harmonic leakage reactance and/or increase to slot harmonic magnetizing reactance, opposite the theoretical impact of skew, to reproduce the dip at high slip in

the measured torque speed curve. The impact of inter-bar currents to the effective rotor resistance and effective skew factor can help to better calculate the observed behavior of the skewed motors.

An additional correction can also be included to account for the slight decrease in bar area from the incremental offset of successive rotor laminations to create the bar skew. In normal cases, this is again, insignificant. However, the reduced bar area can have a greater impact than the increased length and could significantly impact rotor behavior with extreme skews and bar shapes with thin sections.

2.4.4 Skew Variation

Variation of the manufactured rotor skew partially explain the observed variations among nominally identical rotors. All of the five horsepower copper rotors and the skewed aluminum rotors were designed for a rotor bar skew of twelve degrees, eighty percent of a stator slot pitch. Measured skew angles vary significantly between rotors. Rotor skew can be a difficult to identify source of variation between otherwise identical rotors and is an important variable for inter-bar loss equations.

Comparing a group of four skewed to four otherwise identical but non-skewed rotors, the motors with skew measured increased variation in all quantities. The skew angle is difficult to accurately measure on a completed rotor. Binns, Hindmarsh, and Short planned to compare three rotors, one non-skewed, one with 1.0 rotor slot pitch, and the last with 1.3 rotor slot skew.[24] The machines were 100 hp with 52 rotor slots and 60 stator slots. The final rotors ended up measuring 0.024, 0.936 and 1.263 rotor slot skews. The difference is small, but more than typical care and attention must have been spent on these experimental rotors and the actual skew values still varied somewhat from the nominal design values.

Measured variations in skew and stray load loss are shown in Figure 2-13 below. The skew measurements were rough but repeatable, with a likely range of error around plus or minus 2.5 degrees. The stray losses generally increased with increasing skew, consistent with inter-bar loss.

Approximate estimates of the rotor bar skew were made by measuring the cir-

cumferential length between the center of a bar and an axially straight line from the center of the same bar at the far end of the rotor. The measurements are only as accurate as visual estimations of bar centers, but were consistent and repeatable. The values are not exact but give a reasonable comparison between rotors. The variation in skew alone is insufficient to explain the differences in stray load losses and cannot explain the unexpected differences between skewed and non-skewed rotors. Still, Figure 2-13 shows a rough trend. Stray load loss for these rotors generally increases with increasing skew. Rotor bar skew is an important parameter in determining stray load loss and will also be a key variable in calculating the impact from inter-bar currents.

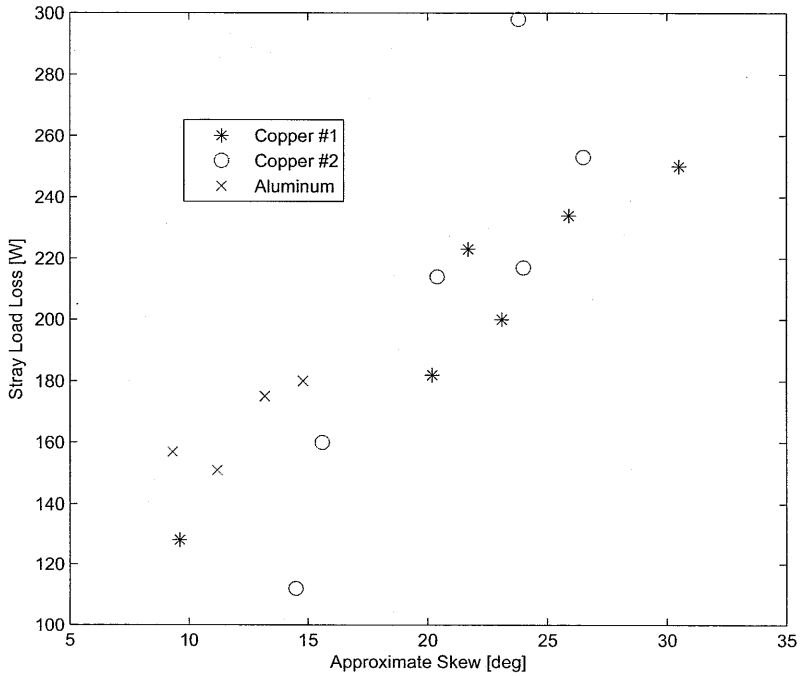

Figure 2-13: Comparison of 5 hp rotor skew and stray load losses

The Copper %1 and Copper %2 are similar rotors, each with twenty nine cast copper rotor bars. The #1 design uses a "double" bar design including a leakage neck and round starting bar and is slightly taller and thinner than the basic tear-drop shaped conductors of design %2. The cast aluminum rotors are slightly longer and operate in a stator with slightly reduced number of turns, so it should not be directly compared. The twenty-nine cast aluminum bars are the same tear-dropped

shape as the #2 copper design.

2.5 Summary and Conclusion

This second chapter has examined the classic induction motor equivalent circuit model and how it can be extended to incorporate multiple space harmonics and adjusted to include the impact of rotor skew. Equivalent circuit calculations have been compared to measured test results for the case of no skew. The reactance values influencing the rotor currents and stray loss have also been introduced. This circuit model provides a common framework for motor calculations and, in Chapter 5, will have the rotor resistance and effective skew factor adjusted to include the presence of inter-bar currents. The next chapter presents the equations for rotor current and total loss including inter-bar currents required for adjusting the equivalent circuit parameters.

Chapter 3

Inter-bar Loss Equations

This chapter presents and evaluates classic inter-bar loss calculations. It begins with the presentation of the differential equation derivation based on the 1955 doctoral thesis by Adnan M. Odok at the Swiss Technical University, Zurich.[10] Odok's approach is compared to a modernized adaption more consistent with equivalent circuit analysis. The differential equation is then solved following Odok's solution process to calculate total rotor bar and inter-bar losses. A condensed version of the derivation and solution process also appears in an often cited April 1958 AIEE paper "Stray-Load Losses and Stray Torques in Induction Machines."[17] Odok's work was based on a 1939 Elektrotechnik und Maschinenbau paper in German by Von V. Rossmaier, the earliest commonly cited publication to use a transmission line approach for rotor bar and inter-bar losses.[9] The results of the derivation are not new but are included here to provide a complete and more accessible derivation of the differential equation commonly solved to determine rotor bar and inter-bar losses. The complete rotor losses can be calculated using these equations only when the motor operating point, in terms of the stator input current and rotor slip, have already been measured or otherwise determined for every point of interest. This chapter compares the calculated fundamental and space harmonic rotor loss to measured rotor loss at specific load points of measured current and slip. Since inter-bar currents can impact the motor operating point, a more general solution to predict motor performance for any operating conditions requires incorporating the full rotor loss equations into an ad-

justed equivalent circuit model. The rotor loss equations from this chapter are later used in the calculations to adjust the equivalent circuit parameters to account for the presence of inter-bar currents, presented in Chapter 5. The only parameter in the rotor loss calculations not available from an extended equivalent circuit model is the average value of total inter-bar resistance. The measurement procedures and estimated average values of inter-bar resistance are presented in Chapter 4.

Following the equation for total rotor losses, new separate calculations for both bar and inter-bar losses are presented and compared to Odok's findings. After deriving an initial general solution, Odok focuses on the simplified case assuming end rings to have negligible impedance compared to the cross-path impedance in the laminations between neighboring bars. This assumption is common and reasonable for the higher order space harmonics on most machines, resulting in negligible difference in calculated losses. Low impedance end rings, compared to the cross-path between bars, do not significantly alter the distribution of inter-bar currents, but unusual machines can be constructed with increased end ring resistance. Plus, even relatively low impedance end rings can still contribute enough loss to adjust the motor operating point, and the changing slip and input current impact the calculation of inter-bar currents. End ring boundary conditions were given in the original Rossmaier paper and later applied in calculations by Weppler, Subba Rao, and others.[9, 11, 15] Calculations including the end ring boundary conditions for the cases of negligible, infinite, and as designed end ring impedance are compared between the adjusted single Odok calculation and separate calculations of bar, inter-bar, and end ring losses.

Plots illustrate the calculated total rotor loss at full load including the end ring boundary conditions under the assumption of near constant current and slip with varied inter-bar resistance for the five and ten horsepower test motors. The motors include variations in bar conductivity, skew, and air gap length. The calculations for each motor are compared to the single points of average inter-bar resistance (from Chapter 4) and full load stray load loss from test measurements. If the input current and rotor slip are known then these calculations using values from a representative circuit model can accurately calculate the total rotor losses. Additional plots and

tables compare rotor fundamental and space harmonic bar currents from calculations and measured tests over a range of eight specific load points. Later, Chapter 5 incorporates the total rotor loss equations into the extended equivalent circuit model allowing the prediction of motor performance at any operating point, under any arbitrary variation in parameters.

3.1 Differential Equation for Rotor Bar Current

The following differential equation has often been used to model total rotor losses, both along and between rotor bars.[9]

$$-\frac{d^2 I_b(y)}{dy^2} Z_{qs} + I_b(y) Z_r = E e^{j\alpha y} \tag{3.1}$$

This equation can be solved for $I_b(y)$, the rotor bar current at axial position y along the rotor length. The remaining terms are known, calculable, or measurable design variables and rotor quantities. Z_{qs} is a scaled version of the average impedance per unit length between neighboring bars, Z_q, with units of ohm meters, calculated according to the following equation.

$$Z_{qs} = \frac{Z_q}{4\sin^2(\frac{\delta}{2})} = \frac{Z_q\, e^{-j\delta}}{(1 - e^{-j\delta})^2} \tag{3.2}$$

The variable δ is the electrical phase angle between neighboring bars, equal to $\frac{2\pi n P}{N_R}$ for the n^{th} space harmonic field. P is the number of fundamental pole pairs, and N_R is the number of rotor bars. In general, the inter-bar impedance could be a complex quantity, but only real values of inter-bar resistance measured from Chapter 4 are used for Z_q in all calculations. This is discussed in more detail in Chapter 4.

Z_r, nominally the "bar impedance," is a per bar rotor impedance value including bar impedance, additional rotor leakage reactance, and per bar magnetizing reactance terms. E is the working axial electric field along the rotor length, equal to the induced voltage per rotor bar per unit length with no skew, in units of volts per meter.

Odok gives the following equation for E:

$$E = j\, X_{2h\nu}\, I_1\, \ddot{u}_\nu = \frac{j I_1 12 \mu_0 R f_2 N_c k_w}{g P^2 \nu^2} \tag{3.3}$$

In this equation N_c is the number of stator conductors per phase, equal to twice the number, N_a, of series turns per phase. I_1 is the input stator current; μ_0 is the permeability of free space; R is the rotor radius in meters; and f_2 is the rotor frequency. The total stator winding factor is k_w; g is the effective air gap length; P is the number of poles; and ν is the space harmonic number.

Finally, α represents the electrical angle of rotor bar skew per unit length, the twist built into usually the rotor conductors, measured as the angle of rotation of each bar from one end to the other around the motor shaft.

As the rotor bars become perfectly isolated with no inter-bar currents, the current remains constant along the bar length and the first term in (3.1) drops out. In this case the current is the ratio of voltage to impedance and the rotor losses can be calculated as the square of the bar current (typically assumed sinusoidally distributed across all bars) multiplied by the frequency and temperature adjusted bar impedance, consistent with standard induction machine theory.[6]

With non-insulated rotor bars, (3.1) is solvable when the machine geometry, material properties, and operating conditions are known. The electromagnetic interaction between the motor rotor and stator dictate the solution of the rotor losses. The induced rotor bar voltage, E, arises from linked flux and relative motion driven by the input stator current. The resultant air gap field in the machine is a function of both the rotor and stator currents. The rotor impedance, Z_r, is a function of the magnetic interaction between rotor and stator in addition to the bar geometry and material properties. The solution at any particular point is an equilibrium condition that changes with stator current and rotor slip.

The remainder of this section presents and compares interpretations of the derivations of the differential equation (3.1) based on work by Odok and Kirtley, both following the circuit approach originally from Rossmaier's paper, examining a short segment along two neighboring rotor bars. Assuming a sinusoidal distribution of rotor

current around all of the N_R rotor bars, the values of current in successive neighboring bars, end ring sections, or inter-bar paths are all phase-shifted by an angle $\delta = \frac{2\pi P}{N_R}$ around the rotor outer diameter, where P is the number of pole pairs.

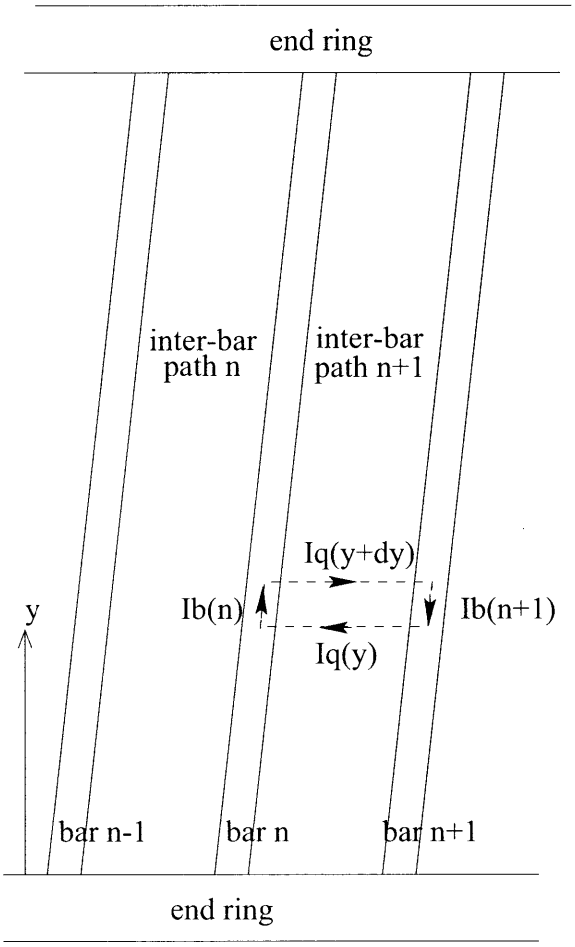

Figure 3-1: Rotor section used in inter-bar loss equation derivation

Kirchhoff's current law applied at a point along a bar gives the change in current along the bar as the net change in current flowing in or out from both neighboring bars. The change in current at a point on the center, n^{th}, bar shown in Figure 3-1 must be equal to the sum of the currents between the $n-1$ and n^{th} and between the n^{th} and the $n+1$ bars, all at the same position y along the bar length.

$$\frac{dI_b}{dy} = K_q(1 - e^{-j\delta}) \tag{3.4}$$

Here I_b is the bar current in amperes and K_q is the current per unit length in amperes per meter between bars. Equation (3.4) can also be solved for the inter-bar cross current.

$$K_q = \frac{dI_b}{dy}\frac{1}{(1 - e^{-j\delta})} \tag{3.5}$$

Similarly, Kirchhoff's voltage law can be applied around a loop formed by thin lengths dy of the n^{th} and $n+1$ neighboring bars linked by the two lamination sections across the $n+1$ inter-bar path at positions y and $y+dy$ as shown in Figure 3-1. The sum of the total voltage around this loop, due to both voltage drops across impedances as well as the source-like total induced voltage around the loop, V, must equal zero.

$$I_{b(n)}(y)\, Z_r\, dy + K_{q(n+1)}(y+dy)\, Zq - I_{b(n+1)}\, Z_r\, \delta y - K_{q(n+1)}(y)\, Z_q = V \tag{3.6}$$

Again, Z_r is the rotor impedance per unit length with units of ohms per meter; the bar current I_b has units of amps; the inter-bar impedance Z_q is in units of ohm meters; and the inter-bar current, I_q, has units of amperes per meter so all terms have units of volts.

Dividing through by dy and substituting in the phase shift for the n+1 bar and inter-bar currents gives the following equation:

$$I_{b(n)}\,(1 - e^{-j\delta})\,Z_r + \frac{dK_q}{dy}\,Z_q\,e^{-j\delta} = \frac{V}{dy} \tag{3.7}$$

Assuming a sinusoidal fundamental distribution of air gap flux, the induced bar voltages will also be phase shifted from bar to bar, and the loop summing the voltages will traverse the bars in opposite directions.

$$V = (E_{(n)} - E_{(n+1)})\,dy = E(1 - e^{-j\delta})dy \tag{3.8}$$

Again, E is the rms value of the sinusoidal distribution of the non-skewed, induced voltage per bar, per meter length. $E\,dy$ gives the voltage induced along the length dy of the rotor bar at the peak of the assumed sinusoidal distribution around the bars, assumed here to be the n^{th} bar. The subscript n or $n-1$ indicates the value of induced voltage at a particular bar, with a corresponding phase shift away from the n^{th} bar.

Substituting (3.5) and (3.8) into (3.7) and dividing through by $(1 - e^{-j\delta})$ gives an equation nearly equivalent to the desired differential equation, (3.1).

$$I_{b(n)}(y)\,Z_r + \frac{d^2 I_b}{dy^2}\,\frac{Z_q\,e^{-j\delta}}{(1 - e^{-j\delta})^2} = E \tag{3.9}$$

Equation (3.9) lacks the phase shift as a function of position along the rotor length, $e^{j\alpha y}$, applied to the induced voltage to account for skew and the substitution of $Z_{qs} = \frac{Z_q\,e^{-j\delta}}{(1-e^{-j\delta})^2}$ to scale the inter-bar impedance. Otherwise, this is the same differential equation as (3.1) solvable for the rotor bar and inter-bar currents required to calculate total rotor losses. The four main parameters are the electrical angle of rotor bar skew per unit length, α, included as a phase shift to the induced voltage, the voltage induced along the bars, E, the rotor per-bar impedance, Z_r, and the impedance between bars, Z_q. The rotor impedance Z_r also includes mutual and leakage reactance terms since the induced voltage depends on both the rotor and stator currents. Approximate values of all four terms are required for accurate loss calculations. Each of the four critical parameters are briefly discussed in order to examine their potential impact on the rotor losses.

3.1.1 Rotor skew

Rotor skew, the electrical angle of twist or slant in each bar from end to end, is a straightforward variable for this chapter. The value of skew is assumed to be known from design data or measured on the completed rotor. The measured skew is used in the loss equations for each rotor. The impact of skew on insulated rotor equivalent circuit parameters was discussed in the previous chapter. The angle of skew will impact each space harmonic differently, with different series of values resulting in minimum and maximum rotor losses. The impact of varied skew is examined on the five horsepower motors with similar characteristics except altered skew. Calculations of the impact of varied skew on a particular motor design are not evaluated here because the constraint of constant input current and slip may produce unrealistic results. Varied skew and inter-bar resistance are considered in the equivalent circuit adjustments and loss calculations in the fifth chapter.

3.1.2 Per-Bar Rotor Impedance

The components of the per-bar rotor impedance are also briefly discussed in the previous chapter as part of the equivalent circuit model. X_r is a combination of the rotor bar impedance together with a per-bar value of magnetizing reactance as well as any additional rotor leakage reactance components, often expressed as zigzag or differential leakage reactance terms. The rotor bar resistance is one of the easier circuit parameters to calculate. Some reduction in the bar conductivity is possible from voids and impurities as a result of the casting process. For the five and ten horsepower cases, the decrease in cast rotor conductivity were small, less than about 10%. Changes even of this magnitude noticeably alter the motor performance. Surface conductivity measurements showed almost no decrease in conductivity following the rotor casting.

Frequency effects must also be taken into account. A routine written by J.L. Kirtley, Jr., is used to calculate the impact of changing rotor frequency on rotor bar resistance and rotor slot leakage reactance values. The method breaks the bars up into many horizontal slices, simplifying the synthesis of complex bar shapes and

building up the total bar impedance from the combination of every slice.[21]

Unfortunately, the slot leakage reactance is not the only reactance term included in the total equivalent per-bar rotor impedance, X_r. The magnetic coupling and interaction between the rotor and stator impact the induced rotor voltage, currents, and loss. The total rotor reactance, representing both the useful fields and leakage magnetic fields not fully linked by both windings, should be included. Odok includes as part of X_r, the reactive component of the per bar rotor impedance, Z_r, a magnetizing reactance term in addition to slot and differential leakage reactance coefficients consistent with those given by Liwschitz-Garrick.[19, 10] The differential leakage reactance term is roughly equivalent to the zigzag leakage reactance as given by Alger.[6] Equations for these reactance values are presented in the second chapter as part of the equivalent circuit discussion. These reactance values, above all for the stator slot harmonics, greatly impact the calculated rotor losses. At least in the case of the five horsepower motor, unadjusted traditional formulas do not adequately calculate the measured space harmonic rotor loss and torque.

3.1.3 Inter-bar Impedance

The scaled inter-bar impedance, Z_{qs}, is the only new parameter not included in traditional equivalent circuit calculations where the bars are assumed to be perfectly insulated. Previously, Z_{qs} had been defined in 3.19.

$$Z_{qs} = \frac{Z_q\, e^{-j\delta}}{(1 - e^{-j\delta})^2} = \frac{Z_q\, e^{-j\delta}}{e^{-j\delta/2}(e^{j\delta/2} - e^{-j\delta/2})^2} = \frac{Z_q}{4\sin^2(\frac{\delta}{2})} \tag{3.10}$$

The literature generally neglects any reactance associated with the bar-to-lamination interface, and measurements by both Odok and Christofides determined the reactive components to be negligible.[17, 30] However at least one exception by Watterson et al. measured an appreciable variable inductance.[14] As an insulating layer between two conductors, the contact seems like it could add capacitance, but no reactance measurements were taken as part of this investigation. The inter-bar reactance is assumed small enough not to significantly impact the inter-bar losses, and dc mea-

surements determine contact resistance values. The contact resistance measurements and calculations are presented in Chapter 4. Still, identical equations apply with either an inductance or capacitance term included or neglected from the impedance between bars. The inter-bar impedance can easily be updated to reflect the latest measurement results.

The total inter-bar resistance is at least twice the contact resistance, plus the resistance of the section of laminations between bars, if appreciable. The lamination impedance, assumed resistive along with the contact term, contributes a finite resistance, typically negligible compared to the much larger contact resistance, but more significant for rotors with low contact resistance. The lamination impedance also imposes a fixed lower limit on minimum practical value of inter-bar resistance when approaching zero contact resistance. With low enough lamination conductivity, the point of maximum cross-path loss might never be achievable. On the twenty-nine bar, almost three inch diameter, five horsepower rotors, the resistance of the iron path per unit length between neighboring bars was estimated to be around 0.1 micro-ohm meters.

Frequency effects should also be considered in dealing with the inter-bar resistance values. Even though the cross path is assumed purely resistive, the axial path along the bars includes both bar resistance and reactance. The rotor bar currents crowd towards the upper sections of the rotor bars under conditions of high slip and rotor electrical frequency, increasing the equivalent rotor resistance from rotor currents crowding towards the top of the bars. The inter-bar currents will similarly concentrate in the regions of higher current density, increasing the effective inter-bar resistance. As a first order approximation, the increase to the contact resistance is assumed to be proportional to the increase in rotor bar resistance.

3.1.4 Induced Rotor Voltage

The induced rotor voltage is another rotor parameter accounting for the coupling between rotor and stator. Dependent on both the useful reactance terms representing the magnetic fields jointly linked by both rotor and stator and the leakage fields

linking only one or the other winding, the induced rotor voltage varies with the stator operating point as well as the design of the rotor and stator.

The working axial electric field along the rotor, equal to the induced rotor bar voltage per unit length with no skew, can also be calculated as the integral of the induced axial electric field along the bar, divided by the bar length. With radially directed air gap flux density, B_g, the electric field along the bar is equal to the cross product of B_g and the bar velocity. Integrating the electric field over the full bar length, L, and dividing by the total length of the bar gives the induced voltage per unit length, E. There is no induced voltage in the orthogonally oriented end rings. Normally, the air gap magnetic flux density and the induced rotor electric field are assumed sinusoidally distributed around the air gap and uniform along the bar length in the absence of skew.

$$E = \omega \, s \, R \, B_g P \tag{3.11}$$

In this equation, R is the rotor radius in meters, B_g the rms air gap flux density in tesla, P the number of pole pairs, ω the stator electrical frequency, and s the rotor per unit slip. The induced bar voltage for each space harmonic is the only rotor source term driving the rotor currents. With no end ring impedance, the magnitude of induced voltage per unit bar length exactly matches the voltage drop along the bars, calculated as the bar current multiplied by the bar impedance per unit length with a uniform bar current. With appreciable end ring impedance and otherwise identical conditions, the same induced voltage now drives a somewhat reduced current through both the bar and ring impedances.

Still assuming a sinusoidal distribution, the next bar will be phase shifted by an angle δ, and the total induced voltage, V, around the loop of a small section of neighboring bars, as illustrated in Figure 3-1 can be calculated as the difference between the induced voltages of the two neighboring bars.

$$V = \frac{\omega_r \, R \, B_g \, dy}{p} (1 - e^{-j\,\delta}) \tag{3.12}$$

Kirtley uses a slightly different equation than Odok for B_g, with the vector difference in stator and rotor currents determining the magnetizing current and air gap flux density. This more clearly shows the interaction of rotor and stator and leads to the additional per-bar magnetizing reactance term, X_b combined with the rotor bar reactance, Z_b, to give Odok's full per-bar rotor impedance, Z_r.

$$B_g = j\,\mu_0 \frac{3}{2}\frac{4}{\pi}\frac{N_s\,k_w}{2\,p\,g}(I_1 - I_2) \tag{3.13}$$

Here the stator and rotor currents are defined positive when directed into the motor stator terminal or rotor branch.

The rotor current, I_2, referred to the stator and the physical current per bar, I_b, are related by the normal referral ratio as shown in Equation (3.14) for a three-phase squirrel cage machine with no skew or skew evenly split between stator and rotor. The skew factor can also be included as a rotor winding factor, depending on how the equivalent circuit incorporates the skew.

$$I_2 = I_b \frac{N_R}{6\,N_a\,k_w} \tag{3.14}$$

In this equation, N_R is the number of rotor bars, N_a the series turns per phase, and k_w the total stator winding factor. Substituting into the equation for induced rotor voltage, (3.11), gives the following equation:

$$E = \frac{j\,3\,\mu_0\,\omega_r\,R\,N_s\,k_w}{\pi\,p^2\,g}(1 - e^{-j\,\delta})(I_1 - I_b\frac{N_a}{6\,N_s\,k_w}) \tag{3.15}$$

Plugging this induced voltage into the differential equation from (3.9) results in an expanded form.

$$I_b\,Z_b\,(1-e^{-j\,\delta}) - \frac{dI_b^2}{dy^2}Z_q\frac{e^{-j\,\delta}}{(1-e^{-j\,\delta})} = \frac{j\,3\,\mu_0\,\omega_r\,R\,N_s\,k_w}{\pi\,p^2\,g}(I_1 - I_b\frac{N_a}{6\,N_s\,k_w})(1-e^{-j\,\delta}) \tag{3.16}$$

Dividing through by $(1 - e^{-j\,\delta})$ slightly simplifies the equation.

$$I_b(\frac{j\,\mu_0\,\omega_r\,R\,N_R\,dy}{3\,\pi\,p^2\,g}\,Z_b) - \frac{dI_b^2}{dy^2}\frac{Z_{qs}\,e^{-j\,\delta}}{(1-e^{-j\,\delta})^2} = \frac{j\,3\,\mu_0\,\omega_r\,R\,N_s\,k_w}{\pi\,p^2\,g}\,I_1 \tag{3.17}$$

And substituting in

$$X_g = \frac{\mu_0\,\omega\,s\,R\,N_R}{3\,\pi\,p^2\,g} \tag{3.18}$$

as well as

$$\frac{Z_q\,e^{-j\,\delta}}{(1-e^{-j\,\delta})^2} = \frac{Z_q}{4\sin^2(\frac{\delta}{2})} = Z_{qs} \tag{3.19}$$

gives the final version

$$I_b(Z_b + jX_g) + Z_{qs}\,\frac{d^2I_b}{dy^2} = Xg\,\frac{N_a\,k_w\,6}{N_R}\,I_1 e^{\frac{j\,\alpha\,y}{L}} \tag{3.20}$$

This derivation from J.L. Kirtley, Jr. based on the method used by Odok and Rossmaier more clearly shows how both the rotor and stator currents impact the air gap flux density and how the additional reactance, X_g, combines with the bar reactance Z_b.

3.2 Rotor Loss Solution

This section initially presents Odoks solution for rotor bar and inter-bar losses before solving for arbitrary end ring boundary conditions. Odok starts with the following homogenous and particular solutions to (3.1) for the rotor bar current, verifiable by evaluation in the differential equation.

$$I_H(y) = C_1 e^{\gamma y} + C_2 e^{-\gamma y} \tag{3.21}$$

$$I_P(y) = \frac{E e^{j\alpha y}}{Z_{qs}(\gamma^2 + \alpha^2)} \tag{3.22}$$

In these and future equations, the new term γ is a propagation constant given by

$\sqrt{\frac{Z_r}{Z_{qs}}}$ while C_1 and C_2 are complex integration constants set by applying boundary conditions. Combining these two equations gives the total solution for the rotor bar current.

$$I_b(y) = C_1 e^{\gamma y} + C_2 e^{-\gamma y} + \frac{E e^{j\alpha y}}{Z_{qs}(\gamma^2 + \alpha^2)} \tag{3.23}$$

Expressions for the current and voltage between bars in terms of the bar current can also be used to calculate the losses from currents between bars. The current between bars, I_q, can be determined by current continuity along a thin section of bar. The difference in the bar current must equal the difference in cross currents entering and leaving the bar along the section. Taking the limit as the length of the section approaches zero gives the derivative of the bar current in terms of the two adjoining inter-bar currents.

$$I_q(y) = \frac{dI_b(y)}{dy} \frac{e^{j\delta/2}}{2j\sin(\frac{\delta}{2})} \tag{3.24}$$

In this equation δ is the phase angle between adjacent rotor bars. The bar-to-bar voltage, $V_q(y)$, is the product of the inter-bar current and impedance.

$$V_q(y) = I_q(y) Z_q \tag{3.25}$$

Evaluating the inter-bar voltage in terms of the bar current produces the following equation for the voltage between bars.

$$V_q(y) = -Z_{qs} 2j \sin(\delta/2) e^{j\delta/2} \frac{d}{dy} \left[C_1 e^{\gamma y} + C_2 e^{-\gamma y} + \frac{E e^{j\alpha y}}{Z_{qs}(\gamma^2 + \alpha^2)} \right] \tag{3.26}$$

Odok first solved for the integration constants, C_1 and C_2, in terms of generic boundary conditions given by $I_b(y = 0) = I_1$ for the bar current at the starting end of the rotor and $V_q(y = 0) = V_1$ for the voltage between bars. This exchanges the two unknown constants for functions of two other, more specifically defined unknown constants.

$$C_1 = \frac{I_1}{2} - \frac{V_{1s}}{2\gamma Z_{qs}} - \frac{E(j\alpha + \gamma)}{2Z_{qs}\gamma(\gamma^2 + \alpha^2)}$$

and

$$C_2 = \frac{I_1}{2} + \frac{V_{1s}}{2\gamma Z_{qs}} + \frac{E(j\alpha - \gamma)}{2Z_{qs}\gamma(\gamma^2 + \alpha^2)}$$

The substitution $V_{1s} = \frac{V_1}{2jsin(\delta/2)e^{j\delta/2}}$ makes the equations a little cleaner. Now, plugging in the results for C_1 and C_2 and simplifying using the hyperbolic functions $2\cosh(x) = e^x + e^{-x}$ and $2\sinh(x) = e^x - e^{-x}$ yields equations (3.27) and (3.28) for the bar current and inter-bar voltage.

$$I_b(y) = I_1\cosh(\gamma y) - \frac{V_{1s}}{Z_v}\sinh(\gamma y) - \frac{j\alpha E}{Z_v\beta}\sinh(\gamma y) - \frac{E}{Z_{qs}\beta}\cosh(\gamma y) + \frac{E_i e^{j\alpha y}}{Z_{qs}\beta} \quad (3.27)$$

$$V_{qs}(y) = -I_1 Z_v\sinh(\gamma y) + V_{1s}\cosh(\gamma y) + \frac{j\alpha E}{\beta}\cosh(\gamma y) + \frac{EZ_v}{Z_{qs}\beta}\sinh(\gamma y) - \frac{j\alpha V_i e^{j\alpha y}}{\beta} \quad (3.28)$$

In both of these equations substitutions have been made for $\beta = \gamma^2 + \alpha^2$ and $Z_v = \sqrt{Z_{qs}Z_r}$. There are a number of different ways these equations can be used to find the rotor power loss. Odok uses the most direct approach to find the total rotor losses, the sum of losses along and between bars. He integrates along the bar length the product of the bar current and the complex conjugate of the induced voltage for the case of no skew. The non-skewed induced voltage is multiplied by a phase shift dependent on the position along the bar to account for the rotor bar skew. This allows the calculation of the sum of the rotor bar, inter-bar, and end ring losses by evaluating a single integral. In any loop between bars along the rotor length, as shown in Figure 3-1, the sum of the induced voltage along the bars drives all rotor current, both along and between bars, and must be equal to the total voltage drop, both along and between bars. The end rings are included as boundary conditions with altered inter-bar resistance, cross-current, and voltage drop at either end of the bar.

With insulated rotor bars and negligible impedance end rings, the voltage drop along a section of a rotor bar equals the induced voltage along the bar. Add in end ring impedance and inter-bar paths and now the induced voltage along a length of a bar equals the sum of the voltage drop along the same bar length, plus the voltage drop between a section of the rotor bars, and a voltage drop accounting for a proportional section of both end rings. The phase shifted induced voltage E represents the combination of all three areas of voltage drop. The total rotor loss both in the rotor bars, end-rings, and paths between bars can be simultaneously calculated using the single expression below, multiplying the total number of rotor bars by the integral of the IV^*, with the complex conjugate of the phase shifted voltage drop for the total voltage drop.

$$P_2 = N_R \Re e \left\{ \int_{y=0}^{y=L} \left[I_b(y) E^* e^{-j\alpha y} dy \right] \right\} \tag{3.29}$$

The starred variable, E^* represents the complex conjugate of the induced bar voltage in the case of no skew, E. The variable N_R is the number of rotor bars, and $\Re e\{\}$ represents the real component of a complex number.[17] Inserting I_b from equation (3.27) and evaluating the integral results in equation 36 from Odok's AIEE paper or, equivalently, equation 30 from his thesis.[17, 10]

$$\begin{aligned} P_2 = & N_R \Re e \left(\frac{E^2 L}{Z_{qs}\beta} + \left(I_1 E^* - \frac{E^2}{Z_{qs}\beta} \right) \left[\frac{e^{-j\alpha L}}{\beta} (\gamma \sinh(\gamma L) + j\alpha \cosh(\gamma L)) - \frac{j\alpha}{\beta} \right] \right. \\ & \left. - \left(\frac{V_{1s} E^*}{Z_v} + \frac{j\alpha E^2}{Z_v \beta} \right) \left[\frac{e^{-j\alpha L}}{\beta} (\gamma \cosh(\gamma L) + j\alpha \sinh(\gamma L)) - \frac{\gamma}{\beta} \right] \right) \end{aligned} \tag{3.30}$$

Still including the generic I_1 and V_1 boundary conditions, equation (3.30) could be applicable to any case. However, one of the most practical and easiest to evaluate cases assumes the rotor end rings behave as ideal short circuits with negligible impedance.

3.3 Negligible End Ring Impedance

Physical rotor end rings contain a finite impedance value, generally less than the bar impedance and typically negligible compared to the resistance of the lamination path between bars. In the low current dc voltage measurements of Chapter 4, even copper tendrils of millimeter dimensions squeezed between the outer most lamination layers could effectively short out the voltage measurable between neighboring bars.

The larger solid copper or aluminum rings cast together with the rotor bars as a single conductor cage provide an even closer approximation to a short circuit in typical machine designs. Negligible end ring impedance gives effectively zero voltage between bars at both ends of the rotor and $V_1 = 0$. The value of Odok's other boundary condition value, I_1 is not as obvious but can be determined using the second boundary in equation (3.28), solving $V_{qs}(y = L) = 0$ with $V_1 = 0$ for I_1.

$$I_1 = E\left[\frac{j\alpha\, cosh(\gamma L)}{Z_v\beta\sinh(\gamma L)} + \frac{1}{Z_{qs}\beta} - \frac{j\alpha e^{j\alpha L}}{Z_v\beta\sinh(\gamma L)}\right] \tag{3.31}$$

Substituting these values for V_1 and I_1 into equation (3.30) yields equations 37 and 31 from the Odok AIEE paper and doctoral thesis, the equation for total rotor losses in the case of negligible end ring resistance, reproduced below as equation (3.34). Alternatively, when only considering the case of negligible end ring impedance, the boundary conditions, $V_{qs}(y = 0) = V_{qs}(y = L) = 0$, can be applied earlier to equation (3.26) to directly determine the integration constants, C_1 and C_2, for this particular case.

$$C_{1o} = \frac{j\alpha E\left(e^{-\gamma L} - e^{j\alpha L}\right)}{2\gamma Z_{qs}\beta\sinh(\gamma L)} \tag{3.32}$$

$$C_{2o} = \frac{j\alpha E\left(e^{\gamma L} - e^{j\alpha L}\right)}{2\gamma Z_{qs}\beta\sinh(\gamma L)} \tag{3.33}$$

These alternate integration constants can be substituted into the equations for bar current and inter-bar voltage, (3.23) and (3.26). Repeating the integration of the product of this new bar current and the induced bar voltage identically reproduces

equation (3.34) for total rotor losses under the assumption of negligible end ring impedance. Again, this equation gives the combined total of both the traditional rotor bar losses along with the inter-bar losses but omits any end ring loss.

$$P_2 = N_R|E|^2 \Re e \left[\frac{L}{Z_{qs}\beta} + \frac{2\alpha^2(\cosh(\gamma L) - \cos(\alpha L))}{\beta Z_v \sinh(\gamma L)} \right] \tag{3.34}$$

While this equation is derived and written for the fundamental air gap field and rotor currents, the same equation with adjusted parameters for the higher order harmonics can be used to calculate non-fundamental frequency rotor losses. Frequency effects must be taken into account when determining the bar and inter-bar impedances. The physical rotor skew angle, if about equal to one stator slot pitch, may be a small percentage of the fundamental field pole pitch but will be more significant for the higher order harmonics.

3.4 Infinite End Ring Impedance

The opposite extreme provides equally simple, if less realistic, boundary conditions. Infinite end ring impedance is equivalent to removing both end rings. This case can be used as a sanity check to verify the equations are behaving as expected. With infinite end ring impedance, total rotor losses should go to zero as the inter-bar impedance gets large, no currents flow, and the motor fails to operate. Inter-bar losses will still approach zero as the bar-to-bar impedance approaches zero, matching the previous case with no end ring impedance. Again, this extreme model does not represent physical reality for normal machines. These equations are calculated using a fixed current and slip that will only remain approximately constant provided that the additional rotor losses do not significantly alter the motor operating point. Especially without end rings, the original full load operating point does not apply and incorrect values of stator current and slip are used. Still, the no end ring case can be useful for comparison against separate bar and inter-bar loss equations.

Applying the new boundary conditions, $I_b(y = 0) = I_b(y = L) = 0$, produces new integration coefficients.

$$C_{1\infty} = \frac{-\alpha E\left(e^{-j\alpha L} - e^{\gamma L}\right)}{2Z_{qs}\beta \sinh(\gamma L)} \tag{3.35}$$

$$C_{2\infty} = \frac{-E\left(e^{-\gamma L} - e^{j\alpha L}\right)}{2Z_{qs}\beta \sinh(\gamma L)} \tag{3.36}$$

Substituting these coefficients into the equation for bar current and repeating the integration of the bar current multiplied by the phase shifted induced bar voltage gives the following equation for total rotor losses in the case of no, or infinite impedance, end rings.

$$P_{2\infty} = N_R|E|^2 \Re e\left[\frac{L}{Z_{qs}\beta} + \frac{2\gamma(\cos(\alpha L) - \cosh(\gamma L))}{\beta^2 Z_{qs}\sinh(\gamma L)}\right] \tag{3.37}$$

3.5 Separate Bar and Inter-bar Loss Equations

The total rotor losses can also be found by separately integrating the square of the bar current times the bar impedance to find the rotor bar losses, P_{2b} , and then adding the integral of the square of the voltage between bars divided by the inter-bar impedance for the inter-bar losses, P_{2q}, with both integrals taken over the full rotor length. Since both bar current and inter-bar voltage are complex quantities, the squared term for both power equations must multiply each value by its complex conjugate. This more complicated method separately calculates the rotor losses physically located either in the rotor bars or in the lamination paths between bars. With non-insulated bars, new loops between bars allow currents to flow along and between sections of bars. These currents cannot exist in the case of an insulated rotor. The total change in loss due to inter-bar currents arises from the new currents and total losses in both bar and cross-path. The total rotor losses from each case should be compared in order to determine the impact from non-insulated rotor bars, but the separately calculated bar and inter-bar losses provide a useful check against the previous total rotor loss calculation.

$$P_{2b} = N_R \Re e \left[\int_0^L I_b(y) I_b^*(y) Z_r^* dy \right] \tag{3.38}$$

$$P_{2q} = N_R \Re e \left[\int_0^L \frac{V_q(y) V_q^*(y)}{Z_q} dy \right] \tag{3.39}$$

Evaluating these integrals gives separate nine term equations for the bar and inter-bar rotor losses. Substituting in the integration constants for the negligible end ring impedance case and evaluating, the sum of these two equations matches the single total rotor loss from equation (3.34).

$$\begin{aligned} P_{2b} =& N_R \Re e \Bigg\{ Z_r^* \Bigg\{ \frac{C_1 C_1^*}{2\gamma_r}(e^{2L\gamma_r} - 1) - \frac{C_2 C_2^*}{2\gamma_r}(e^{-2L\gamma_r} - 1) \\ & - \frac{jC_1 C_2^*}{2\gamma_i}(e^{j2L\gamma_i} - 1) + \frac{jC_2 C_1^*}{2\gamma_i}(e^{-j2L\gamma_i} - 1) + \frac{E^2 L}{\mathbf{QB}} \\ & - \frac{EC_1}{Z_{qs}^* \beta^*(\gamma - j\alpha)}(e^{L(\gamma - j\alpha)} - 1) + \frac{EC_2}{Z_{qs}^* \beta^*(\gamma + j\alpha)}(e^{-L(\gamma + j\alpha)} - 1) \\ & + \frac{EC_1^*}{Z_{qs}\beta(\gamma^* + j\alpha)}(e^{L(\gamma^* + j\alpha)} - 1) - \frac{EC_2^*}{Z_{qs}\beta(\gamma^* - j\alpha)}(e^{-L(\gamma^* - j\alpha)} - 1) \Bigg\} \Bigg\} \end{aligned} \tag{3.40}$$

$$\begin{aligned} P_{2q} =& N_R \Re e \Bigg\{ Z_{qs}^* [\frac{\Gamma C_1 C_1^*}{2\gamma_r}(e^{2L\gamma_r} - 1) - \frac{\Gamma C_2 C_2^*}{2\gamma_r}(e^{-2L\gamma_r} - 1) \\ & + \frac{j\Gamma C_1 C_2^*}{2\gamma_i}(e^{j2L\gamma_i} - 1) - \frac{j\Gamma C_2 C_1^*}{2\gamma_i}(e^{-j2L\gamma_i} - 1) + \frac{\alpha^2 E^2 L}{\mathbf{QB}} \\ & - \frac{\alpha\gamma EC_1}{Z_{qs}^* \beta^*(\gamma - j\alpha)}(e^{L(\gamma - j\alpha) - 1}) + \frac{j\alpha\gamma EC_2}{Z_{qs}^* \beta^*(\gamma + j\alpha)}(e^{-(L(\gamma - j\alpha) - 1)}) \\ & - \frac{\alpha\gamma EC_1 *}{Z_{qs}^* \beta^*(\gamma^* + j\alpha)}(e^{L(\gamma + j\alpha) - 1}) - \frac{\alpha\gamma^* EC_2^*}{Z_{qs}^* \beta^*(\gamma^* - j\alpha)}(e^{-L(\gamma^* + j\alpha) - 1})] \Bigg\} \end{aligned} \tag{3.41}$$

The following plots compare the sum of the bar and inter-bar losses, $P_{2b} + P_{2q}$, to the loss calculated first using Odok's equation with negligible end ring impedance in Figure 3-2 and second, assuming the opposite extreme case of infinite end ring impedance in Figure 3-3. The exact matches suggest the separate bar and inter-bar

loss equations are functioning correctly.

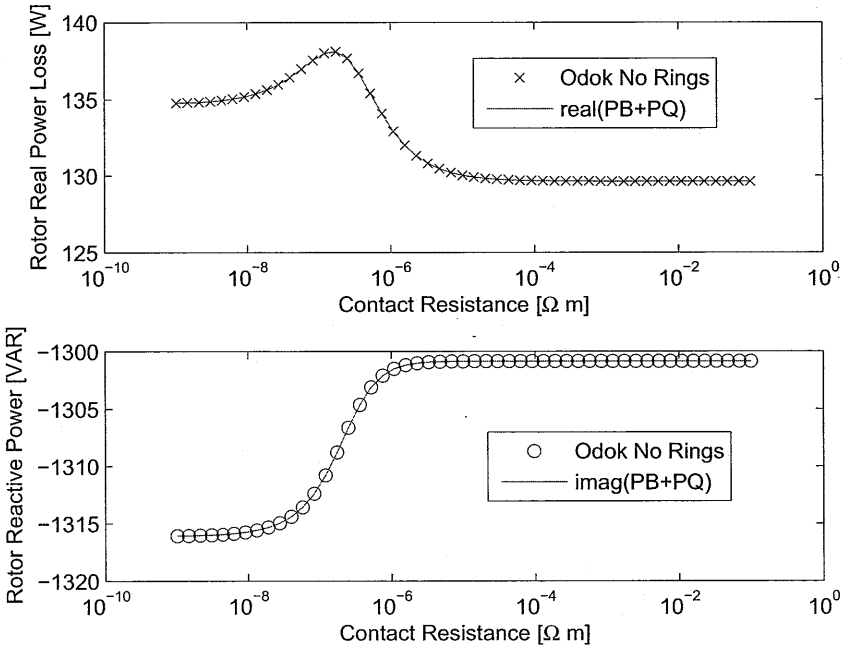

Figure 3-2: Comparison of calculated total rotor power loss between the single equation and the combination of separate bar and inter-bar losses with negligible end rings

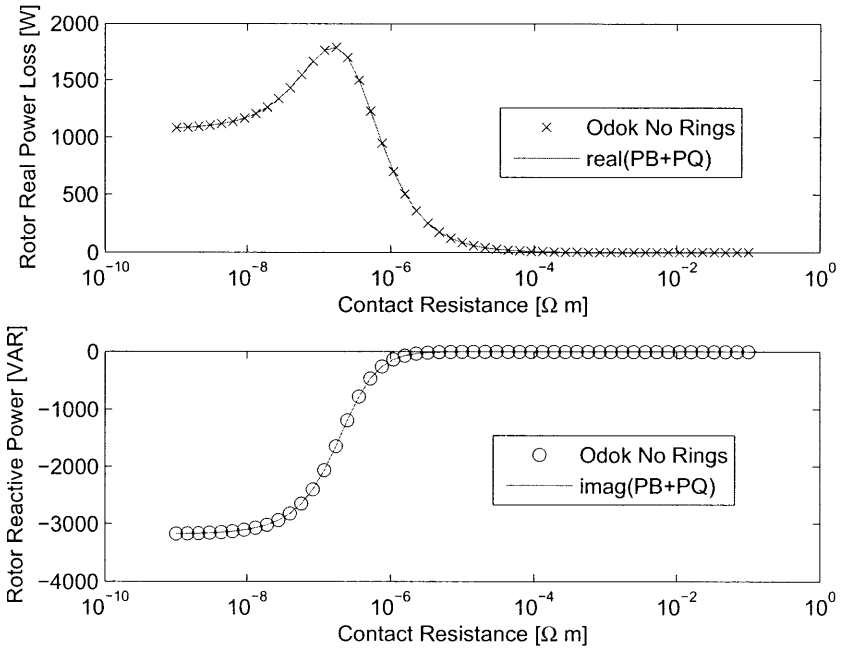

Figure 3-3: Comparison of fundamental real and reactive power calculated between the single total equation and the combination of separate bar and inter-bar losses with no end rings (infinite end ring impedance)

Since the Figures 3-2 and 3-3 compare only the sum of both bar and inter-bar power equations, there could still be an error in the division between the two categories. The next two plots show the separate calculations of bar and cross-path loss for the same two cases of negligible end ring impedance, in Figure 3-4, and infinite end rings, in Figure 3-5. The results make sense for the zero impedance case, where all of the cross-path losses go to zero as the rotor resistance gets large enough to prevent any rotor currents from flowing. Similarly, the inter-bar losses will approach zero and the bar currents a maximum value as the inter-bar resistance goes away. For the less realistic case of completely removed end rings, all losses vanish as expected as the cross-path impedance increases and all rotor currents approach zero. Again, the bar current and loss should reach a maximum as the inter-bar resistance and loss approach zero.

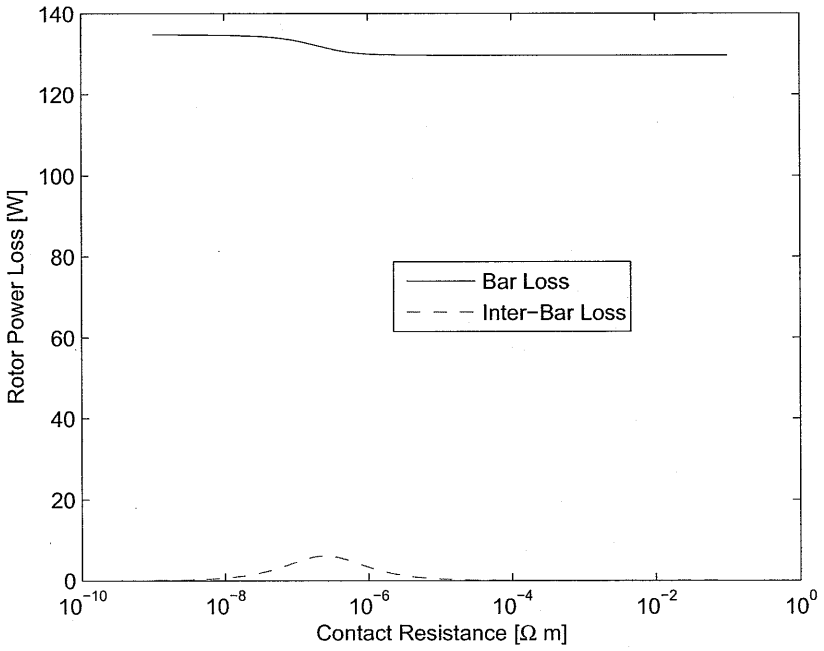

Figure 3-4: Plot of calculated fundamental bar and inter-bar losses for skewed cast aluminum 5 hp rotor with negligible end rings

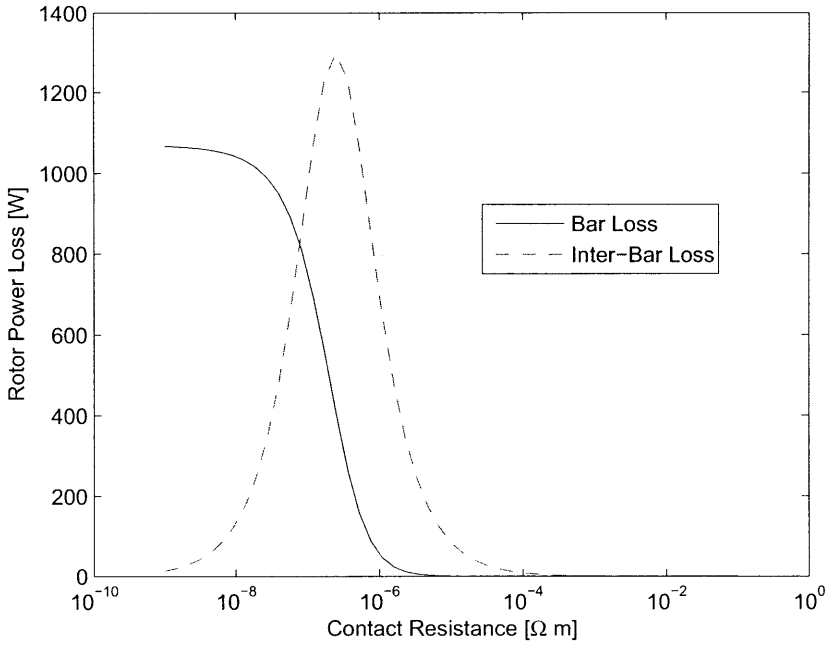

Figure 3-5: Plot of calculated fundamental bar and inter-bar losses for skewed cast aluminum 5 hp rotor with no end rings

Lastly, since all of these plots examined only the fundamental rotor losses, Figures 3-6 and 3-7 show the 23rd space harmonic power for the case of negligible end rings. First, Figure 3-6 again compares the real and imaginary component of the sum of both to the independently calculated power. Then, the real power is plotted broken down into bar and inter-bar losses in Figure 3-7. The inter-bar losses are more significant on this slot harmonic than on the fundamental.

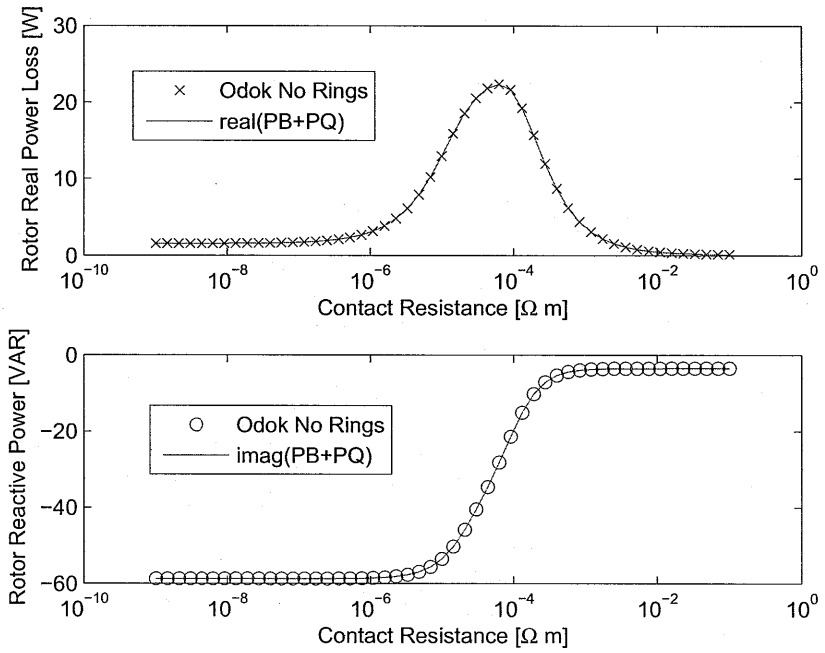

Figure 3-6: Comparison of 23rd space harmonic real and reactive power calculated between the single total equation and the combination of separate bar and inter-bar losses

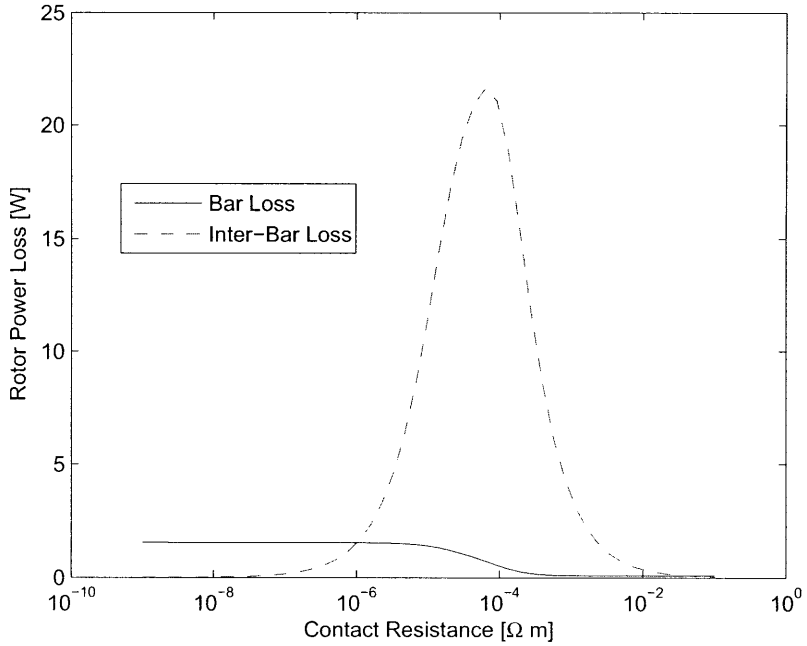

Figure 3-7: Plot of calculated bar and inter-bar losses for 23rd space harmonic skewed cast aluminum 5 hp rotor

3.6 Arbitrary End Ring Conditions

Both of the rotor loss equations with assumed zero or infinite end ring impedance do not consider end ring losses. In most typical machines, the end rings may act as ideal short circuits when compared to the much larger cross-path impedance, but each ring retains a small, non-zero, impedance. The bar currents still travel through the copper or aluminum end rings and can produce significant I^2R losses and heat despite the relatively low end ring impedance. Adjusting the equivalent rotor conductivity, or equivalently, assuming a somewhat longer effective bar length, are two common equivalent circuit strategies to calculate more accurate total rotor losses by examining only the bar losses with appropriate adjustment to account for the impact of the end rings. The inter-bar losses vary with both the bar length and rotor bar conductivity, so both of these strategies will introduce additional error in the calculated inter-bar currents. An improved but more complicated solution considering arbitrary end ring

impedance can be used to more accurately calculate the total rotor losses of any rotor. This is the most general and realistic case that will be used for all future calculations.

3.6.1 Alternate Integration Constants

The goal is to solve the same differential equation using alternate boundary conditions to determine the new rotor bar current, now including end rings of arbitrary impedance. A hybrid strategy combining methods from Rossmair and Alger, consistent with the equations given by Weppler and Subba Rao, determines integration constants for any given end ring impedance while aligning with equivalent circuit calculations. Odok's original simplified expression assumes end ring impedance to be negligibly small and was applied only to higher order harmonics. Applying this approximation to the rotor fundamental can significantly underestimate losses. The difference may be on the order of 10-20% in typical induction machines but are closer to 30% on the tested five hp machines. The end ring impedance is much less significant for the higher order harmonics, with smaller pole pitch and reduced ratio of end ring path to bar length.

The diagram of a section of the rotor, repeated here as Figure 3-8, will again be examined, now with arbitrary end ring resistance between neighboring bars, R_R, at both ends.

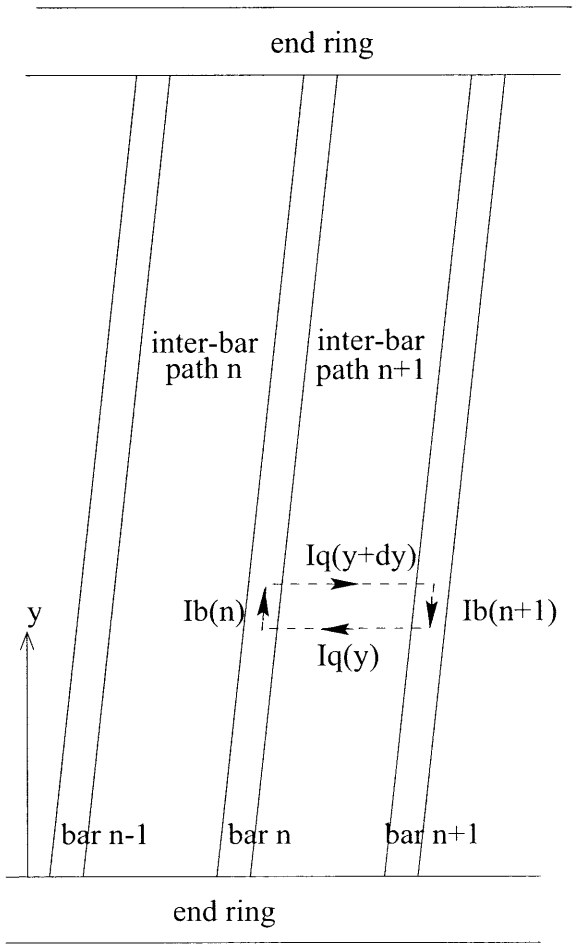

Figure 3-8: Rotor section used in inter-bar loss equation derivation

The voltage between bars at either end of the rotor will be equal to the current in the ring times the resistance of that section. The bar current at either end of the stack is $I_b(y = 0)$ or $I_b(y = L)$. However, the bar currents flow a varying distance around the end rings, with currents from multiple bars combining at any point along the ring. Assuming an approximately sinusoidal distribution of rotor currents around the rotor bars, Alger integrates the bar currents over a half pole pitch to obtain the ratio of end ring to bar current as $\frac{N_R}{2Pn\pi}$ where N_R is the number of rotor bars and P the number of pole pairs.[6] Multiplying the square of this ratio with the end ring impedance gives the effective end ring resistance for use with the rotor bar current to calculate equivalent total end ring loss without using the actual, larger end ring currents combined from multiple bars.

Rossmaier applied an additional constraint to the end ring current. Still assuming a sinusoidally distributed end ring current results in a phase shift between consecutive end ring sections. As with the also sinusoidal bar or inter-bar currents, the current in the "n^{th}" end ring segment is equal to the next section phase shifted by the angle between neighboring bars.[9]

$$I_{R(n)} = I_{R(n+1)}\, e^{-j\delta} \tag{3.42}$$

Current continuity at each bar end also requires that the bar current at either end must equal the difference in neighboring end ring currents.

$$I_{R(n)} = I_{R(n+1)} + I_{B(n)} \tag{3.43}$$

These two equations, (3.42) and (3.43), combine to give the following relation between the ring and bar current.

$$I_R(n) = \frac{I_B(n)}{1 - e^{-j\delta}} \tag{3.44}$$

Using this ratio to refer the actual end ring resistance to a value for use with the bar current results in another correction factor, this time equal to the square of the

magnitude of $\frac{1}{1-e^{-j\delta}}$, or $\frac{1}{4\sin^2(\delta/2)}$ as given in Rossmaier's equation (5).

The above equations are correct regardless of the bar and end ring currents, but the correction factors applied to the end ring resistance relate the peak or rms value of the sinusoidally distributed rotor bar current to the peak or rms value of the also sinusoidally distributed end ring current. However, the peak ring current occurs physically near the minimum bar current, out of phase by $\frac{\pi}{2}$ with the peak bar current. Minimum actual ring current flows either into or away from the bar carrying peak current. This generates some difficulty and error in the simple application of end ring boundary conditions. Ideally, results from analyzing a single bar and section between two neighboring bars could be multiplied by the number of bars to account for the full rotor.

The actual, physical resistance of a section of end ring combined with the rotor bar current will underestimate end ring losses, neglecting the combination of bar currents in the end rings, and result in an underestimated stator current and rotor losses. Conversely, employing the effective, adjusted resistance of an end ring section together with the bar current calculated correct total end ring losses. This calculation overestimates the voltage across the section of end ring acting. The values of peak bar current and effective end ring section resistance are both greater than the physical end ring current near the peak bar and the actual resistance of an end ring section and calculate an inflated end ring boundary voltage. However, for typical machines, even this overestimated voltage for the end ring section still does not significantly impact the distribution of inter-bar currents.

The fundamental end ring losses may be appreciable and should be included, but the error in end ring voltage has had negligible impact on the current and loss calculations for the motors examined. The end ring impedance is necessary for calculating total fundamental rotor losses and determining the stator current and rotor slip of the motor operating point but otherwise has not significantly impacted the calculation of either fundamental or harmonic rotor losses.

The final effective resistance of a single section of end ring between neighboring bars, R_{Re}, not yet referred to the stator winding, is given by equation (3.45).

$$R_{Re} = \left(\frac{2\,\pi\,R}{N_r\,\sigma_r\,L_E\,h_E}\right)\left(\frac{N_r}{2\,\pi\,n\,P}\right)^2\left(\frac{1}{4\sin^2(\frac{/delta}{2})}\right) \tag{3.45}$$

With both inter-bar and end rings currents defined positive as flowing from left to right in Figure 3-8, the two boundary conditions for determining the integration constants in (3.46) and (3.47) equate the end ring and bar-to-bar voltages across the end ring and lamination sections at either end of the rotor.

$$V_{R0} = V_q(y = 0) \tag{3.46}$$

$$V_{RL} = V_q(y = L) \tag{3.47}$$

The physical resistance, R_R, of a section of end ring between neighboring bars is roughly approximated as the length between bars divided by the area of the end ring cross section and conductivity. This assumes that the current is roughly equally distributed over the end ring. If the end ring is over sized, the current may not be equally distributed resulting in a larger effective ring resistance. The length between bars is slightly overestimated here as the total rotor circumference divided by the number of bars. This distance could be taken at the middle of the end rings or averaged from the inner to outer end ring radius, but there is more significant uncertainty in the exact value of the as-cast ring conductivity.

$$R_R = \frac{2\,\pi\,R}{N_R\,\sigma_R\,L_E\,h_E} \tag{3.48}$$

In calculating the end ring segment resistance, R is the rotor radius, N_R the number of rotor bars, σ_R the ring conductivity, L_E the axial ring length, and h_E the radial ring height.

The solution for the rotor bar current, I_b, as a function of axial position along the rotor, y, in terms of the complex integration constants C_1 and C_2, is repeated below as (3.49). End ring boundary conditions can be applied to solve for the unknown complex constants, C_1 and C_2.

$$I_b(y) = C_1 e^{\gamma y} + C_2 e^{-\gamma y} + \frac{E e^{j\alpha y}}{Z_{qs}(\gamma^2 + \alpha^2)} \tag{3.49}$$

The inter-bar current I_q can be found as a function of the bar currents, repeated below as (3.50).

$$I_q(y) = \frac{dI_b(y)}{dy} \frac{e^{j\delta/2}}{2jsin(\delta/2)} \tag{3.50}$$

In these equations, as before, Z_{qs} is a scaled version of Z_q, the impedance between bars, E is the induced voltage per bar per unit bar length, and the per bar impedance Z_r also includes mutual and leakage reactance terms since the induced voltage depends on both the rotor and stator currents. The term δ is the phase angle between adjacent rotor bars, α is the rotor bar electrical skew angle per unit length, and γ is a propagation constant given by $\sqrt{\frac{Z_b}{Z_{qs}}}$.

The voltage between bars can be found by multiplying the inter-bar current and resistance values.

$$V_q(y) = -Z_{qs} 2jsin(\delta/2) e^{j\delta/2} \left[\gamma C_1 e^{\gamma y} - \gamma C_2 e^{-\gamma y} + \frac{j\alpha E e^{j\alpha y}}{Z_{qs}(\gamma^2 + \alpha^2)} \right] \tag{3.51}$$

The two arbitrary, complex integration constants can be solved by substituting the equations for V_q and I_y into the two boundary conditions at either end of the rotor given by (3.46) and (3.47) and simplifying.

The first boundary condition including the equations for inter-bar voltage and bar current is evaluated at $y = 0$.

$$X\,\gamma C_1 - X\,\gamma C_2 + \frac{j\alpha\, X\, E}{Z_{qs}\,\beta} = C_1 + C_2 + \frac{E}{Z_{qs}\,\beta} \tag{3.52}$$

A number of terms have been grouped together and written as X to simplify the expression.

$$X = \frac{4\pi P Z_{qs} \sin(\delta/2) e^{j\delta/2}}{N_R R_R} \tag{3.53}$$

This first boundary condition can be solved for the integration constant C_1 in terms of C_2.

$$C_1 = \frac{C_2(X\gamma + 1) + \frac{E}{Z_{qs}\beta}(1 - j\alpha X)}{X\gamma - 1} \tag{3.54}$$

Similarly, the second boundary condition is evaluated at $y = L$.

$$X\left[\gamma C_1 e^{\gamma L} - \gamma C_2 e^{-\gamma L} + \frac{j\alpha E e^{j\alpha L}}{Z_{qs}\beta}\right] = C_1 e^{\gamma L} + C_2 e^{-\gamma L} + \frac{E e^{j\alpha L}}{Z_{qs}\beta} \tag{3.55}$$

The second boundary condition can be solved for C_2 by substituting the solution for C_1 in terms of C_2.

$$C_2 = \frac{E(1 - j\alpha X)(e^{\gamma L} - e^{j\alpha L})}{Z_{qs}\beta(X\gamma + 1)(e^{-\gamma L} - e^{\gamma L})} \tag{3.56}$$

Comparing calculations using these new integration constants, the sum of the bar and inter-bar losses still agree exactly with the single equation calculations for the extreme cases as the ring resistance approaches zero or infinity. These two complex integration constants can be used along with the equations for bar and inter-bar losses to determine the losses for any rotor, regardless of end ring impedance.

3.7 Comparison of Rotor Loss From Calculation and Measured Tests

The restriction of the fixed operating current and slip restrict the application of the rotor loss calculations to known test points. Examination of variations in rotor parameters remains for Chapter 5, using the rotor loss calculations as part of a full circuit model. The following set of plots compare values of stray load loss and fundamental rotor conduction loss from measured test results and calculations. The calculated stray load loss consists of the rotor I^2R conductor losses from eight calculated harmonics, the four lowest, "belt," space harmonics of order 5, 7, 11, and 13 as well as the first and second order pairs of stator slot space harmonics, $\frac{N_s}{p} \pm 1$ and

$\frac{2N_s}{p} \pm 1$, where N_s is the number of stator slots and p the pole pairs. The harmonics generally decay as the inverse of the square of the harmonic number, so this limited set is expected to be representative of the appreciable harmonic bar losses in the rotor for most cases. Eight different load points from no load to 150% of the full load are displayed for a selection of cast five and ten horsepower motors in the remaining plots, Figures 3-9 to 3-15 in this section. For all of these plots, an error of less than plus or minus ten percent is a reasonable estimate for the error in "measured" fundamental rotor and stray load loss. As shown in Chapter 5, the worst case measured stray load loss error could reach as high as plus or minus thirty or forty percent, but that is an unlikely extreme, and the non-skewed aluminum rotors showed about a 10% variation in measured stray load loss.

The triangular points compare the calculations of the fundamental rotor loss to values determined according to the IEEE 112 test standard as the measured slip multiplied by the air gap power, calculated by subtracting the stator copper and no load core losses from the measured input power. The calculations of fundamental rotor losses generally agree with the test data, across all of the machines and rotors.

Calculations of stray load loss are more difficult and variable, but including the impact of inter-bar currents universally improves the correlation between predictions and test values. Stray load loss calculated assuming infinite inter-bar impedance is equivalent to traditional equivalent circuit calculations without inter-bar currents. With insulated rotor bars, skew can effectively reduce slot harmonic rotor bar currents and losses, minimizing stray loss from slot harmonic rotor conductor loss.

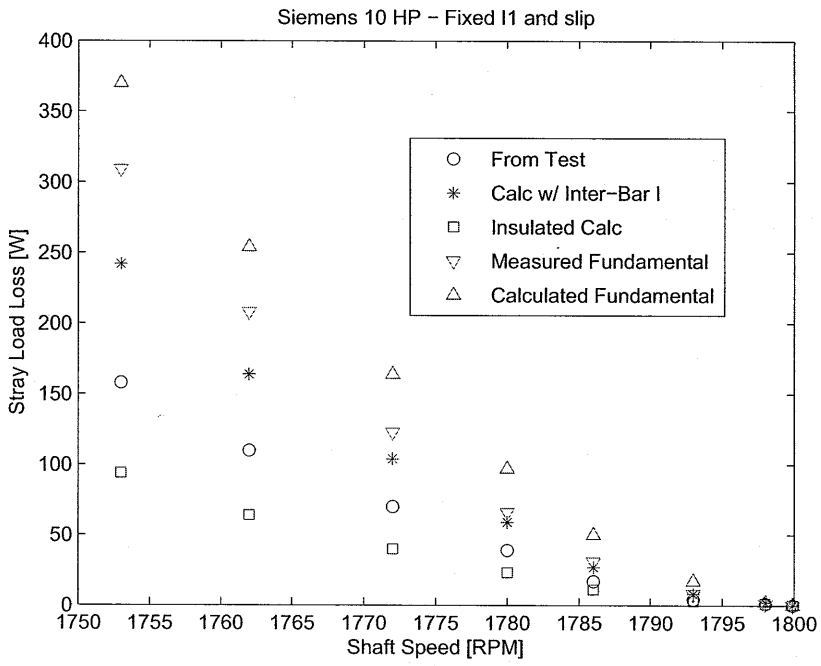

Figure 3-9: Design #1 10 hp cast copper load points with fixed speed and stator current without combining core and air gap reactances

Initial calculations overestimate the stray load loss for the Design #1 ten horsepower machine in Figure 3-9. However, using the parallel combination of the air gap reactance and a core excitation reactance for an effective value of magnetizing reactance in the calculations of harmonic reactance values produces a much closer match. The core excitation reactance represents the energy stored and mmf drop over the non-infinitely permeable motor laminations and can be calculated similarly to the core loss using manufacturer excitation power data and calculated mass and magnetic flux density for the motor teeth and back iron.

All harmonics have magnetizing and components of leakage reactance calculated as a function of the fundamental air gap reactance. The fundamental air gap reactance is typically reduced through an effective Carter-corrected air gap length, greater than the physical dimension to account for the redistribution of air gap magnetic fields from the stator and rotor slots. An additional "saturation" correction factor is also often applied to further reduce the fundamental air gap reactance.[19] The equivalent reactance as the parallel combination of core and air gap values is consistent with the

"saturation" factor, used to account for the mmf drop in the core laminations.[20]

The next plot repeats the calculations on the same design #1 cast copper ten horsepower motor, but now, the effective, combined air gap and core reactance value, is used in the harmonic reactance calculations. The calculated stray load loss in Figure 3-10 now agrees with the test values.

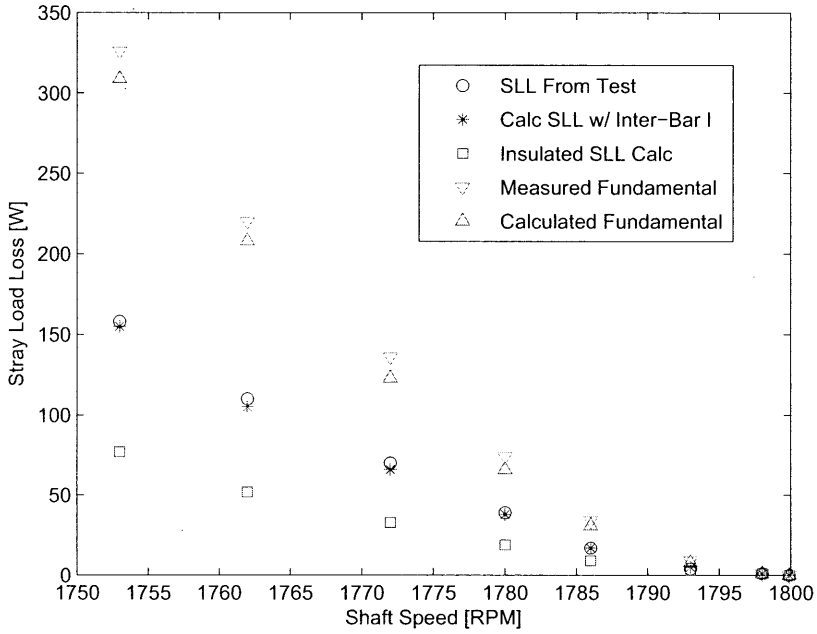

Figure 3-10: Design #1 10 hp cast copper load points with fixed speed and stator current with combined core and air gap reactance

The next two figures compare results for a completely different ten horsepower cast copper motor, design #2. The original motor of Figure 3-11 includes an 18 mil air gap. This motor measured higher than expected stray losses. Including the impact of inter-bar currents increase the calculated loss closer to the test results, but the predictions still significantly underestimate the measured stray loss. Additional sources of potential stray loss are examined briefly in Chapter 5. Figure 3-11 gives results for the exact same motor except with the rotor outer diameter machined down to give a 25 mil air gap. The increased air gap effectively reduced the stray load losses and improved the correlation between prediction and test.

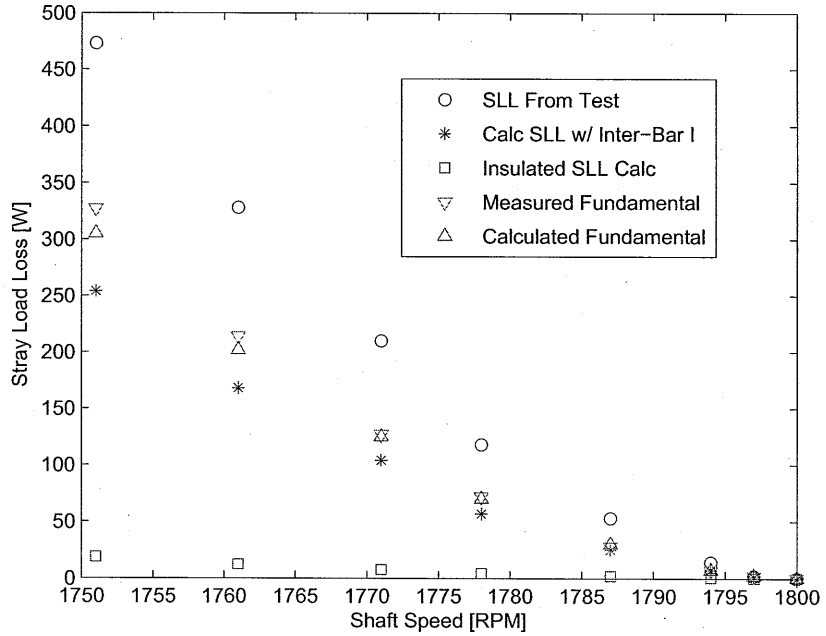

Figure 3-11: Design #2 18 mil gap "High SLL" 10 hp cast copper load points with fixed speed and stator current

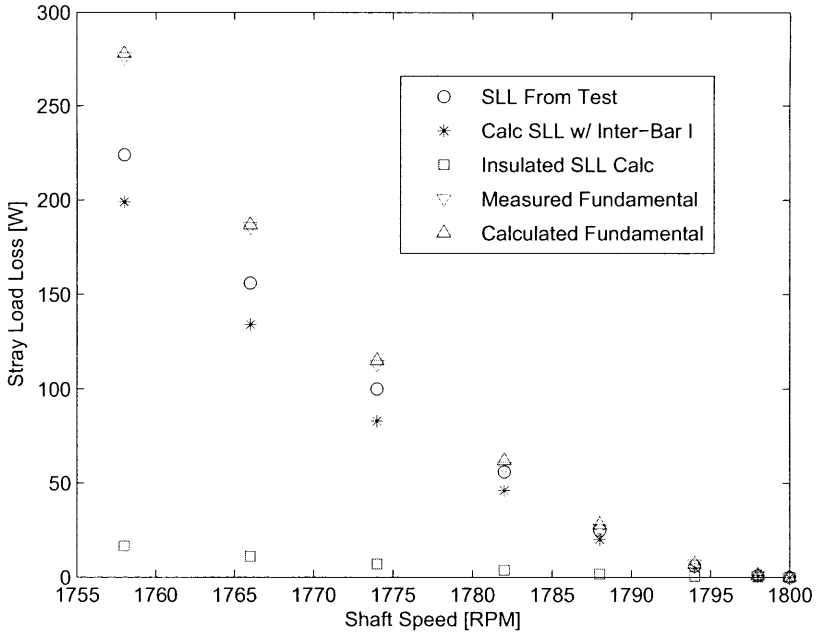

Figure 3-12: Design #2 25 mil gap "Low SLL" 10 hp cast copper load points with fixed speed and stator current

The next plot, Figure 3-13, compares calculations to values from test on a cast aluminum five horsepower motor with skew. As with the non-skewed rotors, the predicted stray loss falls well below the test value.

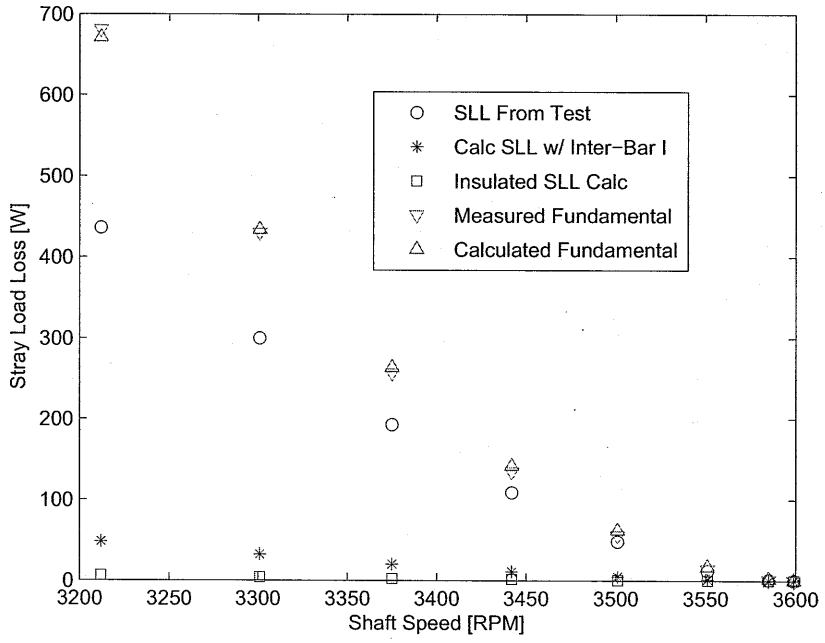

Figure 3-13: 5 hp cast aluminum load points with fixed speed and stator current

As designed, with reactance values as calculated and one stator slot of skew, the predicted losses are low on the five horsepower machines. The calculation including inter-bar currents is still an improvement, slightly closer to the measured values when compared to the insulated case. The remainder of the stray losses could be from a completely different source, but the pronounced dip in the measured torque speed curves for these machines in the high slip region around the synchronous speed of the slot harmonics suggests that the stator slot space harmonic losses are more significant than predicted. This is consistent with the equivalent circuit calculations of the non-skewed aluminum rotors from the previous chapter. Calculations of space harmonic loss and high slip torque appeared to significantly underestimate the impact of slot harmonic loss and torque. Reducing the differential or zigzag leakage reactance terms is one option to increase the predicted rotor losses closer to measured levels.

The final rotor examined in this section is a skewed, five horsepower cast copper motor. Figure 3-14 shows an example plot of six different rotor harmonic losses plotted against a varied value of average inter-bar contact resistance. In this case, the stator current and slip are assumed constant at the measured full load values

and the measured full load stray loss was about 112 watts. The total stray loss peaks rather strongly at values of inter-bar contact resistance of around 10 micro-ohm meters. The measured value of inter-bar resistance in this case (from Chapter 4) was about 2 micro-ohm meters.

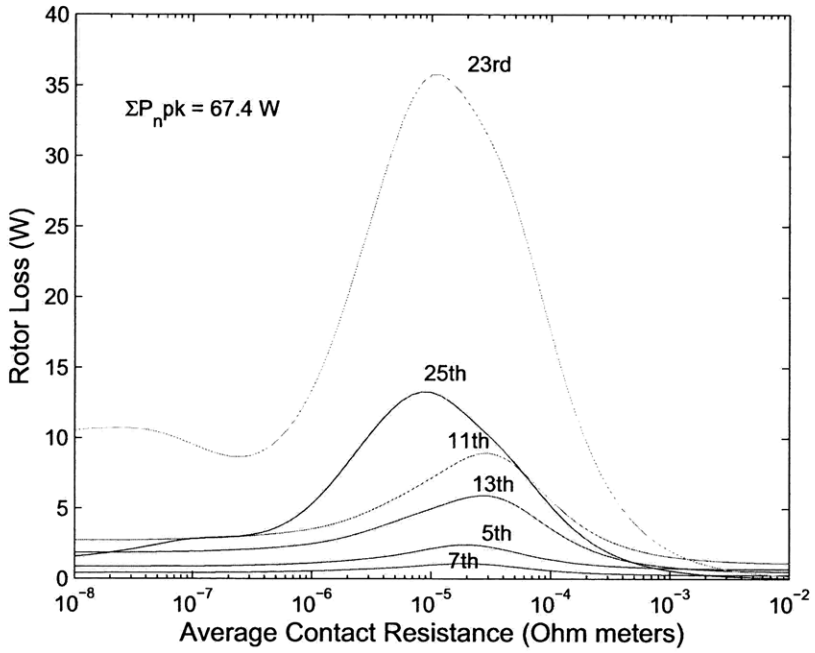

Figure 3-14: Baseline case Cu in Al rotors with 1 slot skew and unadjusted reactance

Adding an arbitrary adjustment factor of 0.6 to the harmonic leakage reactance terms increases the harmonic losses as shown in Figure 3-14. The total sum of the peak values of all six harmonics, at about 108 watts is now very close to the 112 watt "measured" value.

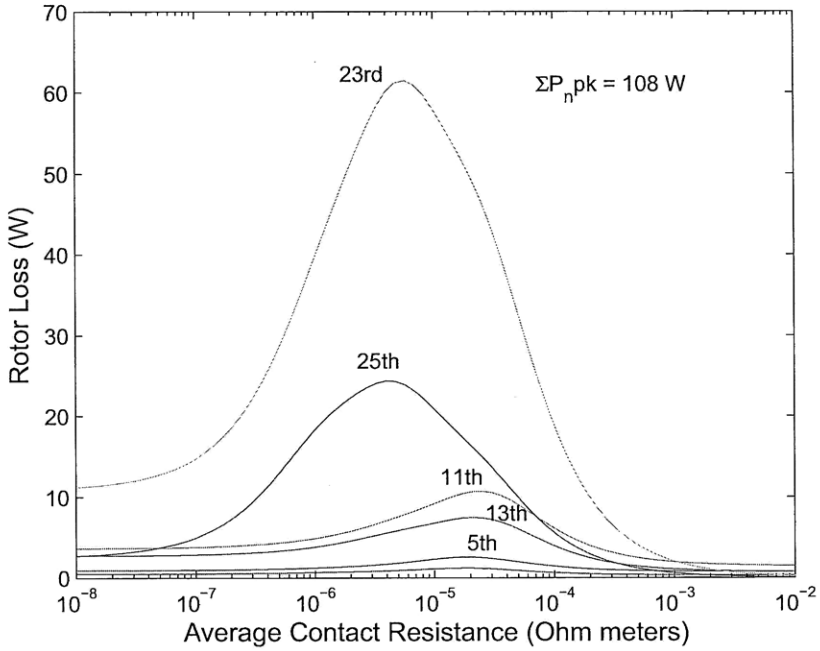

Figure 3-15: Cu in Al rotor with 1 slot skew and 0.6 reactance

3.8 Summary and Conclusion

This chapter re-derived and then re-solved the classic differential equation for rotor bar current as a function of position along the rotor length. Total rotor loss calculations have been checked by comparing single evaluations of the total loss to separate calculations of bar, between bar, and end ring loss. The full range of possible boundary conditions have been examined from negligible to infinite end ring resistance, with the arbitrary resistance case applicable for these extremes as well as any intermediate value. Finally, plots compared calculation results for rotor loss to measured values for a series of load points on a number of different machines. The rotor losses including inter-bar currents were an improvement over the insulted case, producing results closer to the measured values. However, as with the cast aluminum rotors with no skew from the previous chapter, the equivalent circuit reactance values required some adjustment in order to calculate more realistic values. These rotor equations depend on a number of motor design and operating point values that must be previously de-

termined through measurement or calculation. Incorporating the rotor loss equations into an equivalent circuit framework will allow for predictions of motor performance under any operating conditions. An average value of inter-bar resistance is the only new variable. The next chapter describes the measurements of inter-bar resistance, before using the values in the adjusted equivalent circuit calculations of Chapter 5.

Chapter 4

Inter-bar Resistance Determination

Accurate rotor current and loss calculations require an approximate average value of bar-to-bar resistance. The cross resistance includes the bar-to-lamination contact resistance from each bar together with the impedance of the lamination path between bars. All of the measured rotors fit into one of two classes of inter-bar resistance. The large contact resistance values on some rotors dominate the total bar-to-bar resistance and allow direct calculation of the contact resistance from measured dc voltage and current. On other rotors, smaller values of contact resistance were closer to the now appreciable values of bar and lamination resistance, and comparison between measured and calculated voltage profiles were used to determine approximate resistance values. In all cases, the value of contact resistance appears to vary with the rotor bar shape, conductor composition, and casting procedure and is difficult to predict or measure. Values can vary significantly, and seemingly arbitrarily, among nominally identical rotors and among individual bars around a particular rotor. This chapter describes the procedure and results of the determination of rotor bar-to-bar resistance on sets of five horsepower (about 3.75 kW) cast copper and aluminum and ten horsepower (about 7.5 kW) cast copper rotors. The determined resistance values will later be used to calculate total rotor loss for comparison to stray load loss from measured tests.

4.1 DC Voltage Measurements

Only dc voltages have been used in this study to determine values of contact resistance which, more generally, could be impedance values. The literature also usually neglects any inter-bar reactance. Independent measurements over a wide range of frequencies by both Odok and Christofides concluded that the inter-bar impedance was dominantly resistive, although adjustments were included to account for the concentration of current towards the bar tops as the rotor frequency increases.[17, 30] However, at least one dissenting opinion more recently by Watterson et al. measured an appreciable inductance as part of the inter-bar impedance term.[14] It also seems plausible that a thin insulating layer between the conducting rotor bar and laminations could contribute a small amount of capacitance. Any small contact reactance would also assume greater significance for rotors with low contact resistance. No inter-bar reactance has been measured or included in this study, although the resistance value in later equations can easily be adjusted to include additional reactance values. The main contribution of previous inter-bar loss studies has been identifying that maximum stray loss due to inter-bar currents can exist at intermediate, as opposed to extreme high or low, values of bar-to-iron contact resistance. Increasing or decreasing the contact resistance can either raise or lower losses depending on the motor design and initial value of inter-bar resistance. The actual value of contact resistance must be known in order to identify the starting location on the loss curve and to predict how a change impacts rotor loss.

A variety of methods have been used in the past to measure the approximate bar-to-lamination contact resistance. Odok used a non-destructive method, applying current to the rotor shaft and one end ring while measuring the average voltage drop between the open-slot rotor bars or opposite end ring and laminations.[17] A number of other authors performed destructive rotor measurements where the rotor shaft is pressed out and the end rings removed.[30, 15, 13, 14, 31, 32] This procedure allows contact to be made directly at the end of each bar. While requiring more preparation and ruining the rotor, this method exposes the variation between bars and reduces

the number of unknowns in the rotor model by removing the shaft resistance and the shaft-to-lamination contact resistance.

The rotors of this study were prepared for dc voltage measurement following the destructive method of removing the rotor end rings to provide contact points to each individual rotor bar.[30] With the end rings removed, a current can be applied to or removed from the ends of any two rotor bar, and voltages can be measured between any two points on the rotor, typically other bar faces. For all dc voltage measurements in this study, a fixed ten amp current was driven through the exposed ends of different pairs of bars while measuring the voltage between the same two bars at the free ends. The voltage measurements are taken at the bar ends opposite the current connections to eliminate any error from varied current distribution on the bar face around the connection point and because the bars with current connections are easy to identify and are separated by relatively large voltages. Current connections using brass screws in each bar or banana clips attached directly to each bar yielded identical results.

As the rotor is one solid block of conducting metal, any measured voltages are small, typically in the range from micro-volts to milli-volts when applying a ten amp current, depending also on the rotor resistance values and location of the current leads. Four wire measurements were used to prevent any resistance from the current source or measurement leads from impacting the measured voltages. Two sets of measurements, often used for inter-bar resistance measurements, applied current to bars faces at either the same side or opposite ends of the rotor while measuring the resistance between the same two bars at the ends opposite the current leads.[31] These two types of tests can be repeated with any number of bars separating the bars where current is applied and removed, as shown in Figure 4-1 for the case of a single intervening bar. Measurements are repeated on every bar, using successive pairs of rotor bars rotated around the rotor, in order to observe variation between bars and provide an accurate average value over the entire rotor.

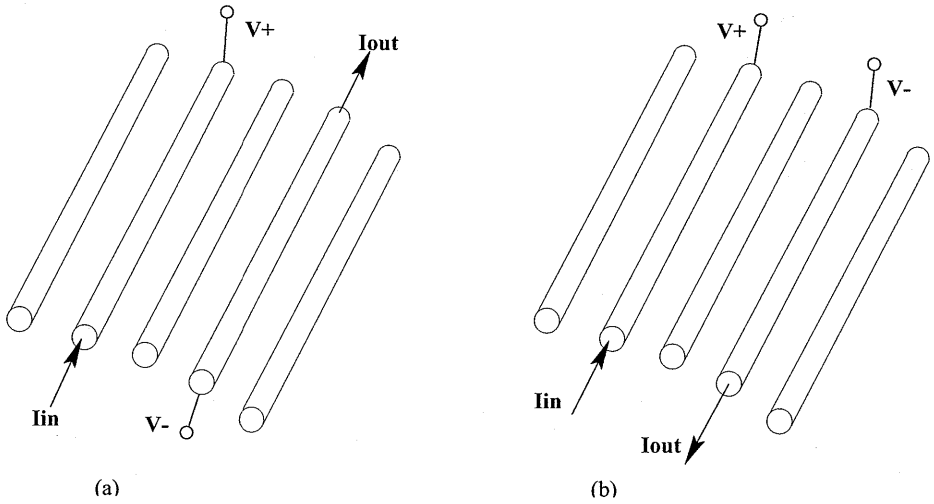

Figure 4-1: Common rotor dc voltage measurements

The measured dc voltage profiles can be grouped into one of two different categories. The two classes of rotors display either "high" or "low" contact resistance compared to the bar and lamination resistances. Different sets of measurements and methods of solving for the contact resistance are more effective for each type.

For the "high" contact resistance rotors, the contact resistance is much greater than the bar or lamination resistance. The voltage drop across the contact resistance dominates the equivalent circuit calculations. Each rotor bar may be treated as an equipotential node with the total resistance between any two bars equal to the sum of the contact resistance of the two bars and found by dividing the voltage measured between bars by the applied current.

Rotors with "low" contact resistance require a more complicated procedure because the voltage drop along bars is significant. The contact resistance is determined by comparing a number of dc voltage measurements to calculated voltages using a lumped parameter resistor model of the rotor and identical current conditions. An approximate average contact resistance can then be determined as the value that minimizes the total error between the predictions and the average measured voltages. This strategy requires a relatively accurate model of the rotor. Both the structure, including the position and interconnection of different resistors to recreate the available current paths, as well as the values for each of the individual elements, must ade-

quately represent the physical rotor. The measurement and calculation procedures for the "high" contact resistance case will be briefly discussed before examining the resistor model and calculations for the "low" contact resistance rotors.

4.2 "High" Contact Resistance

The bar-to-lamination contact resistance in the "high" case is much simpler to determine than on rotors with "low" contact resistance. In the inter-bar current literature traditionally measuring cast aluminum rotors, the resistance of the iron path between bars is typically assumed to be negligible compared to the much greater rotor bar contact resistance. For the case of "high" contact resistance rotors, the contact resistance per unit length must also be much greater than the bar resistance per unit length.

The two types of dc voltage measurements, with connections at the same side or opposite ends of the rotor, yield essentially identical results on the "high" contact resistance rotors. The spacing, in number of skipped bars, between the current connections is also irrelevant. With the contact resistance far greater than the bar or lamination resistance, any measurement records only the sum of the contact resistances of the two bars with the current connections. The dc inter-bar currents (on the rotor with no end rings) distribute uniformly along the rotor length to minimize the voltage drop over the contact resistances between bars, and each rotor bar can be treated as a single voltage point.

As the current injection and removal points are spread out, with higher numbers of bars between the two points, there is a slight voltage increase from the greater resistance of the longer path length through the iron laminations between the two bars. However, this slight increase is obscured by the much greater variation in contact resistance among particular bars. Voltages on neighboring bars with contact resistance on the higher end measure much larger than similar readings taken on bars with lower contact resistance, even if they are on opposite sides of the rotor.

The rotors having relatively high contact resistance can be modeled by a two dimensional, star-like resistor arrangement shown in Figure 4-2. Each resistor rep-

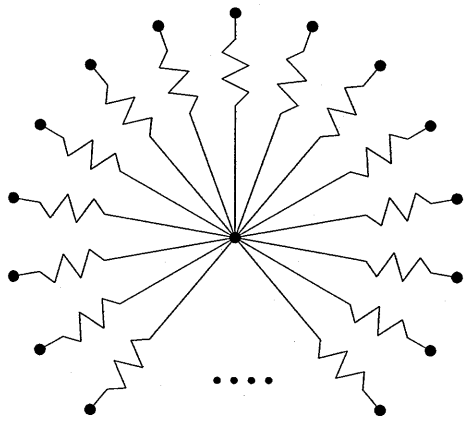

Figure 4-2: "Large" contact resistance dc rotor circuit model

resents the full length contact resistance in ohms of a different rotor bar and should be multiplied by the total stack length in order to compare per-unit-length values in units of ohm meters between machines. The total resistance between bars is multiplied by the rotor length because if the contact resistance for each bar is treated as a traditional, linear, $\frac{L}{\sigma A}$, resistance, the resistance value is inversely proportional to the bar length and total contact area, A. The "length" term, L, directly proportional to the contact resistance, would be a function of the thickness of the oxide layer or the depth for an average conductivity value, σ, around each bar.

The contact resistance, and variation in contact resistance from bar to bar, are large and dominate the measured rotor voltages for the rotors with the "high" type of inter-bar resistance. In this case, the bar and iron resistances can be ignored with negligible error. There appears to be insignificant change along the length of this type of rotor because measurements show negligible difference taken with currents applied either at one end or end-to-end across the rotors, using any combination of ends for each particular pair of bars. Every bar acts as a single equipotential node.

Measurements are simplified on these rotors with "large" contact resistance as the only measurable quantities are the contact resistances for each bar. Voltage measurements between any two bars divided by the applied current give the sum of the contact resistances for those two bars. Contact resistance values for each individual bar can be solved directly by combining measurements on bar pairs. For example, voltage measurements of all three combinations of bar pairs on any group of

three bars could be combined to solve for each of the three contact resistance values. However, only a single average value of contact resistance per rotor is required for inter-bar loss approximations, so one half of the contact total resistance from each pair of bars can be averaged directly. The contact resistance for each individual bar is unnecessary. However, an accurate average of the varying bar values around the rotor requires the measurement of pairs of contact resistance including every bar. Figure 4-3 below shows the measured contact resistance values for all twenty-nine bars on a five horsepower cast copper rotor. The three sets of measurements were taken with current injection and removal points on neighboring bars or separated by seven or thirteen intervening bars. Typical error in the contact resistance values and dc voltage measurements was less than plus or minus two percent of the measured total for the cast aluminum rotors, with measured voltages around 1 millivolt. This combines possible variation in input current, rotor temperature, and a worst case plus or minus five microvolt drifting offset in the voltmeter. The copper rotors measured dc voltages in some cases around one-hundred microvolts, so typical error could be as high as plus or minus six percent for those cases. However, even though the percent uncertainty in measurement voltage values and determined contact resistance increase with the smaller measured voltages, the variation in values from bar to bar also reduce. As shown in Figure 4-3, the total bar contact resistance varies by at least about a factor of five from the lowest to the highest measured bars. As the final rotor equations use only a single average value of inter-bar resistance, this factor of five variation is much more significant than the measurement uncertainty and is an important source of error in the approximate average values of inter-bar resistance and calculated total rotor loss.

Total average values of contact resistance increased slightly when comparing measurements taken on bars on opposite sides of the rotor (skipping 13 bars) compared to neighboring bars (skip 0). On a few rotor bars near the end rings, visible conductor dendrites had leached between laminations to make contact between neighboring bars. If not removed, these pathways reduced or fully short circuited the measured voltages between neighboring bars. In a few cases, insufficient laminations were re-

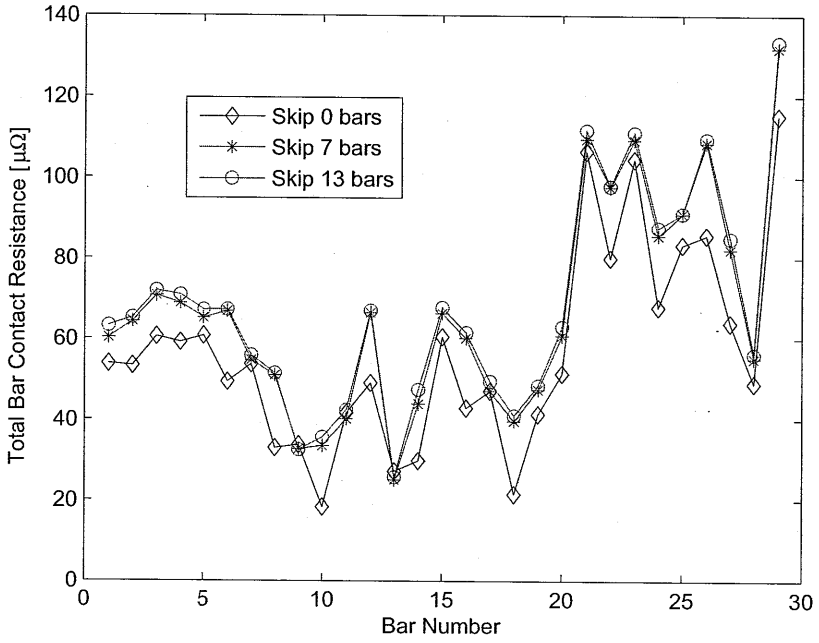

Figure 4-3: Variation in cast aluminum bar contact resistance

moved to eliminate all of these small connections between bars, and the low voltage measurements between these adjacent bars provided no information on the value of contact resistance. This contributes to the lower contact resistance values measured between neighboring bars.

The border between "high" and "low" values of contact resistance depends on the ratios between contact, rotor bar, and lamination resistance values rather than fixed numerical limits. Average contact resistance values down to 1.0 $\mu\Omega m$ were measured on a "high" contact resistance rotor while a 1.2 $\mu\Omega m$ value was determined for a "low" contact resistance rotor. Despite the similar magnitude of contact resistance values for these cases, the measured voltages still clearly fit either the "high" or "low" contact resistance profile. With "low" contact resistance rotors, the measured voltages consistently increase with bar spread and are different for the two sets of tests with current applied and removed from one same side or opposite ends of the rotor. The voltages from "high" rotors are independent of the testing arrangement, depending only on the particular bars measured. The "high" type rotors could be described more accurately as "contact resistance dominated," independent of the actual value

of contact resistance. The more general "low" category of contact resistance describes any rotor where the contact resistance is not completely dominant, again independent of the actual resistance value.

4.3 "Low" Contact Resistance

For "low" contact resistance rotors, the voltage drop along both the rotor bars and the lamination sections between bars become appreciable. For this case, the same side and opposite end current configuration tests yield different results, and the measured voltage between bars rises significantly as the length of the path through the laminations increases with bar spacing. The current crowds toward one end of the rotor if the current is injected and removed from the same side. The current travels into and along multiple bars if the current leads are on opposite rotor ends. With both the bar and lamination conductivities as well as the test setup impacting the voltages, additional measurements are necessary to determine the values of "low" contact resistance rotors.

4.3.1 Voltage Measurements

Again, the same two sets of measurements record the voltage difference between the exposed bar faces opposite the current leads either both on the same or on opposite ends of the rotor, as shown in Figure 4-1. After initially recording these same side and opposite end measurements at every possible separation, from neighboring bars to half a circumference with maximum intervening bars between current leads, five measurement points distributed between the spacing extremes give approximately equivalent results in far less time. The twenty-nine bar rotors use sets of measurements with currents applied to and removed from neighboring bars and bars separated by three, seven, ten, and thirteen bars. For each of these spacings, both same side and opposite end measurements are recorded between different bar pairs until every bar has been included in order to obtain the impact of each bar on the total average. To determine an average value of bar-to-lamination contact resistance the averages

of the sets of voltage measurements are compared to calculated voltages using a rotor resistance model. The average measured voltages for both the same side and opposite end measurements on four different five horsepower, cast copper rotors with "low" contact resistance are shown below in Figures 4-4 and 4-5. Typical error in the measured values is less than plus or minus six micro-volts. The voltages are measured opposite the bar ends where current is injected. This results in negative values for the tests with current applied and removed from opposite ends of the rotor and few intervening bars. With the low contact resistance, currents disperse through nearby bars before flowing along the rotor length, and the bar faces around the current input bar are at a higher potential than the bar faces around the current output bar. As the spacing and resistance between current leads increase, the current more uniformly distributes along the input and output bars to take advantage of all available iron lamination paths around the rotor between bars. All four of these different rotor designations are nominally of identical cast copper #1 design. All four rotors include rotor bars with the "double" rotor bar design and were expected to perform close to identically.

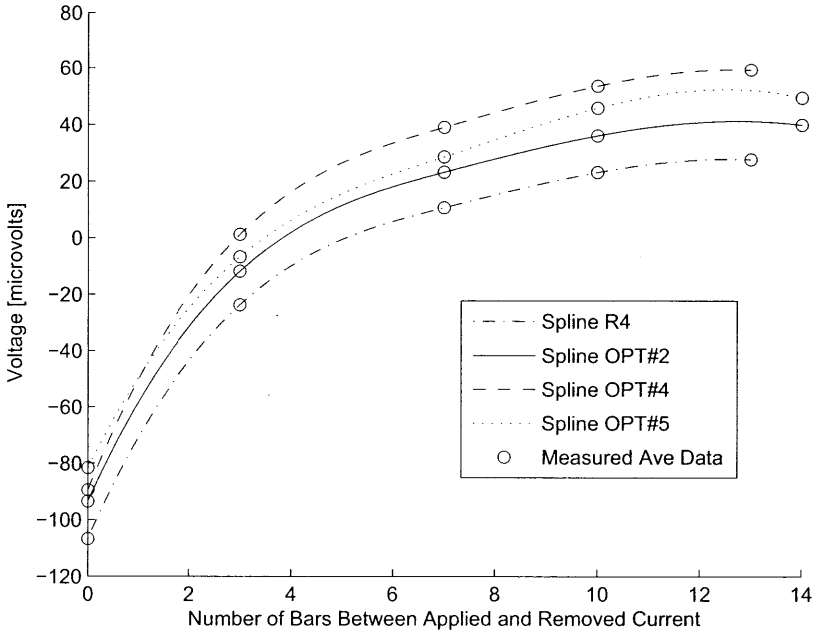

Figure 4-4: Average measured voltages on 4 different low contact resistance, Copper #1 5 hp rotors - Opposite side tests

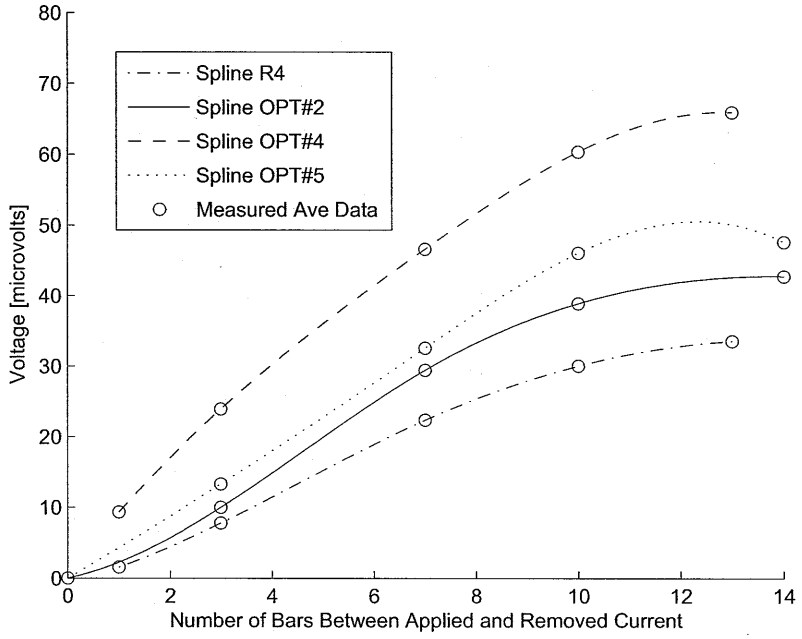

Figure 4-5: Average measured voltages on 4 different low contact resistance 5 hp rotors - Same side tests

4.4 Rotor Resistance Models

A variety of lumped parameter resistor combinations can model the physical rotors. The ideal configuration correctly recreates the voltage and current distribution across the rotor with a minimum number of elements. One of the simplest models includes only two neighboring bars of uniform conductivity and a uniform total resistance between them as shown below in Figure 4-6. R_a represents the resistance of axial subdivisions of the rotor bars and R_b the resistance of a section between neighboring bars, the sum of twice the contact resistance and the resistance of the iron path between bars.

The discrete model sections the rotor into any given number of slices, with the resistance values adjusting with the number of slices to give a finer or coarser representation of the rotor. If only two bars are considered, a set of ordinary differential equations can solve for the voltages continuously along the entire length of the ro-

tor, giving the limiting result of the discrete model with a large enough number of slices. The analytical solutions become difficult beyond the two resistor model considering only two neighboring rotor bars. The error between the exact and approximate solutions decreases as the number of slices increases, ranging from 7% of the total equivalent impedance between same side bar ends for the simplified two bar case at 50 slices down to 2% at 200 slices. This exact solution verifies the performance of the discrete rotor model in the simplest case. Later, the complexity of the discretized model is increased with additional bars, three-dimensional looping of the first and last bars through another inter-bar resistor, and additional resistors to provide alternate current paths.

The voltage at every bar face can be calculated with the lumped circuit model for any given current condition and compared to the actual measurements. With a representative model of the rotor and appropriate element values the voltages should closely match. The two element model works well when considering only two neighboring bars or when the contact resistance is negligibly small. However, this simplest model does not include all of the possible current paths and fails to accurately represent the measured voltages. Especially with higher contact resistances and greater separation of the current probes around the rotor, currents can circulate through the iron laminations, around any intervening bars. Current can travel in the iron from one bar to any other, bypassing the high contact resistance of every bar in between, as opposed to having to pass into and out of each bar while traveling around the rotor as in the first model. An additional resistance accounting for the voltage drop and conduction losses in the laminations between bars can be added to the total resistance between bars. This additional element also provides the path for current to flow from one bar to another without having to cross the potentially large contact resistance of each intervening bar.

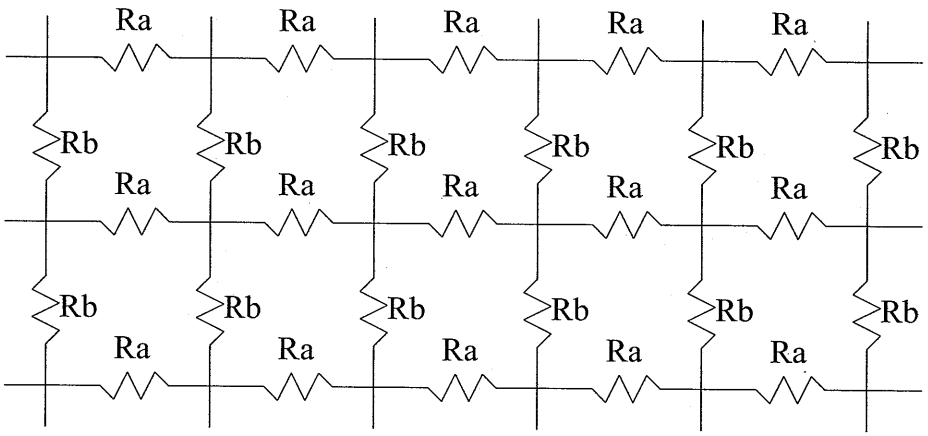

Figure 4-6: Simplest equivalent dc rotor circuit with shaft and end rings removed

Figure 4-7 shows a modified rotor resistance model, now including the resistance of the iron path, R_i, between the bars. R_a is again the resistance of an axial slice of a rotor bar. R_c is the average bar-to-iron contact resistance. The total resistance between two adjacent bars, R_b (not shown), would be the sum $2R_c + R_i$. Behdashti and Poloujadoff proposed a similar model in 1979 with the rotor shaft providing a zero resistance current path around the rotor and Watterson et al. in 1989 used this same model with a single resistance value for current paths between and around rotor bars.[25, 14] The average bar-to-lamination contact resistance for the "low" contact resistance rotors is determined by minimizing the error between the average measured voltages and those calculated using the resistor model shown in Figure 4-7 with varied resistance values.

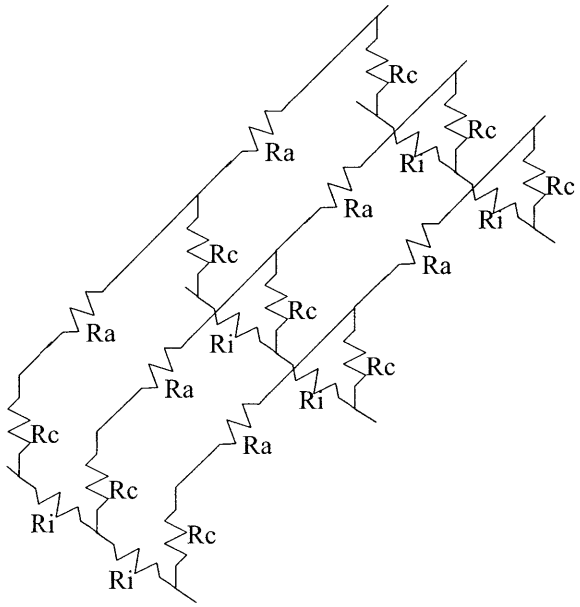

Figure 4-7: Reduced equivalent dc rotor circuit including iron path

4.5 Contact Resistance Determination

For the "low" case when the magnitude of the contact resistance is comparable to the resistance of the rotor bars, there is appreciable voltage drop across bar and iron resistances and determining the contact resistance becomes more complicated. The resistance along the length of an isolated, single bar can be approximately calculated using the standard resistance equation.

$$R_{bar} = \frac{L_{bar}\rho_{bar}}{A_{bar}} = \frac{L_{bar}}{\sigma_{bar}A_{bar}} \tag{4.1}$$

Here σ is the bar conductivity or ρ is the bar resistivity, L is the length of the conductor, and A is the area of the bar cross-section. Using the rotor length, cross sectional area of a bar, and 100% IACS (International Annealed Copper Standard) copper conductivity (58 MS/m) give an end-to-end dc resistance of about 73.7$\mu\Omega$ for a single, isolated bar on a five hp cast copper rotor. The actual, as-cast conductivity will be somewhat decreased by any impurities or voids from the casting process, giving an even higher bar resistance. Rough measurements of the dc resistance across each bar,

taken as the end-to-end voltage drop divided by the current applied across the same bar, revealed a significantly lower average resistance of about 22.1 $\mu\Omega$. With perfectly isolated rotor bars (infinite inter-bar resistance), the only current path is straight down the rotor bar. As the bar-to-bar resistance decreases, current takes advantage of the available parallel paths, flowing through and between increasing numbers of bars, and decreasing the measured voltage drop and total equivalent resistance across a single bar for a given applied current. For these low contact resistance cases, simulated rotor voltages must correctly account for all of the rotor current paths.

Rotors with "low" contact resistance measure zero or near zero voltage between neighboring bars on the same side tests with current applied and removed at one end of the rotor. The contact resistance is small enough compared to the bar resistance that all of the applied current flows between bars before reaching the far end of the rotor, as opposed to being evenly distributed along the bars as in the "high" contact resistance case. With "low" contact resistance, the voltage drop along the bar is a significant factor and comparable to the drop between bars through a lamination at any point along the rotor.

Determining the contact resistance for this case is complicated by having to also consider the current paths and voltage drops along bars and around the rotor laminations. The two sets of opposite end and same side dc voltage measurements from Figure 4-1 are compared to calculated voltage predictions using the resistance model of the rotor and consistent current placement. The final contact resistance average value minimizes the error between the measured and predicted voltages. Multiple points of local minimum error exist at different combinations of resistance values. Combining optimization for both the same side and opposite end tests, where changes to the resistance parameters can have opposite impact, results in convergence to a best fit set of voltage values.

Ideally, this strategy should be able to observe changes in "as-cast" bar or iron conductivity while simultaneously determining the average contact resistance. However, this has not yet been accomplished. There is significant variation between the actual measurements for each bar and the average value, and the model applies a

single value of average contact resistance to all of the rotor bars. This average value provides a realistic approximation to the averaged measured dc voltages and is the required parameter for motor inter-bar loss equations. However, this inherent variation adds significant error to the average calculation and makes accurate determination of the rotor bar or lamination iron resistance values difficult.

The value of rotor bar conductivity in the rotor model and calculations was manually constrained to fall in the reasonable range of 80% to 100% IACS. An approximate bar conductivity of about 90% IACS was used to calculate final contact resistance values. Surface conductivity measurements had recorded about 100% IACS after casting so this value may be low but remains a safe estimate in the neighborhood of the actual conductivity. For all of the "low" contact resistance five hp rotors tested except "R4", the unconstrained optimization process converged to a solution with too low of a rotor bar resistance, resulting in an impossibly high copper bar conductivity in the range of 10% above the maximum limit near 100% IACS. In the unconstrained optimization program, the range of possible resistance values ran from 10^{-5} to 10^{5} micro-ohm meter (10^{-11} to 10^{-1} ohm meters) for the iron and contact resistance values or 10^{-5} to 10^{5} micro-ohms per meter for the bar resistance term. Again, the difference in units arises from how the rotor length is included, directly or inversely proportional to the given resistance value. The rotor "R4" was the only sample to yield reasonable bar resistance values when unconstrained. The rotor "R4" also measured the lowest voltage magnitudes and variations, so the measured averages align closest with the actual measurements. The contact and iron resistance values, though more difficult to bound, remained in realistic ranges for all of the tested rotors.

An approximate sanity check for the resistance per unit length of the iron path through the laminations between bars can be calculated from the rotor geometry and lamination conductivity. The total iron resistance between neighboring bars is approximately equal to the average distance between bars divided by the lamination conductivity, the stack length, and the bar height. Multiplying by the stack length gives the resistance per unit length in Ωm, because the resistance of the iron path between bars can be approximated as directly proportional to the average distance

between bars and inversely proportional to lamination conductivity and the area of the iron path calculated as the bar height multiplied by the bar length. With a conductivity of about 1/20th 100% IACS, the iron resistance value is predicted to be in the vicinity of 0.1 micro-ohm meter. Similarly, the calculated contact resistance values are expected to be lower but of a similar order of magnitude as the values measured on the "high" contact resistance cast aluminum rotors with simpler bar shape.

The solutions, with the bar conductivity constrained, converge to realistic values of bar, lamination, and contact resistance, but the solutions are not unique. Equally good solutions, with similar total difference between calculation and measurements, can be obtained with small variations in the resistance values. These small variations are not as important for the roughly determined average value of contact resistance where even an order of magnitude estimation is generally sufficient for loss calculations. However, the variations prevent the differentiation of a five percent change in rotor bar conductivity that could be another potentially important variation between cast rotors. Approximate, reasonable values have been determined for total inter-bar resistance, but it has not yet been possible to precisely determine the rotor bar or lamination resistances or observe changes to these parameters between rotors. More accurate determination of all three resistance values may be possible if individual values of contact resistance are used for each rotor bar. The present method successfully generates order of magnitude estimates of the rotor-bar contact resistance and provides consistent results for comparison between similarly measured rotors. The following table and plots summarize the contact resistance values determined for each of the measured rotors.

4.6 Contact Resistance Results

A summary of the determined contact resistance along with the measured stray loss for both the five and ten horsepower, "high" and "low" resistance rotors is given below in Table 4.1. The data shows a general trend of increased stray load loss with

increasing contact resistance. The estimated average values of inter-bar resistance vary between rotors, but the OPT and R4 rotors of design #1 with the double rotor bars measured uniformly lower contact resistance than the CuinAl and R3 rotors, all of design #2 including the teardrop shaped bars. The cast aluminum rotors also measured significantly higher inter-bar resistance than the cast copper rotors, by as much as a factor of around 250 to 300 in some cases.

Table 4.1: Comparison of measured inter-bar resistance and full load stray loss

Rotor ID	**Full Load Stray Loss [W]**	**Inter-bar Resistance [microΩ meters]**
10 HP 5	95	2.5
10 HP 7	156	101.2
10 HP 11	92	1.8
10 HP 15	164	4.0
10 HP C6	126	4.6
10 HP C9	181	14.2
10 HP C10	250	21.6
10 HP G4	92	3.6
10 HP S	65	2.5
5 HP R4	128	0.8
5 HP OPT 2	182	0.9
5 HP OPT 4	234	1.6
5 HP OPT 5	250	1.9
5 HP R3	112	2.0
5 HP CuinAl 1	298	21.2
5 HP CuinAl 2	253	4.2
5 HP CuinAl 3	160	3.8
5 HP Al 1N	77	290
5 HP Al 4N	79	276
5 HP Al 2S	180	244
5 HP Al 3S	157	236

Figure 4-8 below compares the measured and simulated results for the five different ten horsepower rotors with "low" contact resistance. The lines show the measured data as best fit splines through five points of increasing separation between the applied and removed currents, with each point averaged from measurements taken on every bar around the rotor. All voltage measurements are recorded while injecting a fixed

ten amp dc current. The individual points using different shaped markers are the calculated voltage values that best fit the measured curves. The value of contact resistance used for each rotor, rc, is given in units of micro ohm meters. All of the ten horse power rotors included a "double" bar shape with a leakage neck and starting bar.

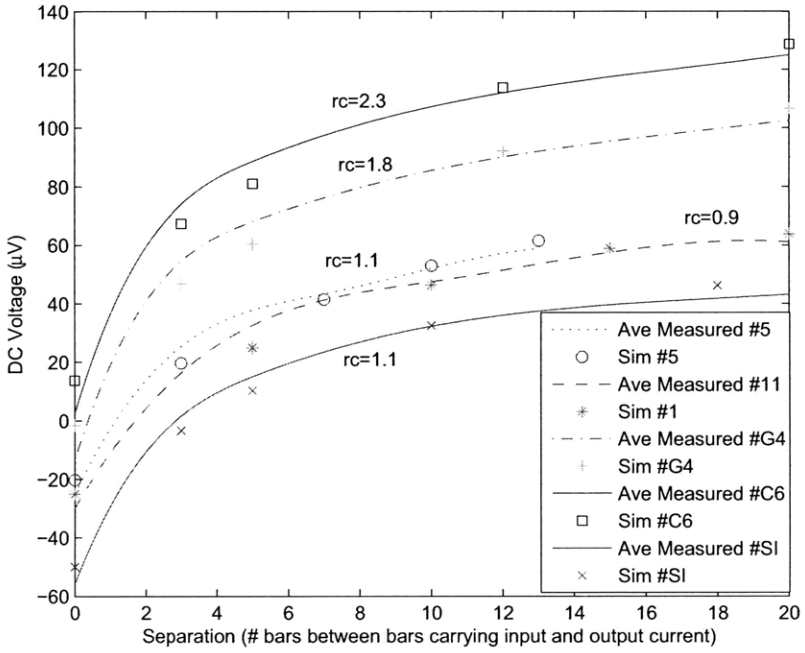

Figure 4-8: Comparison of calculated and measured 10 hp dc rotor voltages

Similar plots for the same side and opposite end tests on the "low" contact resistance cast copper five horsepower machines are shown in Figures 4-9 and 4-10. The inter-bar resistance values for these rotor are presented in Table 4.1. The total inter-bar resistance is twice the contact resistance plus an approximately 0.5 micro-ohm meter impedance of the core path between bars for these machines. The OPT and R4 designated rotors are the copper #1 design with the double bar shape. This more complicated bar shape, with tighter curves and a relatively thin leakage neck must be more difficult to cast and measure lower inter-bar resistance compared to the cast copper in the single, tear dropped shaped bars. For the five horsepower machines, the double bar designs all fit in the "low" category of contact resistance. All of the tear dropped cast copper measured the "high" type of contact resistance, although some were approaching the limit and all were significantly lower than the cast aluminum rotors.

Five different bar spacings between zero, measuring neighboring bars, and skipping fourteen bars halfway around the rotor were measured and used for comparison to

predicted voltages. Adding additional data points did not significantly alter the results. Again, the solid lines are smooth curves through the measured data points for each of the rotors. The star shaped points are the five voltages calculated by applying the resistance value that result in minimized total deviation between calculation and average measurement. The error bars in these plots show plus and minus one standard deviation of the average measured voltage value for that spacing.

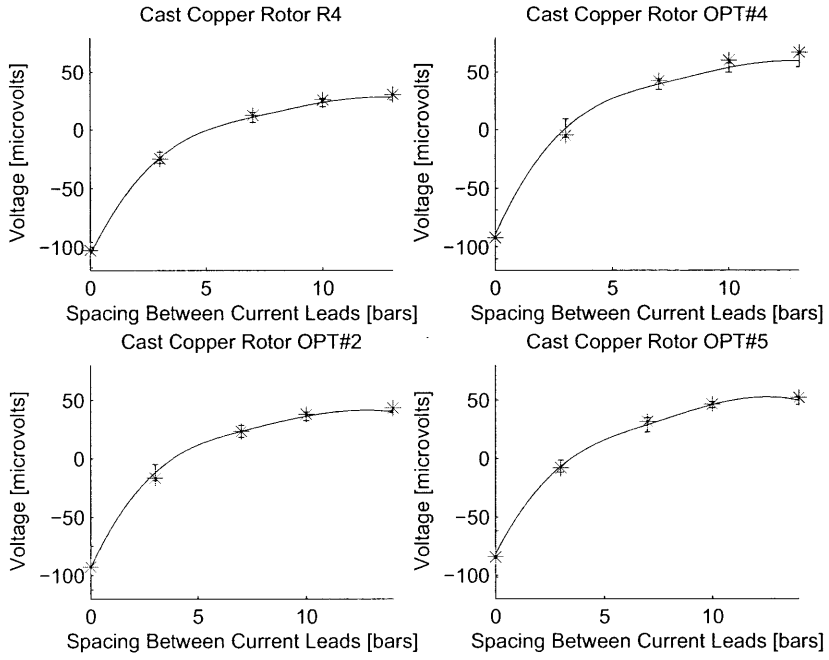

Figure 4-9: Comparison of calculated and measured 5 hp dc rotor voltages - Opposite end measurements

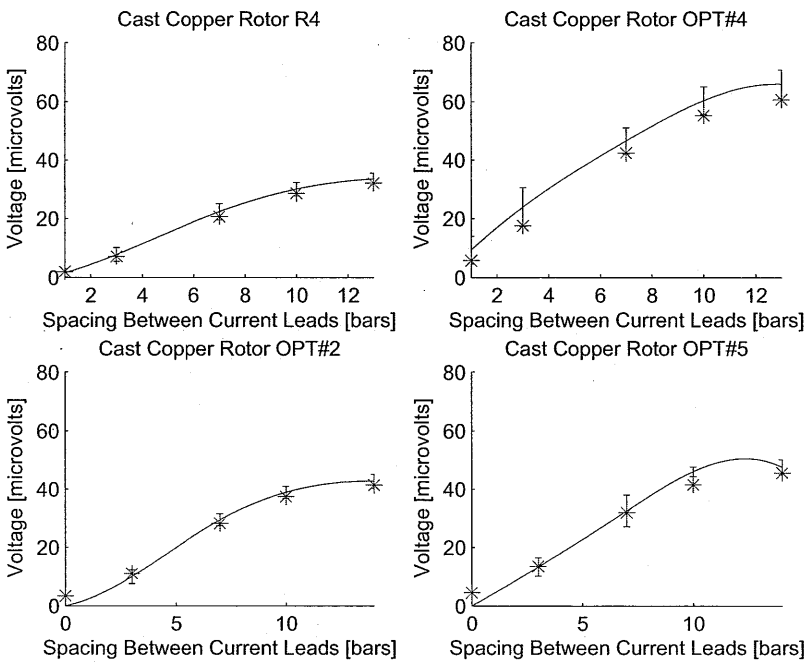

Figure 4-10: Comparison of simulated and measured 5 hp dc rotor voltages - Same side measurements

Finally, the last three plots show the sensitivity of the calculated voltages to changes in the rotor bar, lamination iron, or contact resistance. The solid lines are the spline curve fits through the measured average points. Figure 4-11 illustrates the impact of altering the lamination resistance. Figure 4-12 shows the change in calculated voltages with increased or decreased bar impedance. Figure 4-13 pictures the dependence of the calculated voltages on the bar-to-lamination contact resistance. All of these values are only approximately determined. Curve fitting to the average measured data cannot distinguish between small changes in any of the three resistance parameters, but significant departures from the selected values give unrealistic results. An approximate average value of inter-bar resistance is all that can be determined but this is the unknown value required for calculations of rotor currents and losses.

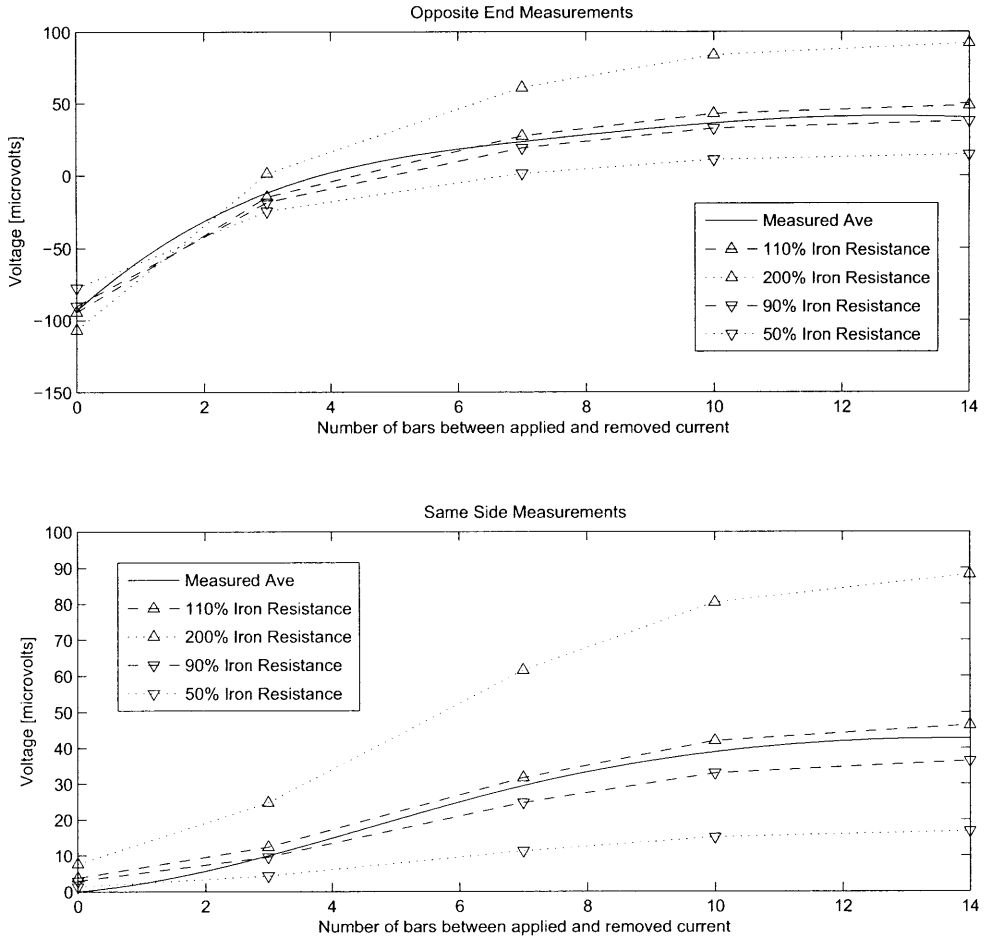

Figure 4-11: Sensitivity of calculated 5 hp voltages to iron lamination resistance

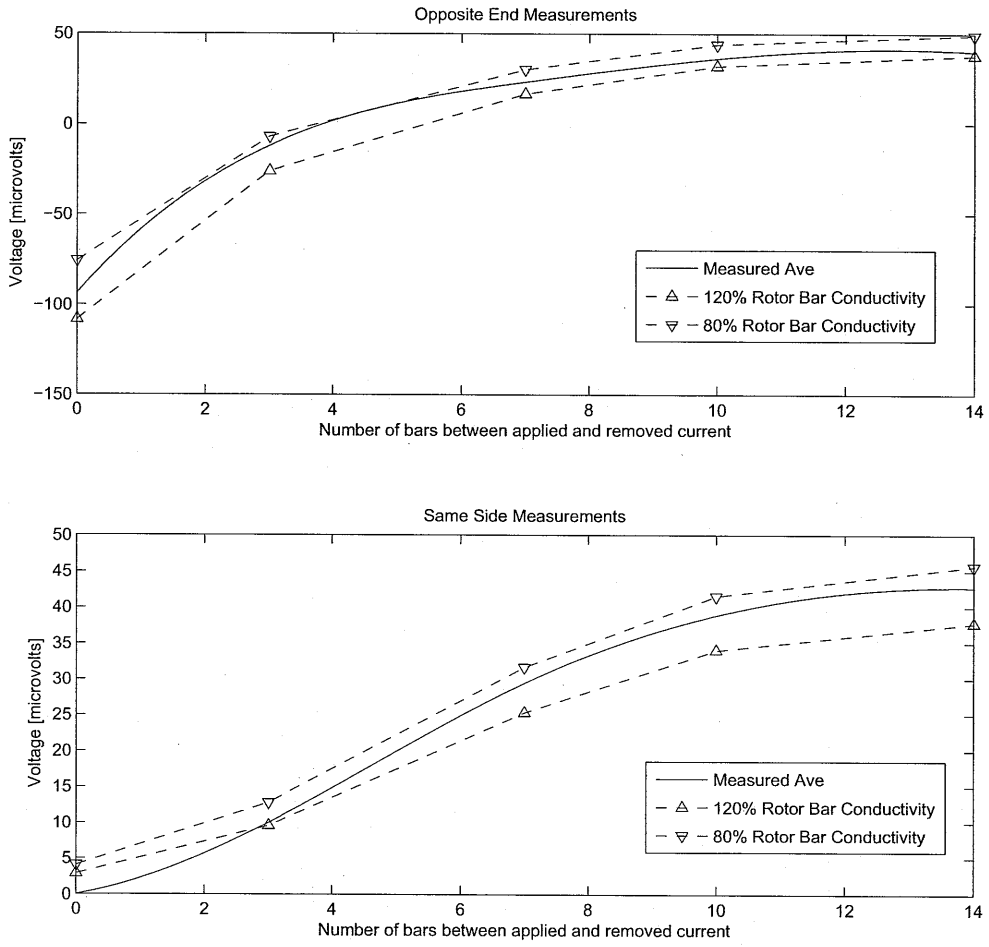

Figure 4-12: Sensitivity of calculated 5 hp voltages to bar resistance

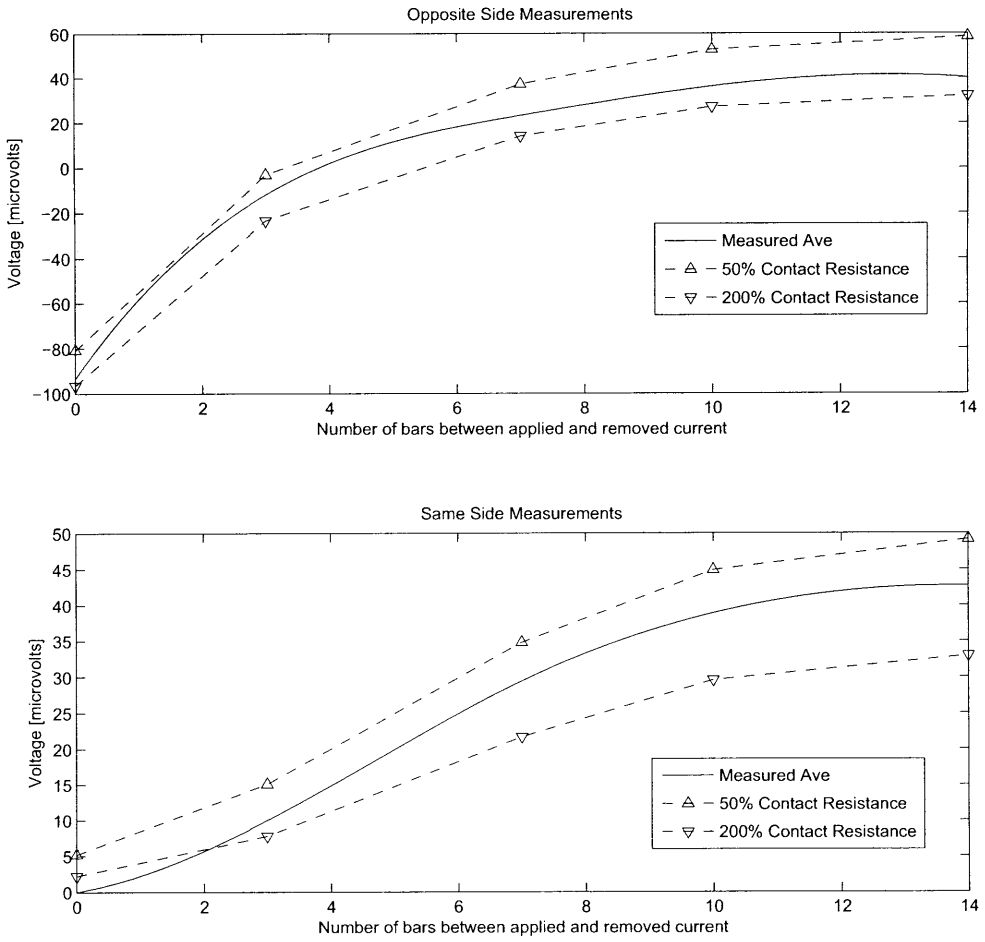

Figure 4-13: Sensitivity of calculated 5 hp voltages to contact resistance

4.7 Summary and Conclusion

This Chapter presented the method and results for determining the average inter-bar resistance for the two different categories of "high" and "low" contact resistance. These values will no be used to evaluate total rotor bar, inter-bar, and end ring losses in the next chapter.

Chapter 5

Equivalent Circuit Modifications for Inter-Bar Currents

This chapter explains how the traditional equivalent circuit model can be adjusted to include the impact of inter-bar currents. Equations for both the fundamental and higher order space harmonics are presented to increase the effective rotor resistance and bring the effective skew factor closer to unity. This strategy is compared to previous methods used by Weppler and Williamson with a single complex skew factor to account for the inter-bar currents.

The adjusted equivalent circuit can now predict the impact of variations in motor parameters like skew, inter-bar resistance, and rotor impedance with appropriately adjusted calculations of motor operating point slip and input current.

5.1 Introduction

With no skew, as long as the end ring impedance is small compared to the cross-impedance between bars through the laminations, as is usually the case, only small cross currents are possible near either end ring. For normal non-skewed machines, these cross-currents are negligible. With skew and non-insulated rotor bars, more appreciable currents are possible, concentrated around the center along the rotor length. Slot harmonics with a pole pitch close to the distance between rotor bars will

be most effective at inducing harmonic inter-bar currents.

The rotor bar skew is intended to prevent neighboring bars from linking slot variations in air gap flux by physically arranging the rotor bar loops to link a net total of near zero slot harmonic flux along their full length. The slot harmonics are specifically targeted because the arrangement and chording of the stator winding and resulting winding factors can be used to reduce lower order harmonics. The slot harmonics depend on the number and geometry of the stator slots and rotor bars. With insulated bars, the skew works to reduce the slot harmonics at the expense of mainly a slight reduction in coupling with a slight increase in leakage reactance, both calculable using the standard skew factor.[6] With imperfect isolation between rotor bars and the surrounding laminations, currents can flow along and between sections of the rotor bars, locally linking changes in slot harmonic air gap magnetic fields. The rotor currents vary continuously along the length of the un-insulated rotor bars, complicating loss calculations. The currents flowing in the laminations between bars contribute a new component of rotor conduction losses. The standard equivalent circuit uses a single value of rotor resistance and rotor current for each harmonic, treating all of the rotor loss as if it were uniformly distributed bar loss. An adjusted, "effective" value of rotor resistance can be used within the standard equivalent circuit to more accurately calculate and represent the total rotor losses including the end rings, inter-bar terms, and the variations along the bars.

In addition to the altered resistance values, the standard skew factor must also be adjusted to reduce the rotor leakage reactance terms and account for the increased coupling compared to the skewed case with insulated bars. In the unrealistic limit of negligible cross-impedance, the effective skew factor becomes unity. In this case the skew and phase shift along the rotor bar are irrelevant when currents can flow freely between any combination of bars. This extreme scenario approaches the limiting case of no skew, but with negligible end ring impedance resulting in reduced fundamental equivalent rotor resistance and input stator current. In both cases, the only rotor loss is along the bars and uniform along the rotor length.

The end ring impedance typically has little impact on the calculations of space

harmonic rotor losses, because of the low end ring impedance and small space harmonic pole pitch. The end ring resistance also appears to have little impact on the distribution of fundamental inter-bar currents. The end rings usually act as effective short circuits. However, both fundamental and harmonic inter-bar currents depend strongly on the input stator current, and the end ring resistance, even though negligible compared to the cross-impedance, can still contribute significantly to the fundamental equivalent circuit effective rotor resistance, loss, and the resultant input stator current. The fundamental end ring impedance must be included in calculating fundamental rotor resistance, loss, and current, but typically will not otherwise impact the distribution of inter-bar currents and losses.

Adjusting both the rotor resistance and skew factor can allow the equivalent circuit rotor resistance and reactance to represent a skewed rotor with un-insulated rotor bars and continuously varying rotor bar and inter-bar currents.

5.2 Effective Rotor Resistance

The following approach is intended to be more straightforward and intuitive than previous methods of adjusting equivalent circuit parameters to account for inter-bar currents. The equations required to calculate the components and final effective values are not especially simple or elegant, but the underlying theory is basic to the equivalent circuit model. Just as the total equivalent circuit rotor losses are calculated as three times the effective rotor resistance times the square of the effective rotor current, the goal is to determine the value of effective rotor resistance by dividing the calculated total, end, bar, and inter-bar rotor losses, by three times the square of an effective rotor current.

Assuming sinusoidal distributions of rotor bar, inter-bar, and end ring currents, the total rotor losses, including bar, inter-bar, and end ring terms, can be calculated using the equations derived from the field equations in Chapter 3. The current in the rotor bar carrying peak current, $I_b(y)$, varies continuously along the rotor length.

$$I_b(y) = C_1 e^{\gamma y} + C_2 e^{-\gamma y} + \frac{E e^{j\alpha y}}{Z_{qs}\,\beta} \tag{5.1}$$

In this solution to the differential equation from Chapter 3, $\beta = \gamma^2 + \alpha^2$, γ is a propagation constant given by $\sqrt{\frac{Z_r}{Z_{qs}}}$, Z_r is the per bar rotor impedance per unit length including resistance, leakage reactance, and per-bar magnetizing terms, $Z_{qs} = \frac{Z_q}{4\sin^2(\delta)}$ is a scaled version of the impedance per unit length between neighboring bars, Z_q, δ is the electrical angle between neighboring bars, E is the induced bar voltage per unit length in the absence of skew, and α is the electrical skew angle per unit length. This equation is equally valid for higher order space harmonics with the terms adjusted for the harmonic frequencies and pole pairs. Also fully defined in Chapter 3, C_1 and C_2 are complex integration constants set by applying end ring boundary conditions.

A number of terms have been grouped together and written as X to simplify the expression.

$$X = \frac{4\pi P Z_{qs} \sin(\delta/2) e^{j\delta/2}}{N_R R_R} \tag{5.2}$$

$$C_1 = \frac{C_2(X\gamma + 1) + \frac{E}{Z_{qs}\beta}(1 - j\alpha X)}{X\gamma - 1} \tag{5.3}$$

$$C_2 = \frac{E(1 - j\alpha X)(e^{\gamma L} - e^{j\alpha L})}{Z_{qs}\,\beta(X\gamma + 1)(e^{-\gamma L} - e^{\gamma L})} \tag{5.4}$$

The solution of the actual rotor current in non-insulated rotors, continuously varying as a function of position along the rotor length, can be multiplied by the skewed, working electric field and integrated to calculate total rotor losses, as in Chapter 3. However, a single, uniform value of effective rotor current is required by the equivalent circuit. A single-value rotor current can be calculated as the spacial rms value of the continuously changing rotor bar current, effectively "averaging" the magnitude of the bar current along the axial length of the rotor, and referred to the stator for comparison to the equivalent circuit value. The following calculations of effective rotor resistance and effective skew factor are a function of the spacial rms bar current.

One method to calculate the total (bar, end ring, and inter-bar) rotor losses, P_r, is to integrate the product of the bar current and the complex conjugate of the skewed, per-unit length, induced bar voltage along the full rotor length and then multiply by the number of rotor bars, N_R. This calculation, presented previously and explained in more detail as (3.29), gives the total rotor bar, inter-bar, and end ring losses when the end rings are considered in the boundary conditions.

$$P_r = N_R \Re e \left\{ \int_{\frac{L}{2}}^{\frac{L}{2}} I_b(y) E^* e^{-j\alpha y} \, dy \right\} \tag{5.5}$$

After integrating, the terms in P_r can be somewhat reduced. One possible form is shown below.

$$\begin{aligned} P_r = N_r \Re e \Bigg\{ \frac{2E^*}{\beta} \Bigg[& \sinh\left(\frac{\gamma L}{2}\right) \cos\left(\frac{\alpha L}{2}\right) [\gamma(C_1 + C_2) + j\alpha(C_1 - C_2)] \\ & + \cosh\left(\frac{\gamma L}{2}\right) \sin\left(\frac{\alpha L}{2}\right) [j\gamma(C_2 - C_1) + \alpha(C_1 + C_2)] \Bigg] \\ & + \frac{EE^* L}{Z_{qs}\beta} \Bigg\} \end{aligned} \tag{5.6}$$

Total rotor losses in the induction motor equivalent circuit model are calculated as three times the product of the equivalent rotor resistance and the square of the single-valued rotor current. In the equivalent circuit, both resistance and current are referred to the stator winding. A single, equivalent value of per-bar rotor resistance consistent with the total bar, inter-bar, and end ring losses can be similarly determined using the calculated net rotor loss, P_r, and the equivalent, single value of effective rotor current, $I_{b_{rms}}$, the spatial rms value of the continually varying bar current.

$$R_b = \frac{P_r}{N_R \, |I_{b_{rms}}|^2} \tag{5.7}$$

R_b is the per-bar, effective rotor resistance not yet referred to the stator. The spatial rms value of the bar current can be calculated using the following equation:

$$I_{b_{rms}} = \sqrt{\frac{1}{L}\int_{\frac{L}{2}}^{\frac{L}{2}} I_b(y)\ I_b^*(y)\ dy} \tag{5.8}$$

The $I_b^*(y)$ represents the complex conjugate of the bar current. The product of bar currents can be evaluated to give the following terms:

$$\begin{aligned} I_{b_{rms}} = \Bigg(\frac{1}{L}\int_{\frac{L}{2}}^{\frac{L}{2}} & C_1C_1^*e^{y(\gamma+\gamma^*)} + C_2C_2^*e^{-y(\gamma+\gamma^*)} + C_1C_2^*e^{y(\gamma-\gamma^*)} + C_1^*C_2e^{-y(\gamma-\gamma^*)} \\ & + \frac{EE^*}{Z_{qs}Z_{qs}^*\beta\beta^*} + \frac{C_1E^*}{Z_{qs}^*\beta^*}e^{y(\gamma-j\alpha)} + \frac{C_1^*E}{Z_{qs}\beta}e^{y(\gamma^*+j\alpha)} \\ & + \frac{C_2E^*}{Z_{qs}^*\beta^*}e^{-y(\gamma+j\alpha)} + \frac{C_2^*E}{Z_{qs}\beta}e^{-y(\gamma^*-j\alpha)}\ dy\Bigg)^{0.5} \end{aligned} \tag{5.9}$$

A few of the terms in this expression combine while evaluating the integral.

$$\begin{aligned} I_{b_{rms}} = \Bigg(\frac{1}{L}\Bigg(\frac{2\sinh(\frac{L}{2}(\gamma+\gamma^*))}{(\gamma+\gamma^*)}(C_1C_1^*+C_2C_2^*) + \frac{2\sinh(\frac{L}{2}(\gamma-\gamma^*))}{(\gamma-\gamma^*)}(C_1C_2^*-C_1^*C_2) \\ + \frac{2C_1E^*}{Z_{qs}^*\beta^*(\gamma-j\alpha)}\sinh(\frac{L}{2}(\gamma-j\alpha)) + \frac{2C_1^*E}{Z_{qs}\beta(\gamma^*+j\alpha)}\sinh(\frac{L}{2}(\gamma^*+j\alpha)) \\ + \frac{2C_2E^*}{Z_{qs}^*\beta^*(\gamma+j\alpha)}\sinh(\frac{L}{2}(\gamma+j\alpha)) + \frac{2C_2^*E}{Z_{qs}\beta(\gamma^*-j\alpha)}\sinh(\frac{L}{2}(\gamma^*-j\alpha)) \\ + \frac{LEE^*}{Z_{qs}Z_{qs}^*\beta\beta^*}\Bigg)\Bigg)^{0.5} \end{aligned} \tag{5.10}$$

The bar current equation can also be rewritten to better align with Equation (5.6) for the total rotor losses.

$$I_{b_{rms}} = \left(\frac{1}{L} \left(\frac{2\sinh(\frac{L}{2}(\gamma+\gamma^*))}{(\gamma+\gamma^*)}(C_1C_1^* + C_2C_2^*) + \frac{2\sinh(\frac{L}{2}(\gamma-\gamma^*))}{(\gamma-\gamma^*)}(C_1C_2^* - C_1^*C_2) \right.\right.$$
$$+ \frac{2E^*}{Z_{qs}^*\beta\beta^*} \left[\sinh\left(\frac{\gamma L}{2}\right) \cos\left(\frac{\alpha L}{2}\right) [\gamma(C_1+C_2) + j\alpha(C_1-C_2)] \right.$$
$$\left. + \cosh\left(\frac{\gamma L}{2}\right) \sin\left(\frac{\alpha L}{2}\right) [j\gamma(C_2-C_1) + \alpha(C_1+C_2)] \right]$$
$$+ \frac{2E}{Z_{qs}\beta\beta^*} \left[\sinh\left(\frac{\gamma^* L}{2}\right) \cos\left(\frac{\alpha L}{2}\right) [\gamma(C_1^*+C_2^*) + j\alpha(C_1^*-C_2^*)] \right.$$
$$\left.\left. \left. + \cosh\left(\frac{\gamma^* L}{2}\right) \sin\left(\frac{\alpha L}{2}\right) [j\gamma(C_1^*-C_2^*) + \alpha(C_1^*+C_2^*)] \right] \right) \right)^{0.5} \quad (5.11)$$

The following term is introduced as a substitution to somewhat simplify the equations for effective rotor resistance. Again, the effective rotor resistance is determined by dividing the total rotor loss by three times the square of the spacial rms bar current. Equivalently, a rotor resistance correction factor is the ratio of the actual effective resistance to the traditionally calculated resistance of an insulated rotor without inter-bar currents.

$$XX = \frac{2E^*}{Z_{qs}^*\beta} \left\{ \sinh\left(\frac{\gamma L}{2}\right) \cos\left(\frac{\alpha L}{2}\right) [\gamma(C_1+C_2) + j\alpha(C_1-C_2)] \right.$$
$$\left. + \cosh\left(\frac{\gamma L}{2}\right) \sin\left(\frac{\alpha L}{2}\right) [j\gamma(C_2-C_1) + \alpha(C_1+C_2)] \right\} \quad (5.12)$$

The following substitution is also made to simplify the equation.

$$ZZ = \frac{2\sinh(\frac{L}{2}(\gamma+\gamma^*))}{(\gamma+\gamma^*)}(C_1C_1^* + C_2C_2^*) + \frac{2\sinh(\frac{L}{2}(\gamma-\gamma^*))}{(\gamma-\gamma^*)}(C_1C_2^* - C_1^*C_2) \quad (5.13)$$

The adjustment factor to include the impact of inter-bar currents and non-negligible end ring impedance in total rotor loss calculations is given below:

$$AFR2 = \frac{\Re e\left\{\frac{EE^* L}{Z_{qs}\beta} + XX\right\}}{RS\left[ZZ + \frac{EE^*}{Z_{qs}Z_{qs}^*\beta\beta^*} + \frac{X}{Z_{qs}^*\beta^*} + \frac{X^*}{Z_{qs}\beta}\right]} \tag{5.14}$$

The adjustment factor can be calculated individually for each harmonic. RS is the bar resistance per unit length for the given harmonic. This rotor resistance correction helps to more accurately model an induction motor with non-insulated rotor bars. The equations are long but easily included in motor analysis and design software. The variables consist of traditional equivalent circuit parameters with the addition of an average value of inter-bar resistance or impedance.

However, this single correction to the equivalent circuit is insufficient for consistent calculations. The rotor current of the equivalent circuit model will not, in general, match the calculated, spacial rms rotor bar current. Errors will result in calculated rotor losses because the inter-bar currents also adjust the reactance of the rotor through the skew factor. An additional correction factor to calculate the effective skew factor is presented in the next section.

5.3 Effective Skew Factor

The adjusted rotor resistance from the previous section is used in calculating the effective skew factor. Skew decreases the coupling between rotor and stator. The skew factor is equal to the reduction in the induced rotor voltage compared to the non-skewed case. The induced rotor bar voltage per unit length in the case of no skew is already calculated as the term E in the previous equations. With negligible impedance end rings and no cross currents, the only voltage drop is along the rotor bars. The induced voltage must equal the total voltage drop, so the induced voltage in the skewed case can be calculated from the total voltage drop. Instead of considering bar, end ring, and inter-bar terms and having to integrate the changing values along the rotor length, the adjusted, effective rotor bar resistance together with the spacial rms bar current, both calculated in the previous section, can be used to estimate the actual, total voltage drop but now taken only along the rotor bars. The effective

voltage drop per unit length is the product of the adjusted bar impedance per unit length with the spacial rms bar current calculated in the previous section. The adjusted bar impedance is the original per-bar slot leakage reactance per unit length (excluding any additional leakage or magnetizing terms here) combined with the newly calculated value of adjusted, effective rotor resistance per unit length. This value of effective rotor voltage drop per unit length can be divided by the non-skewed, induced voltage term, E, to determine the effective skew factor in the case of negligible end rings.

With end rings of non-negligible impedance, the induced voltage along the bar length still must equal the total voltage drop now across both the bars and end rings. The adjusted rotor resistance already accounts for the voltage drop of the end rings in addition to the bar and cross-path components, so the product of the spacial rms bar current and the equivalent bar impedance again gives the skewed total voltage drop per unit length. The effective skew factor can now be calculated as the ratio of the voltage drop per unit length in the skewed bars to the voltage drop per unit length with no skew, now with both terms also including the voltage drop over the rotor end rings. The voltage drop along the bars in the non-skewed case is the induced, non-skewed, voltage per unit length E but now including an average per bar end ring voltage subtracted for each ring and divided by the bar length to uniformly impact the non-skewed bar voltage drop.

$$K_{sk} = \left| \frac{I_{b_{rms}} Z_b}{E - \frac{V_R(y=-\frac{L}{2}) + V_R(y=\frac{L}{2})}{L}} \right| \tag{5.15}$$

The average voltage drop in a section of end ring between bars can be calculated at either end of the rotor from the rotor bar current at that point.

$$V_{ring(y=\pm\frac{L}{2})} = \frac{2\pi R |I_b(y = \pm\frac{L}{2})|}{N_r(1 - e^{j\delta})\sigma_r \; l_e \; h_e} \tag{5.16}$$

In this equation, R is the rotor radius (or effective end ring radius if more accuracy is needed), σ_r is the end ring conductivity, l_e is the axial end ring length, and h_e is

the radial end ring height.

These end ring voltages can be added together for use in the calculation of skew factor, and it is interesting to observe the dissymmetry in the case of inter-bar currents and changing bar current with length. If the casting process also produces an end ring with somewhat decreased conductivity at the end farthest from the entrance of the molten conductor, a very slight decrease in locked rotor current may be possible by ensuring that this higher resistance end ring experiences the higher end ring current. Except in extreme cases, this effect, calculated at only a few watts difference, would be difficult to observe.

A more consistent calculation for an average value of end ring voltage drop can be calculated using the spacial rms bar current. This strategy is simpler and gives effectively identical results. The voltage per end ring section for both rings can be expressed by the following equation:

$$V_{2ring} = \frac{4\pi R|I_{b_{rms}}|}{N_r(1-e^{j\delta})\sigma_r \; l_e \; h_e} \tag{5.17}$$

Substituting into (5.15) and dividing each term by the equation for spacial rms bar current gives the following equation for effective skew factor:

$$K_{sk} = \frac{Z_b}{\frac{E}{\left(ZZ+\frac{EE^*}{Z_{qs}Z_{qs}^*\beta\beta^*}+\frac{X}{Z_{qs}^*\beta^*}+\frac{X^*}{Z_{qs}\beta}\right)^{0.5}} - \frac{4\pi R}{N_r(1-e^{j\delta})\sigma_r \; l_e \; h_e}} \tag{5.18}$$

This effective skew factor combined with the previously calculated effective rotor resistance together allow more accurate calculation of total rotor losses in skewed induction motors with non-insulated rotor bars. These two equations, (5.18) for the effective skew factor, and (5.14) for the effective rotor resistance, can be substituted into motor design software in place of the existing skew factor and as a correction factor to the rotor resistance to account for the impact of inter-bar currents. The next sections compare calculations using the adjusted equivalent circuit to previously existing equations and to measured test data on a variety of rotors.

5.4 Theoretical Verification - Comparison to Previous Calculations

The goal of this section is to use previous work as support for the validity of the new calculations while also differentiating the new method from what has been done in the past. Both Weppler and Williamson et al. use a complex skew factor, including both real and reactive terms, to incorporate the impact of inter-bar currents in the traditional equivalent circuit. This approach seems to apply only when using the equivalent circuit resulting from considering the skew as implemented strictly on the rotor conductors. This skewed-rotor model is usually the most representative of physical reality, since the rotor bars are typically skewed. However, Chapter 2 discussed how equally valid and consistent circuit models for the same physical machine can treat the fixed angle of total, relative skew as divided arbitrarily in any proportion between the rotor and stator conductors. The circuit treating skew as equally split between rotor and stator is also commonly used. With equal (and opposite) skew assigned to both the rotor and stator conductors, no skew factor arises in the referral factor between windings. The equivalent circuit with the skew evenly divided between rotor and stator includes a leakage reactance component in the stator branch of the circuit, so applying a complex skew factor to this circuit alters the stator resistance and reactance, even with insulated stator conductors. Moreover, calculated rotor losses using all three methods agree when using the skewed-rotor circuit, but only the new method gives identical results with the split-skew model. When used with the skewed-rotor equivalent circuit, the complex skew factor gives six new components for the real and reactive parts of the adjusted rotor skew leakage reactance, the adjusted rotor slot and differential or zigzag leakage reactance, and the adjusted rotor resistance. Combining these six terms results in an adjusted, effective rotor resistance and leakage reactance consistent with the previous method of equivalent circuit modification.

5.4.1 Weppler

Rudolf Weppler presented the following equations in his 1966 Archiv fur Elektrotechnik paper.[11] Integration constants U and B are calculated from end ring boundary conditions, similarly to C_1 and C_2 in Chapter 3.

$$U = \left(\frac{R_{RW} \cos(\frac{\alpha L}{2}) - \alpha Z_{qs} \sin(\frac{\alpha L}{2})}{R_{RW} \cosh(\frac{\gamma L}{2}) + \gamma Z_{qs} \sinh(\frac{\gamma L}{2})} \right) \tag{5.19}$$

$$B = \left(\frac{R_{RW} \sin(\frac{\alpha L}{2}) + \alpha Z_{qs} \cos(\frac{\alpha L}{2})}{R_{RW} \sinh(\frac{\gamma L}{2}) + \gamma Z_{qs} \cosh(\frac{\gamma L}{2})} \right) \tag{5.20}$$

In these equations, the same scaling factor as a function of the angle between bars, δ, is used on both the inter-bar resistance and on the end ring section resistance, R_R.

$$R_{RW} = \frac{R_R}{4 \sin^2(\frac{\delta}{2})} \tag{5.21}$$

These values are combined to give the square of the complex skew factor, χ. Shown here for the fundamental, the same equation can be used to calculate complex skew factors for each harmonic.

$$\chi^2 = \frac{L\, Z_r + 2R_{RW}}{L\, Z_r + \alpha^2\, Z_{qs}\, L} \left[1 - (U+B) \frac{\sinh(\frac{L(\gamma+j\alpha)}{2})}{L(\gamma+j\alpha)} - (U-B) \frac{\sinh(\frac{L(\gamma-j\alpha)}{2})}{L(\gamma-j\alpha)} \right] \tag{5.22}$$

Weppler then uses the magnitude and phase of the complex skew factor to determine total rotor resistance and impedance from the real and reactive components associated with the traditional skew leakage, rotor leakage, and rotor resistance values. This total rotor impedance can be compared to alternative calculations, as in Figure 5-1.

5.4.2 Williamson and Smith Calculation

The following equations are slightly adapted from the 2002 IEE paper "Equivalent circuits for cage induction motors with inter-bar currents," by S. Williamson and

A.C. Smith. The original equations use a more general end ring impedance and a less general inter-bar resistance in place of the end ring resistance and inter-bar impedance included in the following equations. More significantly, the factor of $\frac{Z_r}{Z_{qs}\beta}$ is added to the original equations (22) and (23) for F in the Williamson and Smith paper. This is only a regrouping of terms from the complete original equations. The additional factor is not expected to impact the resulting calculations from the paper, where there may have been no reason to use the independently calculated correction factor, F. The adjusted factor is thought to improve substitution into the equivalent circuit model. Calculations including the alteration matched calculations from both Weppler and the new adjusted circuit equations.

The following two integration constants are determined using end ring boundary conditions as in Chapter 3 and Weppler's equations. The sum and difference of A and B can be used to calculate the previously used constants $C1$ and $C2$.

$$A = \frac{-1}{Z_{qs}\beta}\left(\frac{R_R\cos(\frac{\alpha L}{2}) - \alpha z_q \sin(\frac{\alpha L}{2})}{R_R\cosh(\frac{\gamma L}{2}) + \gamma z_q \sinh(\frac{\gamma L}{2})}\right) \tag{5.23}$$

$$B = \frac{-j}{Z_{qs}\beta}\left(\frac{R_R\sin(\frac{\alpha L}{2}) + \alpha z_q \cos(\frac{\alpha L}{2})}{R_R\sinh(\frac{\gamma L}{2}) + \gamma z_q \cosh(\frac{\gamma L}{2})}\right) \tag{5.24}$$

$$\begin{aligned} F = &\frac{Z_r}{Z_{qs}\beta}[1 + \frac{2Z_{qs}}{L}(\gamma A + j\alpha B)\sinh(\frac{\gamma L}{2}) \\ &+ (\alpha\, A - j\,\gamma\, B)\cosh(\frac{\gamma L}{2})\sin(\frac{\alpha L}{2}) \end{aligned} \tag{5.25}$$

Shown here only for the fundamental to avoid additional subscripting, different values of F can be calculated for each harmonic using the same equation and appropriately adjusted variables. The "complex dimensionless harmonic constant" F from (5.25) is used in place of the square of the traditional skew factor in the skewed-rotor equivalent circuit models. This results in real and reactive components in place of each of the traditional skew leakage reactance, rotor leakage reactance, and rotor resistance, but combining real and reactive terms results in an equivalent rotor

impedance comparable to the rotor impedance calculated using Weppler's equations or the new equations for adjusted skew leakage and rotor resistance.

Figure 5-1 compares the amplitude of the 23^{rd} space harmonic, the negative rotating first order stator slot harmonic, rotor impedance for different operating speeds as calculated by the three calculation methods. The arbitrary case is for a cast aluminum five horsepower rotor, using the measured values of skew and inter-bar resistance. The main point is that the three calculations yield identical results. This is true for both real and reactive components for all harmonics. The different calculations, as implemented, give equal results in the case of a skewed-rotor equivalent circuit model.

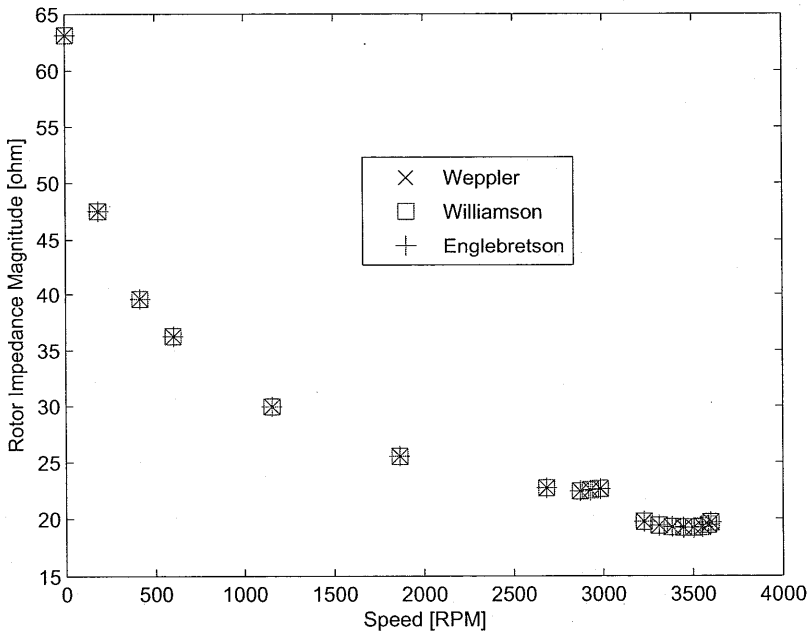

Figure 5-1: Comparison of circuit adjustment equations

5.5 Experimental Validation - Comparison to Test Results

In order to help develop new motor designs or identify means to improve or modify existing designs while minimizing the number of machines built and tested to evaluate alternatives, the circuit model must be capable of accurately predicting motor performance.

The equivalent circuit model can relatively easily match calculations to test data for any individual measured value on a particular machine. Justifiable adjustments to only roughly determined parameters and components, for example the stator end winding reactance or rotor conductivity, allow for custom tuning of the circuit calculations, especially over the near linear, low slip, region of normal operation. Agreement between any particular measurement and test does not necessarily prove a generally accurate circuit model. If, for example, the calculated stray load loss matches measurements but the input current or torque are off by twenty percent or more, then the circuit model fails to accurately represent the motor, and the apparent agreement in loss arises from a coincidental combination of errors.

On the other hand, simultaneous comparison of multiple values, like power, torque, current, and total impedance, over a wide range of operation, and consistently applied among different sizes and types of machines is a significant challenge.

Two of the most important test points for general purpose induction motors are the locked rotor and full load operating points. Comparison between measured and calculated values of current, power, torque, input impedance, and stray loss are compared for these two points are used together with a full torque speed plot to approximate circuit values used for motor predictions in the operating region. The torque-speed curves for some motors show abrupt variations in calculated torque near the locked rotor point because of the impact of the higher order space harmonics used in the calculations. The calculated motor performance includes the fundamental, 5th, 7th, 11th, 13th, and the four lowest stator slot harmonics, $\frac{N_s}{p} \pm 1$ and $\frac{2N_s}{p} \pm 1$. These space harmonics can contribute visible dips to the motor torque and increased stray loss,

especially significant in the high-slip, low-speed region around locked rotor. Half of the slot harmonics have low, positive synchronous speeds, and around these speeds the harmonic torques will swing between peak positive and negative values.

5.5.1 Design #1 Ten Horsepower Motor

Figure 5-2 presents the torque speed curve for a high efficiency, wye-wound ten horsepower motor. Calculations for this machine include a 10% reduction in as-cast rotor conductivity. A stator end turn leakage reactance value of 0.65 ohms is included as part of the 1.28 ohm fundamental stator leakage reactance. The fundamental rotor leakage reactance, including slot, zigzag, and skew leakage reactance components, is about 1.66 ohms. The conditions between the measured points and calculations are not exactly matched. The high slip points are scaled from half voltage, with a lower operating temperature than the full load points. The temperature is held fixed around the full load value for the calculated curve. The strange, non-smooth behavior in predicted torque approaching the locked rotor is believed to arise from interaction of the slot harmonics.

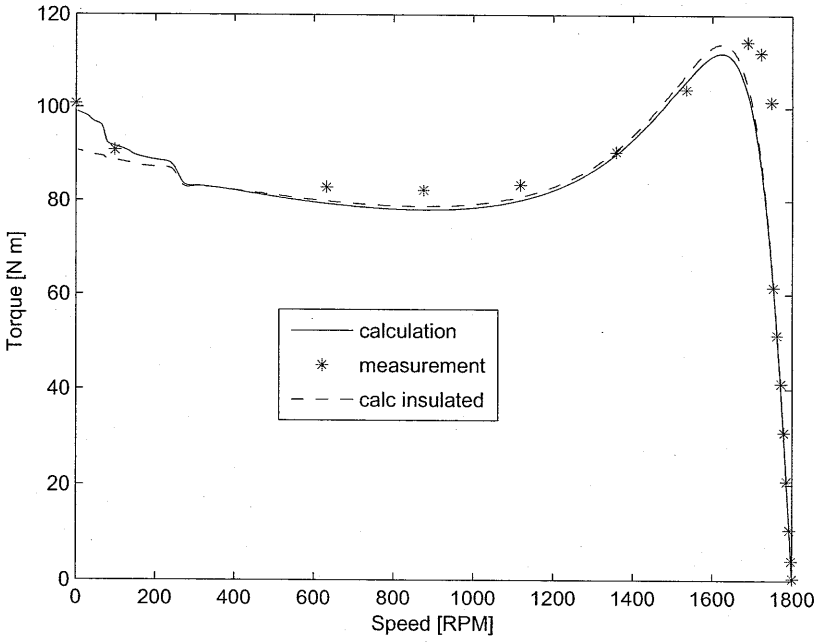

Figure 5-2: Design #1 10 hp cast copper torque speed curve

The following set of plots compare "measured" and calculated values of torque, input current, and fundamental rotor conduction loss. Calculations are presented using the traditional equivalent circuit and the adjusted version to account for inter-bar currents. The measured data is taken at eight different points from no load to 150% load. The calculations assume values of inter-bar resistance equal to the average value determined in Chapter 4 for each motor. Both the ten horsepower motor designs evaluated in this section measured an average inter-bar resistance per unit length of about 2.5 micro ohm meters.

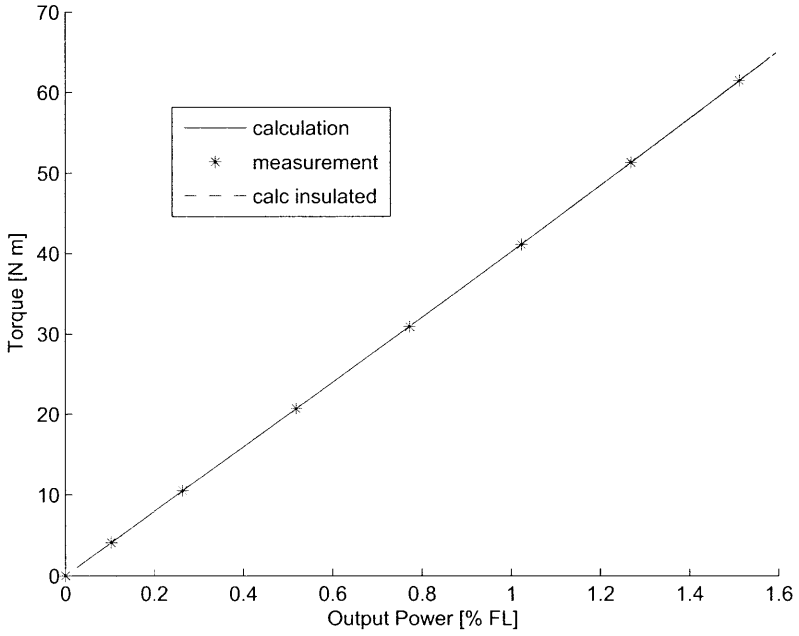

Figure 5-3: Design #1 10 hp cast copper load torque

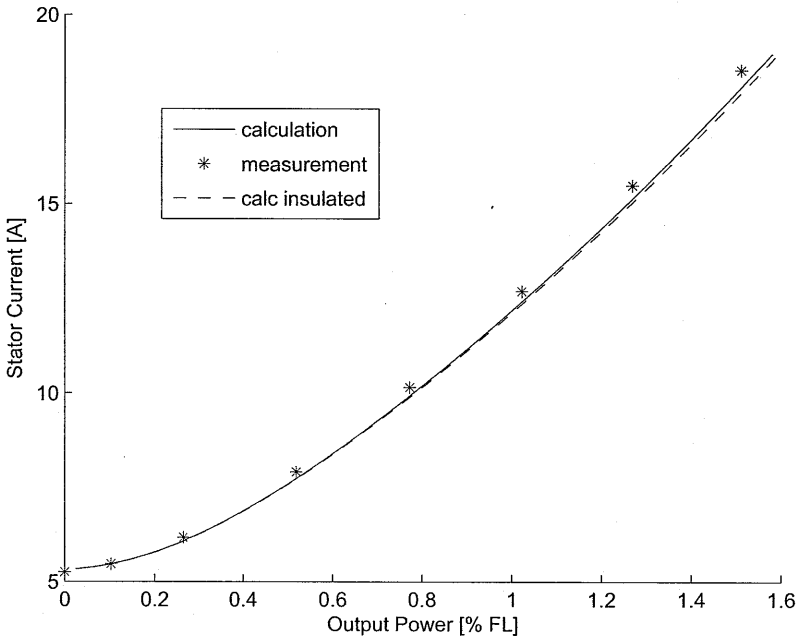

Figure 5-4: Design #1 10 hp cast copper input stator current

The input stator current is somewhat under-predicted, by 0.765 amps or about 6% of the measured 12.7 A stator current.

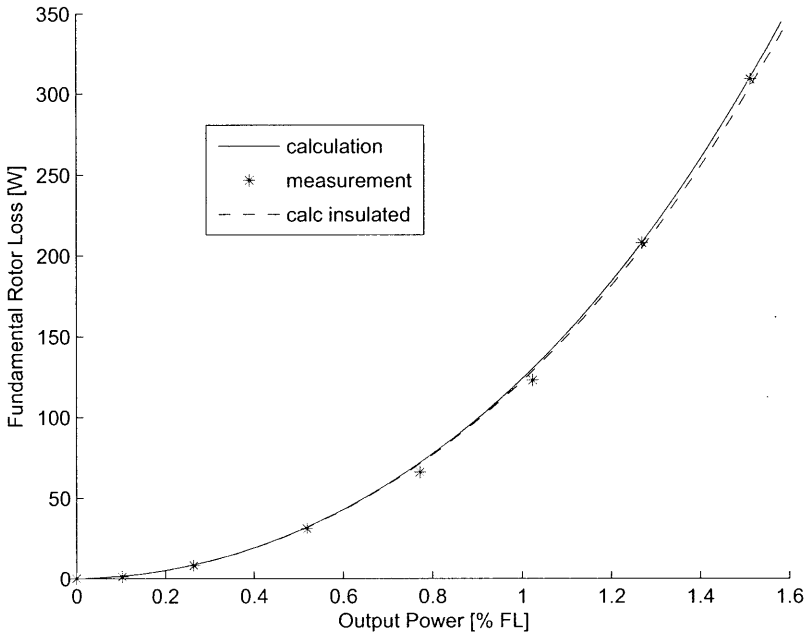

Figure 5-5: Design #1 10 hp cast copper fundamental rotor loss

The stray load loss from measured tests is also compared to calculated stray loss from space harmonic rotor bar currents. This is an important distinction since it is possible that the measured stray load loss includes losses from other sources. The measured value provides only an approximate upper bound for the calculated harmonic rotor bar loss. Additional stray load loss plots include predictions for cases of altered inter-bar resistance and contact resistance.

No error bars are included with the plots of torque, stator current, or rotor fundamental loss because the error is expected to be less than two percent for all points on these graphs, often falling within the size of the starred points. The current and torque are measured directly, with reported precision of 0.001 amps and 0.01 pound feet. Combining error in stator copper loss and no load core loss with a one rpm error in speed and slip, still results in less than a two percent, or plus or minus three watt error on the fundamental rotor loss.

Any error in the individual "measurements" of stator or rotor conductor losses, no load copper loss, input and output power, and friction and windage losses can potentially combine for larger cumulative errors in the determined values of stray load

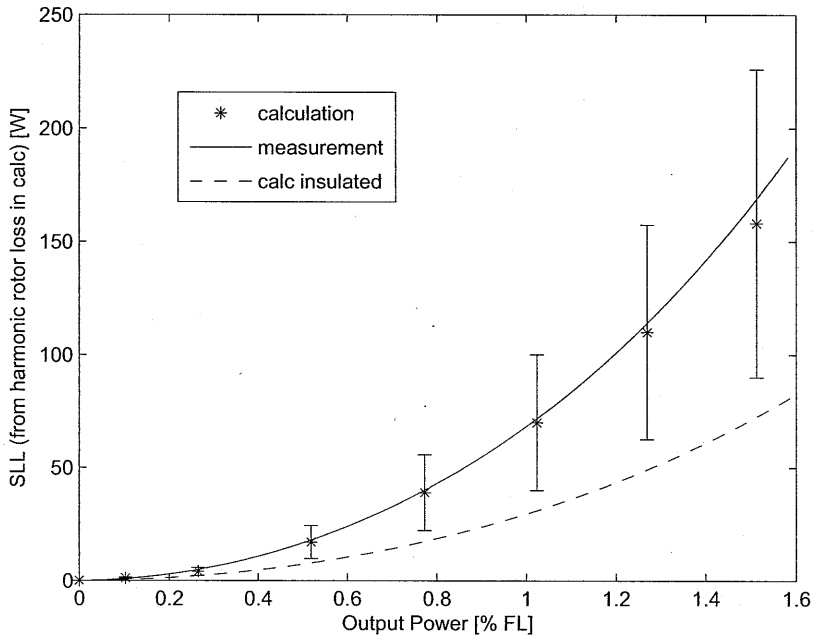

Figure 5-6: Design #1 10 hp cast copper stray load loss or harmonic rotor conduction loss

loss. Typical error should normally fall within plus or minus 10% of the measured stray load loss, but the error bars show the worst case of about 43% of the measured values of stray load loss. At lower loads, the error should be a larger percentage, but the magnitude of the error is much less significant. Around full load, an extreme variation in stator copper losses of about ten watts is possible with an unlikely ten degree error in temperature. Calculations of friction and windage and core loss from measured no load data are repeatable to within a few watts, but a ten watt error is assumed for the combined friction and windage and no load core loss. Since the value of friction and windage loss is subtracted from the measured input power in calculating the no load core loss, most errors will cancel out in the sum of the two values. These errors in stator, core, and rotational losses combine, together with a ± 1 rpm error in measured speed and slip, to give less than a ± 3 watt error in the calculated fundamental rotor losses. Lastly, the IEEE 112 test standard calls for curve fitting the measured stray load loss values to a function of the torque squared. Intended to help smooth out errors in measurements between points, the curve fitting

process was found to alter measured data points around full load by up to about 10%, or 7 watts in the case of the design #1 connected ten horsepower motor. Vibrations in the test setup can impact measured values at particular speeds and loads. These sources of error combine to give a boundary on the potential error in the "measured" value of stray load loss of about 30 out of 70 watts, or 43%. Most measurements are likely to be more accurate, but even on these relatively low power machines, the stray load loss is difficult to exactly determine.

Two different testing facilities independently determined values of stray load loss for this motor. Figure 5-7 compares their results, together with calculations using both sets of measured test values. The results from the second facility do not exactly match but remain within the 43% confidence interval of the original measurements.

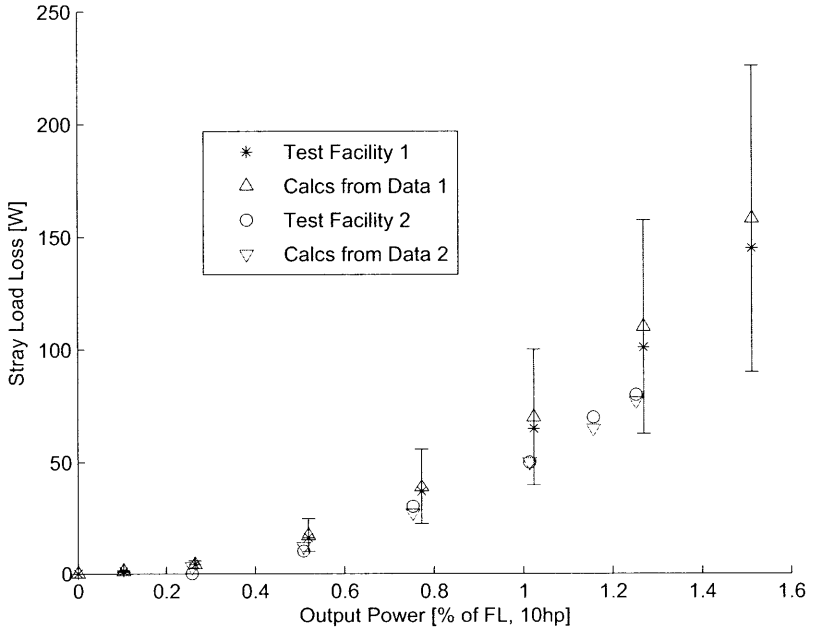

Figure 5-7: Comparison of stray load loss determination on design #1 10 hp cast copper motor

Next, variations in predicted stray, harmonic rotor loss are calculated for variations in rotor skew and contact resistance.

Figure 5-8 suggests the stray load loss of the design #1 ten horsepower motor, with the as measured value of inter-bar resistance, is rather insensitive to changes in

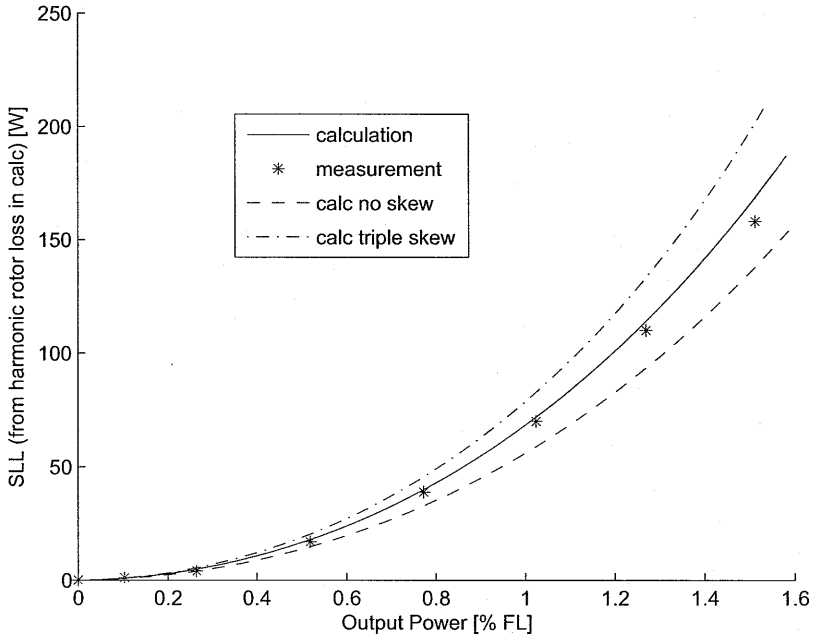

Figure 5-8: Design #1 10 hp cast copper stray load loss or harmonic rotor conduction loss with varied rotor skew

skew. The lowest order, 5th and 7th, belt harmonics contribute more loss than the slot harmonics for this motor. These losses maintain a minimum value of stray loss even as the rotor bars become insulated as plotted in Figure 5-9 along with intermediate values of inter-bar resistance. Generally, small changes in inter-bar resistance have minimal impact, but the stray load loss in this case is expected to decrease with increasing inter-bar resistance. The fully insulated case would also be the result of traditional equivalent circuit calculations not including the adjustments to rotor resistance and skew factor to account for inter-bar currents.

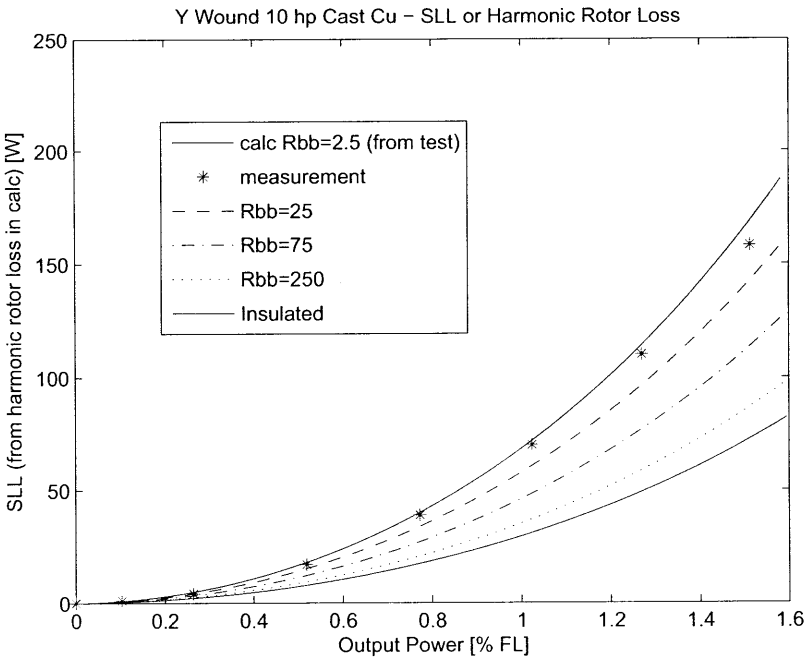

Figure 5-9: Design #1 10 hp cast copper stray load loss or harmonic rotor conduction loss with varied inter-bar resistance

Next, Figure 5-10 examines the impact of variation in inter-bar resistance on the full load harmonic rotor losses. The bar-to-bar resistance varies over the full possible range from the approximate resistance of the of iron path between bars, at around 0.1 micro-ohm meter, up to effectively insulated bars. All of the calculations use a fixed, ten horsepower, output power for a fair comparison. The stator input current and slip are unconstrained but do not vary significantly in this case. The range of speed is around 0.72 rpm and input current around 0.06 A, along with variations in output power of up to 2.3 W. In this case the simplification of constant speed and input current gives negligible error. The single plotted point, $*$, shows the value of stray load loss and inter-bar resistance from measured tests.

The error bars in the "measured" value of inter-bar resistance are also included in this plot. From Chapter 4, the average value of inter-bar resistance for this "low" contact resistance motor was approximately determined by minimizing the error between measured dc voltage profiles and calculated voltages using a rotor resistor model. The voltage measurements on any particular pair of rotor bars are repeatable to within

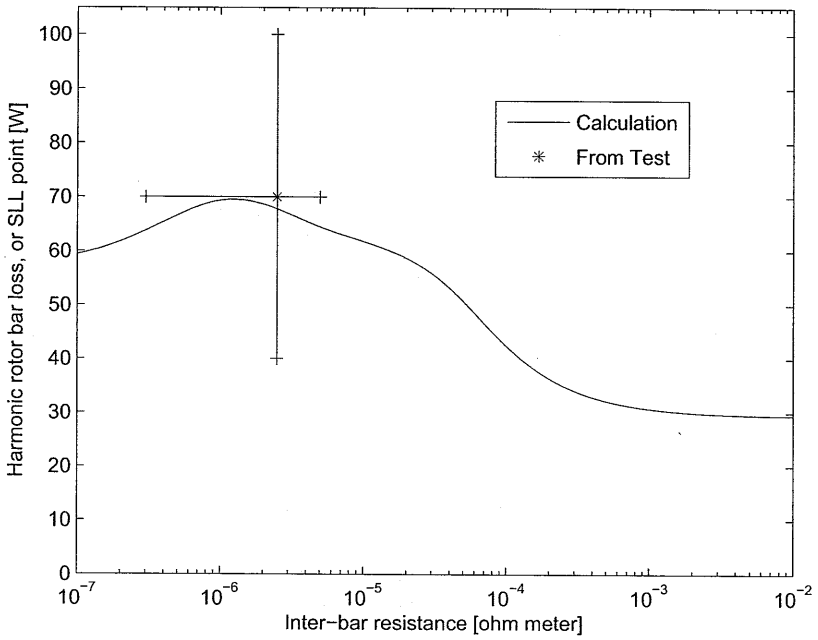

Figure 5-10: Design #1 10 hp cast copper full load stray load loss or harmonic rotor conduction loss with varied inter-bar resistance

a few micro-volts, with minimal error contributed from variations in temperature or applied current. However, measurements of different pairs of bars varied significantly from the changing bar-to-lamination contact resistance values of every bar. Boundaries on the error in inter-bar resistance were found by determining extreme values of inter-bar resistance that resulted in calculated voltage profiles at the boundary of three standard deviations away from the average measured voltages. The points of maximum error reflect the measured variation in rotor voltages but represent unlikely extremes for calculated values. Variations of the average contact resistance around the measured order of magnitude have minimal impact on the calculated stray loss.

The adjusted equivalent circuit model can fairly accurately reproduce the performance of this high efficiency machine. With relatively low stray load, at less than one percent of the full load output power, the harmonic rotor bar and inter-bar currents can account for essentially all of the measured stray load loss on this ten horsepower machine.

5.5.2 Design #2 Ten Horsepower Motor

Another four pole, ten horsepower motor of a completely different design including a delta-wound stator is more difficult to predict. Two versions of this machine were examined. The original motor, designed with an 18 mil air gap, measured surprisingly high stray load loss. The outer diameter around the closed rotor bars was carefully machined to increase the air gap length to 25 mils. The same machine with increased air gap measured significantly reduced stray load loss. The following plots compare calculated and predicted values with and without the inter-bar corrections for this motor design #2, similar to the previous section on the design #1 motor.

The full torque speed curves for the more well behaved motor with increased air gap is presented first. Again, there is visible distortion of the calculated torque approaching locked rotor, presumably from interaction of the four terms representing the first and second order slot harmonics. Both the disturbance as well as the torque dip are more pronounced on the lower air gap, higher stray load loss machine.

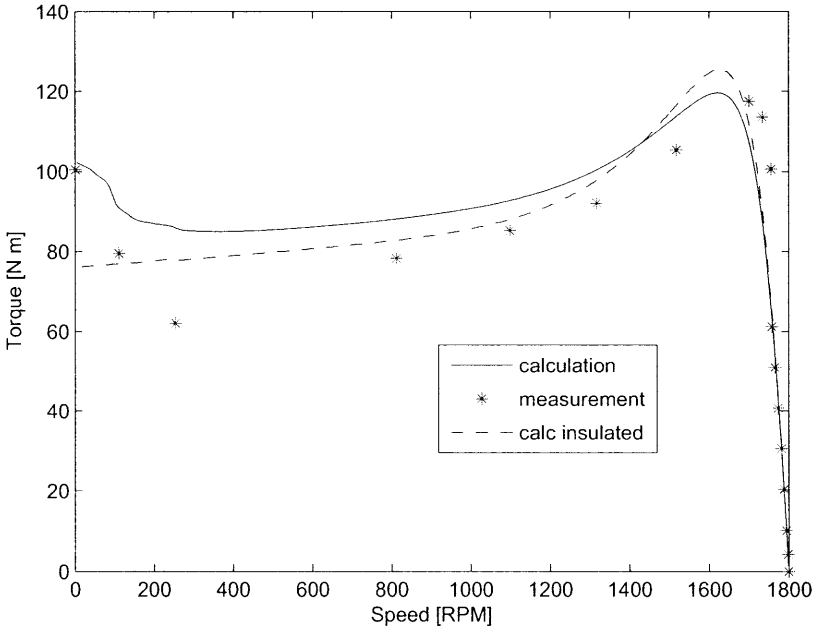

Figure 5-11: Design #2 10 hp cast copper torque speed curve with low stray load loss, 25 mil gap

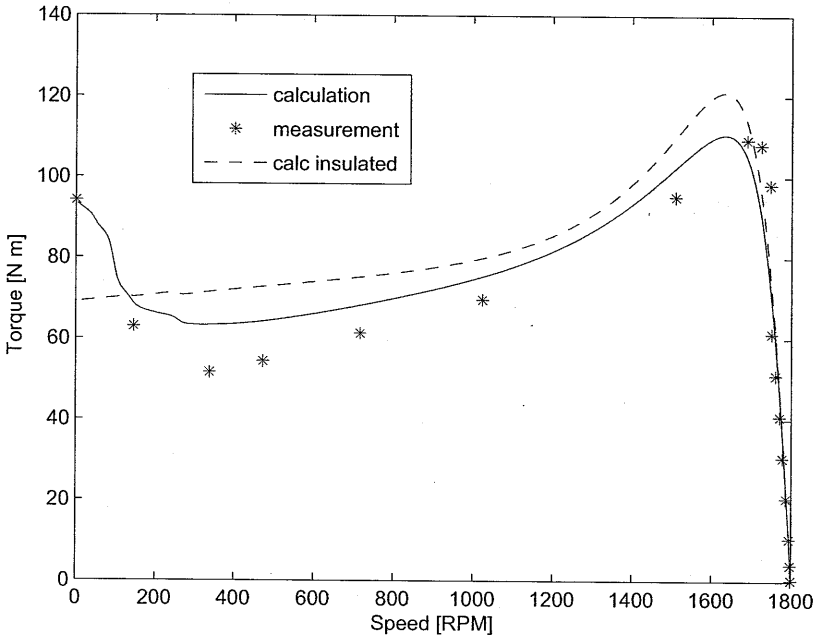

Figure 5-12: Design #2 10 hp cast copper torque speed curve with 25 mil gap and adjusted reactance values

The following set of plots, Figures 5-13, 5-14, and 5-15 compare "measured" and calculated values of torque, input current, and fundamental rotor conduction loss. Calculations are presented using the traditional equivalent circuit and the adjusted version to account for inter-bar currents. The measured data is taken at eight different points from no load to 150% load. The calculations assume values of inter-bar resistance equal to the average value determined in Chapter 4 for each motor, about 2.5 micro ohm meters for the delta connected ten horsepower rotor examined in this section.

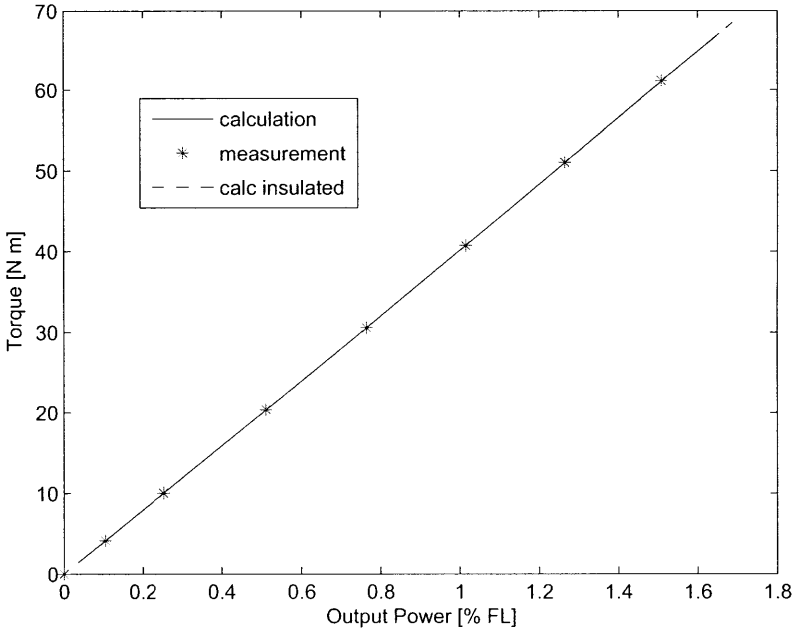

Figure 5-13: Design #2, 25 mil gap, 10 hp cast copper load torque

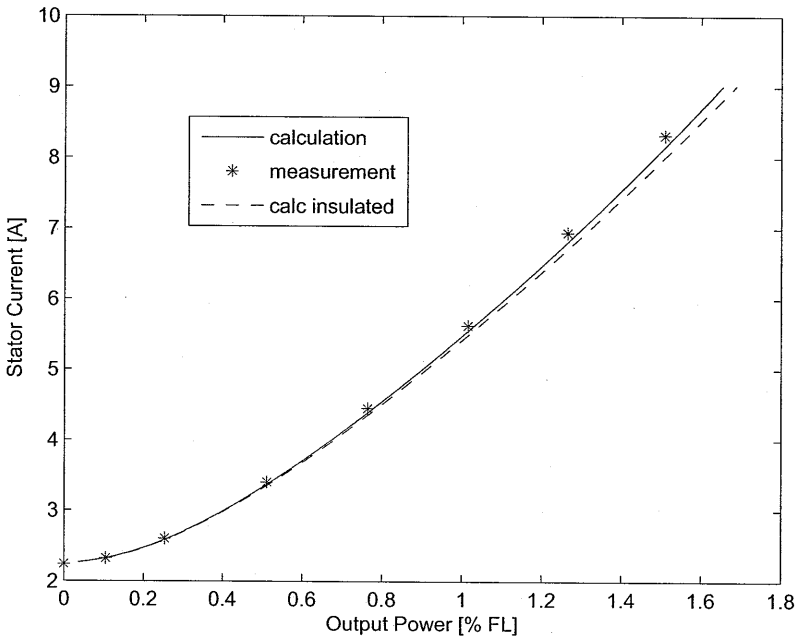

Figure 5-14: Design #2, 25 mil gap, 10 hp cast copper input stator current

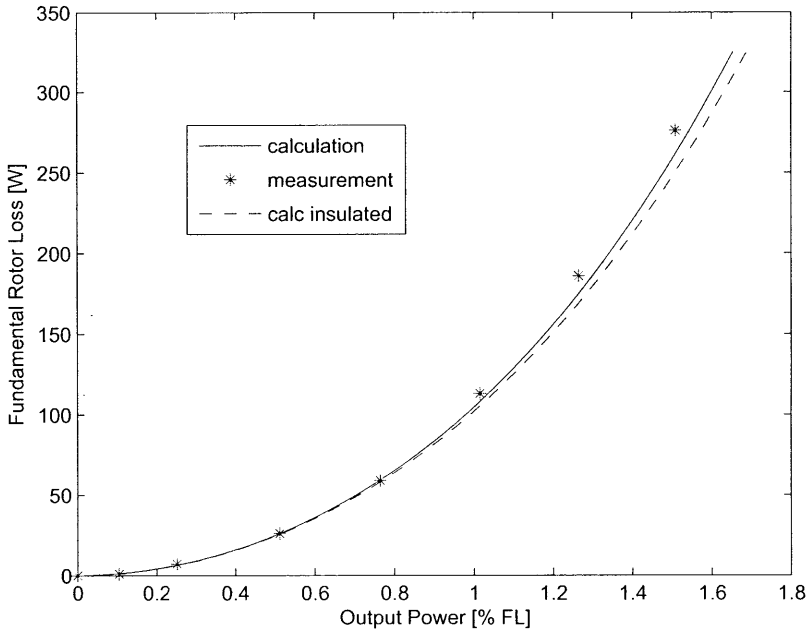

Figure 5-15: Design #2, 25 mil gap, 10 hp cast copper fundamental rotor loss

The overall behavior of the motor is still determined largely from the fundamental fields and circuits of the machine, practically independent of inter-bar currents. The inter-bar currents do not noticeably impact calculated torque, but there is a slight improvement in the calculations of current and fundamental rotor loss, more noticeable at larger loads. The stray load loss from measured tests is also compared to calculated stray loss from harmonic rotor bar currents below in Figure 5-16.

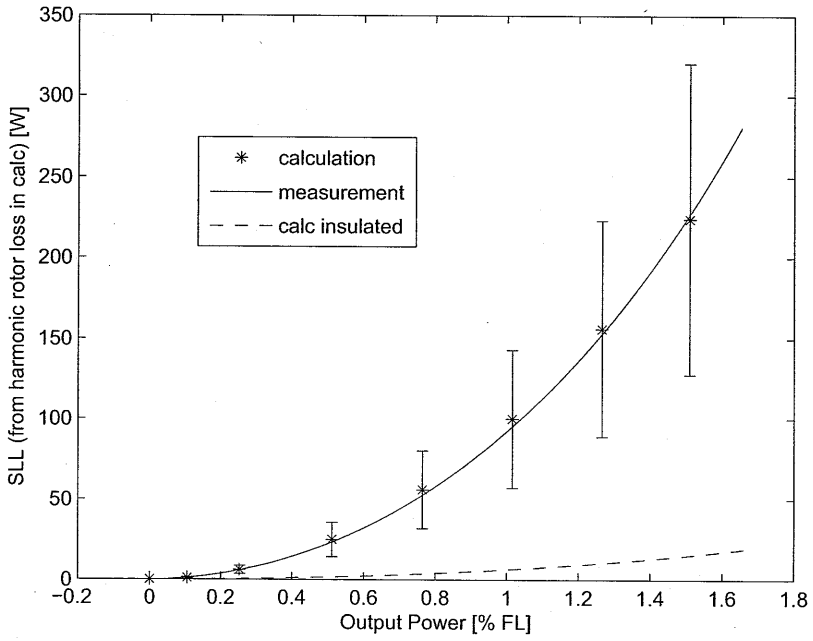

Figure 5-16: Design #2, 25 mil gap, 10 hp cast copper stray load loss or harmonic rotor conduction loss

The motor with smaller air gap and increased stray load loss is more difficult to model. Likely, there is still another source of stray loss not included in the equivalent circuit model as implemented here. The circuit model requires additional refinement, but the correction factors for inter-bar currents still improve predictions of stray load loss in Figure 5-17. Adding the additional harmonic reactance correction factor brings the calculated stray loss even closer to the measured values as shown in Figure 5-18.

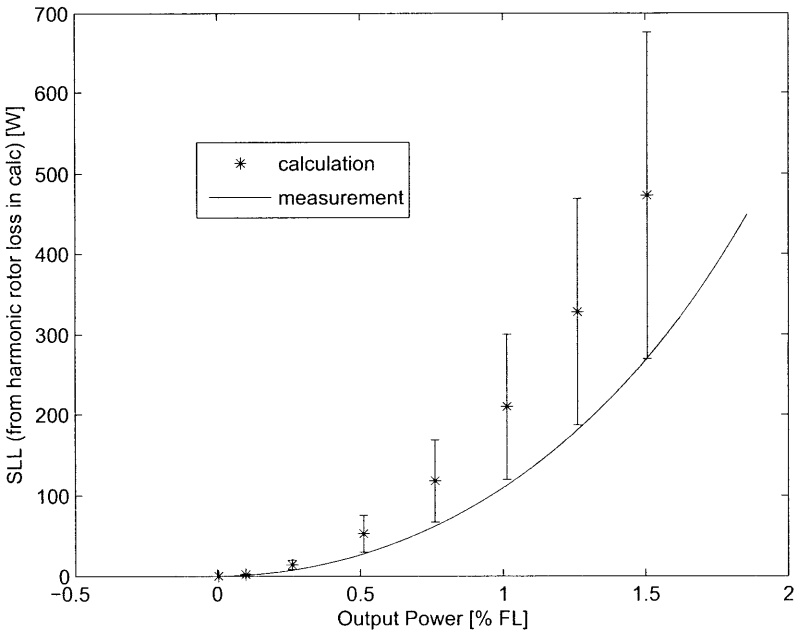

Figure 5-17: Design #2, 18 mil gap, 10 hp cast copper stray load loss or harmonic rotor conduction loss

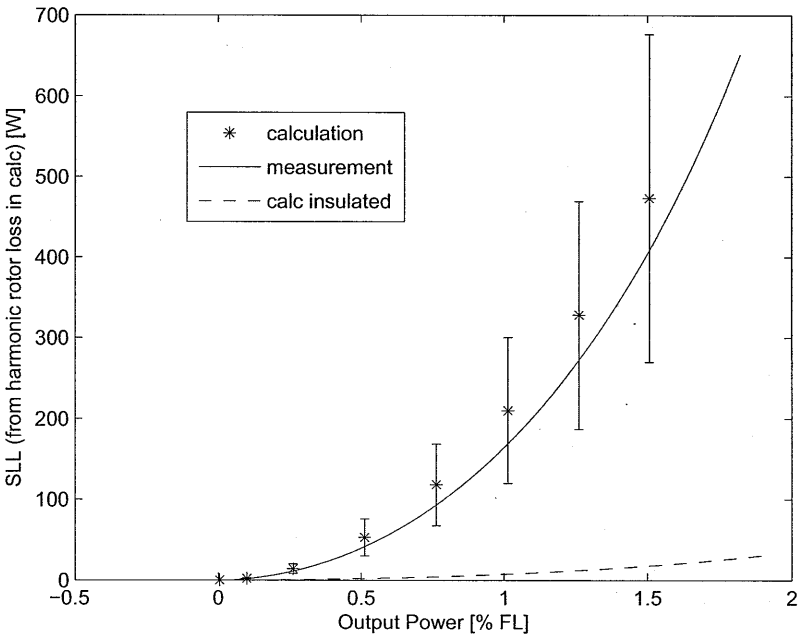

Figure 5-18: Design #2, 18 mil gap, 10 hp cast copper stray load loss or harmonic rotor conduction loss with adjusted harmonic reactances

Next, variations in predicted stray, harmonic rotor loss are calculated for variations in rotor skew and contact resistance for the 25 mil gap rotor in Figures 5-19 and 5-20.

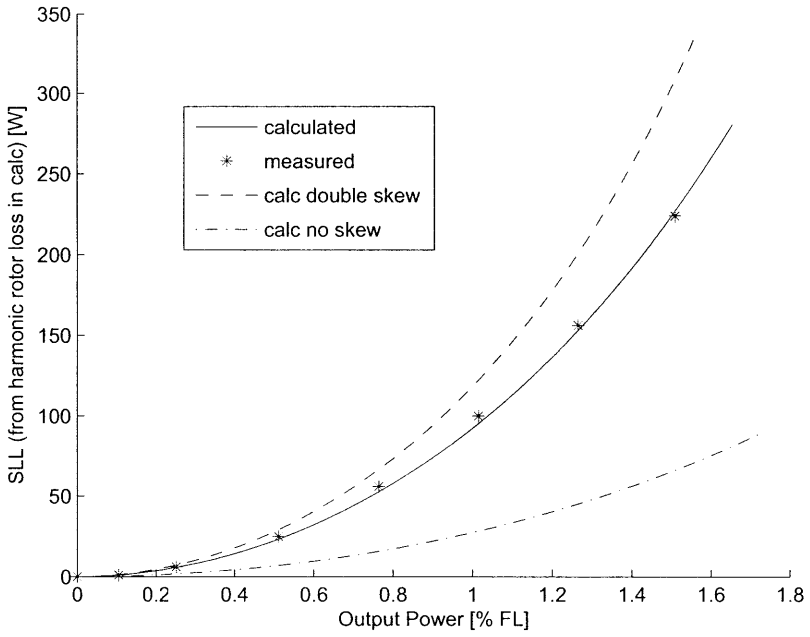

Figure 5-19: Design #2, 25 mil gap, 10 hp cast copper stray load loss or harmonic rotor conduction loss with varied rotor skew

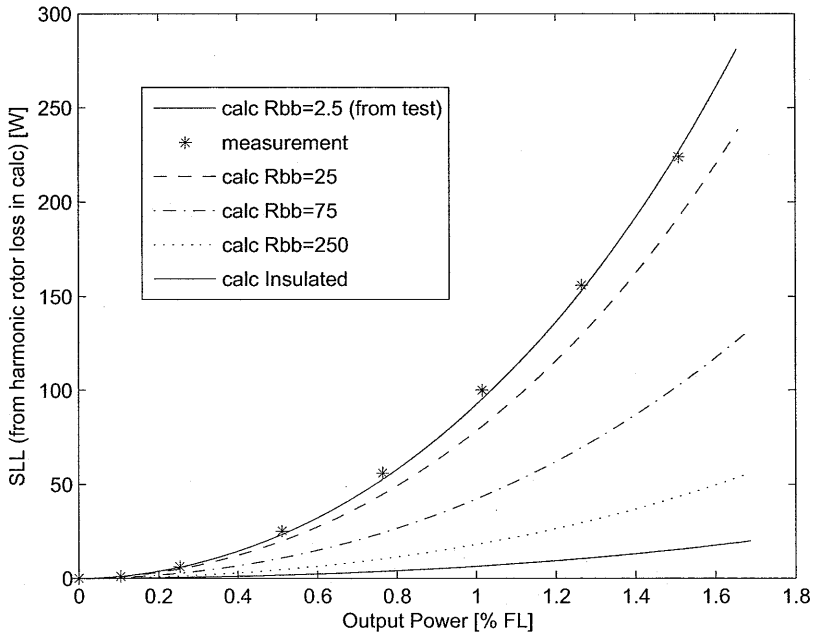

Figure 5-20: Design #2, 25 mil gap, 10 hp cast copper stray load loss or harmonic rotor conduction loss with varied inter-bar resistance

Finally, the last figure of the chapter, Figure 5-21 figure examines the impact of variation in inter-bar resistance on the full load harmonic rotor losses of the 25 mil gap, low stray load loss version of the ten horsepower motor. The bar-to-bar resistance varies over the full possible range from the approximate resistance of the of iron path between bars, at around 0.1 micro-ohm meter, up to effectively insulated bars. All of the calculations use a fixed, ten horsepower, output power for a fair comparison.

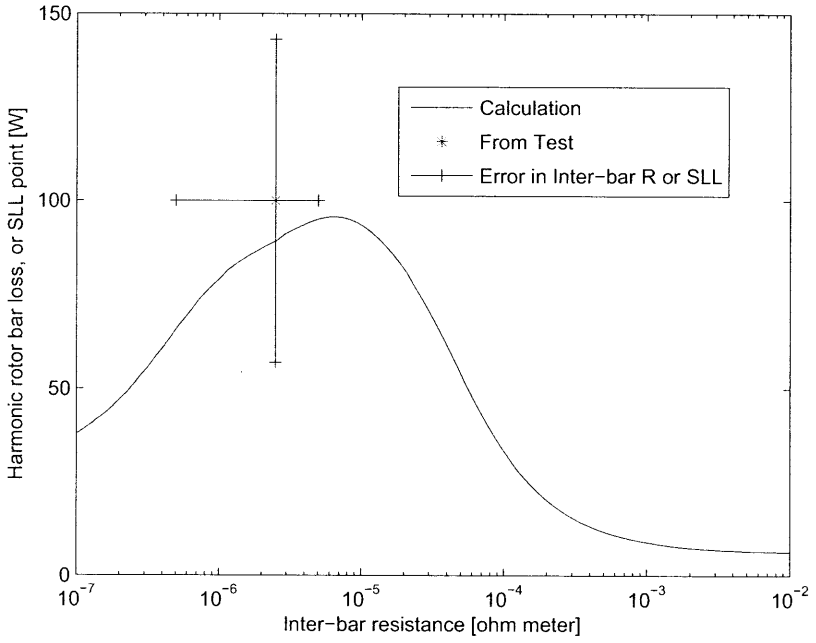

Figure 5-21: Design #2, 25 mil gap, 10 hp cast copper full load stray load loss or harmonic rotor conduction loss with varied inter-bar resistance

Chapter 6

Conclusion and Suggestions for Future Work

6.1 Summary and Conclusion

Inter-bar currents, flowing in loops including sections of rotor bars and circumferential paths through the laminations between neighboring rotor bars, contribute substantial stray load loss to skewed induction motors with non-insulated rotor conductors. The stator slot order harmonics, with a pole pitch closest to the length between neighboring rotor bars, are particularly effective at creating stray load loss. With insulated rotor bars, skew can be used to nearly eliminate these slot harmonic currents and losses, but in general, the effective rotor resistance and skew factor must be adjusted from the traditional values in order to account for the presence of currents between, as well as along, the rotor conductors.

The classic solutions for rotor bar current as a function of axial position use the average values of inter-bar resistance to calculate total rotor bar, inter-bar, and end ring losses, as in Chapter 3. However, these rotor equations depend on a number of motor design and operating point values that must be previously determined through measurement or calculation. Incorporating the rotor loss equation into an equivalent circuit framework allow for predictions of motor performance under any operating conditions.

The second chapter gives an overview of the equivalent circuit model commonly used for evaluating motor performance. The impact of rotor skew, a twisting of the rotor conductors, on the circuit model is examined in detail. The impedance values in the circuit model are also required in the rotor current and loss equations.

The main contribution of this work is the set of equations presented in Chapter 5 to adjust the rotor resistance and skew factor for the fundamental and higher order space harmonics used in equivalent circuit models to include the impact of inter-bar currents. These two equations can be included in any motor design software to improve the calculations of skewed motors with non-insulated rotors. Estimations of minimum and maximum torque as well as stray load loss at any load and locked rotor torque and current all benefit from the adjusted equivalent circuit, including the effects of inter-bar currents. Without the adjusted parameters, stray load losses may be significantly underestimated because the inter-bar currents can greatly reduce the effectiveness of skew in canceling out slot harmonic rotor currents. The new method is consistent with previous efforts, but the new calculations result in a simpler, more intuitive modification of the equivalent circuit and apply more generally, independent of how skew is incorporated into the circuit model. The only additional variable required is the average value of resistance between neighboring rotor bars.

The effective values of rotor resistance and skew factor are calculated as a function of the resistance of the cross path between neighboring bars. Chapter 4 presents the method for determining average values of the inter-bar resistance on a number of cast copper and aluminum rotors. Two general classes of rotors displayed either relatively "high" or "low" inter-bar resistance compared to the bar impedance. The values of inter-bar resistance determined for these machines can be compared to other published results and used for developing estimates of similar machines for future calculations. Ideally, a large enough library of inter-bar resistance measurements could reduce or eliminate the need for additional testing.

Altogether, the circuit model, adjusted to include inter-bar currents, can be used as an improved tool for induction motor design and analysis.

6.2 Calculations of Stray Load Loss

A number of factors can significantly impact predictions of stray load loss. This work has addressed some of these issues and identified additional topics requiring further investigation. Calculations of stray load loss from harmonic rotor bar and inter-bar currents more accurately represent measured values with the resistance and skew factor adjusted to include the impact of inter-bar currents. However, equivalent circuit reactance values also significantly impact harmonic rotor bar currents and stray loss. For each higher order space harmonic, sufficiently high rotor leakage reactance or sufficiently low air gap, magnetizing reactance will nearly eliminate the rotor current and loss, as with a fully effective skew factor much less than unity. As discussed in Chapter 2, these reactance values are difficult to accurately calculate, especially for the higher order slot harmonics. Underestimating space harmonic magnetizing reactance or overestimating the rotor leakage reactance will under predict stray loss from harmonic bar and inter-bar currents, and opposite errors will over predict stray loss.

Two reasonable strategies to adjust the values of magnetizing reactance, in opposite directions, are including the traditional Carter coefficient or adding in an additional reactance parallel to the core resistance and air gap reactance to model the reactive power drawn by the non-infinitely permeable core laminations. The Carter coefficient increases the effective air gap length to account for the stator and rotor slotting, decreasing the calculated air gap reactance. This factor may not be necessary for the slot order harmonics, where the fields cross the gap many times and the majority of the fields concentrate in the positions directly between the teeth. The additional core reactance term has only been included for the fundamental circuit in this study. No load reactive power data can be used to estimate the reactance value. The parallel combination can significantly reduce the net, effective magnetizing reactance value, especially as core flux densities increase. The reduction in fundamental magnetizing, air-gap reactance values can also used impact calculations of higher order reactance values.

Harmonic rotor bar currents account for the majority of inter-bar currents on motors rated under fifty horsepower (37.3 kW), where iron losses are generally less significant than conduction losses, but there are other sources of stray load loss in addition to harmonic rotor currents. Two possible sources of additional stray loss on skewed rotors warranting additional investigation are mentioned here. Lamination eddy current losses in the plane of the laminations, perpendicular to the shaft, are one potential source of stray load loss, driven by the small, circumferential component of rotor bar current in the case of skewed rotor bars. Additionally, the increase in net air gap magnetic field towards one end of skewed machines can also contribute potentially significant stray load loss in the form of traditional hysteresis and eddy current core losses. Similar to inter-bar currents, these two sources of stray load loss exist only on skewed machines.

6.3 Strategies to Minimize Stray Loss

This section discusses strategies to reduce the component of stray load loss from harmonic bar and inter-bar currents. Any design modifications decreasing the air gap harmonic fields will reduce the stray rotor currents and loss. The lower order harmonics can be reduced by stator winding factors from the distribution and pitch of the stator winding. If the rotor bars can be insulated, then inter-bar currents are not an issue, and skew can nearly eliminate the higher order slot order harmonic losses.

With un-insulated rotor bars, the slot harmonics may contribute unexpectedly high stray load losses, increasing with the skew angle. If the skew is not required to reduce noise or increase the starting torque, stray load loss on non-insulated rotors will be lower with no skew. The improvement should be compared to the increase in no load loss without skew. Any individual slot harmonic can also theoretically be nearly eliminated by selecting a number of rotor bars equal to the particular harmonic number, but this also should be weighed against impact to no load and locked rotor conditions.

Increasing the number of rotor and stator bars per pole also increases the order

of the slot harmonics, generally reducing their field strength, current, and loss. The length of the air gap can also be increased as shown for the ten horsepower machine.

6.4 Suggestions for Future Work

Two main issues complicating the comparison between measured test results and calculations including inter-bar currents have been variations in reactance values and additional sources of loss for skewed machines. Determining generally applicable calculations of both magnetizing and leakage reactance values, especially for the slot order harmonics, is a significant challenge that would greatly improve the accuracy of motor performance calculations. Values can change with operating conditions and motor design. This ongoing issue is more than a century old, but modern finite element analysis may provide an increasingly quick and relatively easy method to evaluate motor reactance values. Major manufacturers may already have proprietary equations that work well, but uncertainty in reactance values complicated evaluation of the new, adjusted circuit models.

Similarly, loss predictions for the motors with highest measured stray loss were also inconsistent. Calculated rotor bar and inter-bar conduction losses are not capable of providing all of the measured stray load loss without altering a different measure of motor performance like current or torque. The harmonic rotor conduction losses are a significant, but not the only, source of stray loss. Lamination tooth tip and surface losses from high frequency field variations are another commonly cited source of stray load loss.[6] Motor models must include all appreciable sources of loss to accurately reproduce or predict behavior. Lamination eddy current losses in the plane of the laminations, perpendicular to the shaft, are a potential source of stray load loss, driven by the small, circumferential component of rotor bar current in the case of skewed rotor bars. Additionally, the increase in net air gap magnetic field towards one end of skewed machines can also contribute potentially significant stray load loss in the form of traditional hysteresis and eddy current core losses. Similar to inter-bar currents, these two sources of stray load loss exist only on skewed machines.

One final area of investigation could be inexpensive and effective insulation methods for the higher temperatures required for copper casting, eliminating inter-bar currents altogether.

Bibliography

[1] Xenergy Inc. United states industrial electric motor systems market opportunities assessment. Technical report, U.S. Department of Energy, 1998.

[2] A.D. Little Inc. Opportunities for energy savings in the residential and commercial sectors with high-efficiency electric motors. Technical report, U.S. Department of Energy, 1999.

[3] S. Williamson. The induction motor-a state-of-the-ark technology? *Power Engineering Journal*, 10(6):247–254, December 1996.

[4] R. Schnapp. Electric power industry 2007: Year in review. Technical report, U.S. Department of Energy Information Administration, 2009.

[5] NEMA Motor and Generator Section. Nema premium efficiency electric motors program. http://www.nema.org/gov/energy/efficiency/premium/upload/nemaprem1p.doc, site visited June 2007 program began around 1998.

[6] P.L. Alger. *Induction machines, their behavior and uses.* Gordon and Breach, Science publishers, Inc., 1970.

[7] IEEE Power Engineering Society, New York, NY. *IEEE 112-2004 standard test procedure for polyphase induction motors and generators*, November 2004.

[8] S.S.L. Chang. Physical concepts of stray load loss in induction machines. *Transactions of the AIEE*, 73:10–12, March-April 1954.

[9] V. Rossmaier. Calculation of the stray load losses in induction machines caused by uninsulated bars. *Elektrotechnik und Maschinenbau*, 57:249–255, 1939.

[10] A.M. Odok. *Zusatzverluste und zusatzmomente in kurzschlußankermotoren mit unisolierten staben.* PhD dissertation, ETH Zurich, 1955.

[11] R. Weppler. Ein beitrag zur berechnung von asynchronmotoren mit nichtisoliertem lauferkafig. *Archiv fur Elektrotechnik*, 50(4):238–252, 1966.

[12] S. Williamson and A.C. Smith. Equivalent circuits for cage induction motors with inter-bar currents. *Proceedings of the IEE*, 149(3):173–183, May 2002.

[13] S. Williamson C.Y. Poh and A.C. Smith. Estimation of the inter-bar resistance of a cast cage rotor. *IEEE Transactions on Industry Applications*, 40(2):558–564, March-April 2004.

[14] D.G. Watterson, W. Prescott, M. Bradford, M. Lockwood, and S. Bagk. Mmf and permeance harmonic torques and losses in cage induction motors - the effects of skew, bar-to-bar impedance, and saturation. *Fourth International Conference of Electrical Machines and Drives*, pages 275–281, September 1989.

[15] V. Subba Rao and O.I. Butler. Stray losses of polyphase cage induction motors with particular reference to the condition of imperfect rotor-bar-iron insulation. *Proceedings of the IEE*, 116(5):737–751, May 1969.

[16] C.P. Steinmetz. The alternating current induction motor. *Transactions of the AIEE*, 14:185–217, 1897.

[17] A.M. Odok. Stray-load losses and stray torques in induction machines. *Transactions of the AIEE*, 77:43–53, April 1958.

[18] S. Williamson and C.I. McClay. The variation of cage motor losses with skew. *IEEE Transactions on Industry Applications*, 36(6):1563–1570, November-December 2000.

[19] M.M. Liwschitz-Garik. *Alternating-current machines.* D. Van Nostrand Company, Inc., 1961.

[20] C.G. Veinott. *Theory and design of small induction motors.* McGraw-Hill, New York, 1959.

[21] Jr. J.L. Kirtley. 6.11s class notes chapter 6: Analytic design evaluation of induction machines. Technical report, Massachusetts Institute of Technology, 2005.

[22] J.L. Kirtley Jr., J.G. Cowie, D.T. Peters, and R. Kimmich. Effect of skewing slots on flux distribution in induction machines. *Proceedings of the 2007 IEEE Power Engineering Society Annual Meeting*, June 24-28 2007.

[23] D.S. Babb and J.E. Williams. Circuit analysis method for determination of ac impedances of machine conductors. *Transactions of the AIEE*, 70:661–666, 1951.

[24] K.J. Binns, R. Hindmarsh, and B.P. Short. Effect of skewing slots on flux distribution in induction machines. *Proceedings of the IEE*, 118:543–549, March-April 1971.

[25] S. Behdashti and M. Polojadoff. A new method for the study of inter-bar currents in polyphase squirrel-cage induction motors. *IEEE Transactions on Power Apparatus and Systems*, 98(3):902–910, May-June 1979.

[26] O.I. Butler T.S. Birch. Permeance of closed-slot bridges and its effect on induction-motor-current computation. *Proceedings of the IEE*, 118(1):169–172, January 1971.

[27] C.E. Linkous. Effect of skew on induction motor magnetic fields. *Transactions of the AIEE*, 74:760–765, August 1955.

[28] O.I. Butler and T.S. Birch. Comparison of alternative skew-effect parameters of cage induction motors. *Proceedings of the IEE*, 118(7):878–883, July 1971.

[29] P.L. Alger, Y.H. Ku, and C.H.T. Pan. Speed-torque calculations for induction motors with part windings. *Transactions of the AIEE*, pages 151–160, April 1954.

[30] N. Christofides. Origins of load losses in induction motors with cast aluminium rotors. *Proceedings of the IEE*, 112(12):2317–2332, December 1965.

[31] D. Gersh, A.C. Smith, and A. Samuelson. Measurement of inter-bar resistance in cage rotors. *IEE 1997 Electric Machines and Drives Conference Publication*, pages 253–257, September 1997.

[32] D.G. Dorrell, T.J.E. Miller, and C.B. Rassmussen. Inter-bar currents in induction machines. *Conference Record of the 2001 Thirty-Sixth IEEE Industry Applications Conference*, 2:729–736, September-October 2001.